Variational Perturbation Theory for Quantum Statistics — Introducing a Recursive Calculation of the Imaginary-Time Evolution Amplitude

Diplomarbeit von
Florian Weißbach

Hauptgutachter: Prof. Dr. Hagen Kleinert

vorgelegt dem
Fachbereich Physik der
Freien Universität Berlin
im Februar MMII

Contents

Chapter 1

Introduction

Most physical problems are not exactly solvable. Therefore a wide variety of approximative methods has been developed throughout the history of physics. One of them is perturbation theory. This technique has proven to be extremely useful under innumerable circumstances. Usually, however, the weak-coupling series which are obtained through perturbation theory are not convergent.

The ground state energy of the anharmonic oscillator is the simplest example where this phenomenon can be studied. Recursion relations à la Bender and Wu [1] yield perturbation series for the eigenvalues (energy) and eigenfunctions (wave functions) of the Schrödinger equation up to arbitrarily high orders. The Bender-Wu recursion relation yields a power series for the anharmonic part of the wave function both in the coupling strength g and in the coordinate x. The power series in x can be cut off naturally by comparing the recursive results with results obtained from generating Feynman diagrams. If now the value of the coupling strength g that determines the influence of the anharmonicity is much smaller than one, the series in g converges initially. To higher orders, however, the series diverges. If the coupling strength becomes too large, the series always diverges and no physical results can be obtained at all. This thesis deals with both problems: Obtaining high-order perturbation series and then making them converge for all values of the coupling strength.

In Part I we introduce a new recursive technique that extends the Bender-Wu recursion to solutions of the time-dependent Schrödinger equation. This new, more comprehensive recursion relation enables us to obtain high-order perturbative results for the imaginary-time evolution amplitude of the anharmonic oscillator by solving a set of both differential and algebraic equations. This is in contrast to the Bender-Wu recursion which is a purely algebraic formalism.

We treat our simple model system — the anharmonic oscillator — quantum statistically by performing a Wick rotation. In the beginning of Chapter 2, both the real- and the imaginary-time evolution amplitude and their respective properties are reviewed. The subsequent sections deal with the physical quantities that can be derived from the imaginary-time evolution amplitude, namely the partition function, the density matrix, the ground state wave function, and the correlation functions. At the end of Chapter 2 we take a look at the limits as the temperature goes to zero and to infinity, respectively.

In Chapter 3 we derive the *combined* differential *and* algebraic recursion relation for calculat-

ing the imaginary-time evolution amplitude. To that end we compare two different ansatzes from which the second proves to be the better one. It obeys a symmetry which eventually enables us to change many of the differential equations into purely algebraic ones. Thus our recursion relation assumes a Bender-Wu [1] like shape. We also cut off the power series in the coordinates by comparison to diagrammatic considerations.
In Part II of this thesis variational perturbation theory [2] is applied to the perturbative results gained throughout the first part. This theory is a systematic extension of a simple variational approach, first developed by Feynman and Kleinert in the path integral formalism. Feynman introduced the path integral formalism as a quantization regulation, that represents the operator properties of quantum physics by fluctuations of the dynamical variables [3, 4]. By extending analytically real time to imaginary time, also quantum statistical quantities can be obtained by summing over quantum mechanical and thermal fluctuations with the help of path integrals [4, 5]. In order to evaluate the path integral for the free energy approximatively, Feynman and Kleinert developed a variational method in 1986 [6]. It replaces the relevant system by the exactly solvable harmonic oscillator whose frequency becomes a variational parameter which has to be optimized. Starting with Ref. [7], this method has been systematically enhanced by Kleinert to higher orders [2, 8]. It is now known as variational perturbation theory and yields results for all temperatures and all coupling strengths. It has already been applied to a broad variety of physical problems like, for instance, to effective classical partition functions and potentials [6, 7, 9, 10], to the Coulomb problem with and without homogeneous magnetic field [11, 12, 13, 14][1], semiclassical simulations of molecular dynamics [15, 17], the anharmonic oscillator [18, 19, 20, 21], Sine-Gordon chains [22], Markov processes [23, 24, 25], Bender-Wu singularities [26], the anharmonic oscillator with an x^P-potential [27], as well as to tunneling phenomena [28, 29, 30], to the double-well potential [31], to particle distributions [11, 32, 33, 34], to fluctuating field systems [35], and the fluctuation pressure of membranes [36, 37], to ϕ^4-theory [8, 38, 39] and last but not least to the ground state wave function [40, 41]. Only very recently variational perturbation theory was applied to quantum dissipative systems [42]. For instance Cuccoli et al. applied variational perturbation theory to the density matrix [43] of the Caldeira-Leggett model [44, 45, 46, 47], using techniques developed by Giachetti and Tognetti [22].
In Chapters 4 and 5 the free energy and the ground state wave function of the anharmonic oscillator are discussed and each of them undergoes variational perturbation theory. Using the high-order results for the imaginary-time evolution amplitude from Chapter 3 we study the convergence behaviour of variational perturbation theory up to fifth order for the free energy and up to seventh order for the ground state wave function. As variational perturbation theory especially allows for strong coupling, we concentrate on coupling strengths g equal to or greater than one. The results for the free energy are subject to a numerical cross check and — where appropriate — to classical considerations, whereas our results for the ground state wave function are checked against both numerical calculations and against the well-known asymptotic behaviour [41]. Moreover we study the patterns occurring in the optimization process [2, 48] for the free energy which already have proven to be very regular in the case of the ground state energy [2].

[1]The singularity is ironed out by the thermal fluctuations. This process condensed in the smearing formula [6, 12]. Similar potentials have been treated reverting on wave packages [15, 16].

In Chapter 6 we take a look at a problem from outside quantum statistics, namely the properties of boundary-layers. They can be calculated on a lattice in the limit as the lattice spacing goes to zero. Understanding this limit would enable us to switch from difference equations and numerics to differential equations and symbolic evaluations and vice versa. Here we compare variational perturbation theory with Padé methods. It turns out that they both produce good approximative results, but they do not converge. However, both resummations reveal special properties which have not been observed before. We also study the large-order behaviour of two boundary-layer problems in order to better understand the strong-coupling limit.
Chapter 7 finally sketches advantages and disadvantages of our combined differential and algebraic recursion relation and discusses the convergence of variational perturbation theory. It also provides an outlook on very promising future applications of both recursion relations and variational perturbation theory.

Part I

Perturbation Theory — Recursion Relations

Chapter 2

Quantum Statistics

In this chapter we review the definitions of some quantum statistical quantities based on the time evolution amplitude in quantum mechanics and in quantum statistics. From the imaginary-time evolution amplitude we derive the partition function and the free energy as global quantities of a system. Thereafter we examine local quantities such as the density matrix and correlation functions which can also be derived from the imaginary-time evolution amplitude. We finally go back to quantum mechanics by taking the low-temperature limit from which we obtain the ground state wave function and energy. We shall also study the high-temperature limit in which we obtain the classical statistical properties of the system.

2.1 Real-Time Evolution Amplitude

In the Schrödinger picture, the time evolution of a state vector $|\Psi(t_a)\rangle$ at a time t_b is given by the equation

$$|\Psi(t_b)\rangle = e^{-i(t_b-t_a)\hat{H}/\hbar}|\Psi(t_a)\rangle\,. \tag{2.1}$$

The operator

$$\hat{U}(t_b,t_a) \equiv e^{-i(t_b-t_a)\hat{H}/\hbar} \tag{2.2}$$

is called the time evolution operator. Here $\hat{H} = \hat{H}(\hat{x},\hat{p})$ is a Hermitean Hamilton operator which depends on the canonical variables, position and momentum of the system. We assume that there is no explicit time-dependence. The operator $\hat{U}(t_b,t_a)$ is unitary by construction, so

$$\hat{U}^{-1}(t_b,t_a) = \hat{U}^{\dagger}(t_b,t_a) \tag{2.3}$$

holds for all times t_a, t_b. Also, it fulfills the group multiplication law

$$\hat{U}(t_b,t_a) = \int_{-\infty}^{+\infty} dt_c\, \hat{U}(t_b,t_c)\hat{U}(t_c,t_a)\,. \tag{2.4}$$

The time evolution operator obeys the equation of motion

$$\frac{d}{dt_b}\hat{U}(t_b,t_a) = -\frac{i}{\hbar}\hat{H}\hat{U}(t_b,t_a) \tag{2.5}$$

with the initial condition

$$\hat{U}(t_a,t_a) = 1\,. \tag{2.6}$$

We now introduce another quantity derived from the time evolution operator, namely the real-time evolution amplitude. It is defined by

$$(x_b\,t_b|x_a\,t_a) \equiv \langle x_b|\hat{U}(t_b,t_a)|x_a\rangle\,, \tag{2.7}$$

where the bra $\langle x_b|$ and the ket $|x_a\rangle$ denote the eigenstates of the position operator $\hat{x}$ to the eigenvalue x, obeying the eigenvalue equation

$$\hat{x}|x\rangle = x|x\rangle\,. \tag{2.8}$$

The eigenvectors are orthonormal

$$\langle x|x'\rangle = \delta(x-x')\,, \tag{2.9}$$

and complete

$$\int_{-\infty}^{+\infty} dx|x\rangle\langle x| = 1\,. \tag{2.10}$$

The operator $\hat{U}(t_b,t_a)$ obeys the unitarity property (2.3), such that the matrix elements have the property

$$\begin{aligned}\langle x_b|\hat{U}(t_b,t_a)|x_a\rangle &= \langle x_a|\hat{U}^\dagger(t_b,t_a)|x_b\rangle^* \\ &= \langle x_a|\hat{U}^{-1}(t_b,t_a)|x_b\rangle^* \\ &= \langle x_a|\hat{U}(t_a,t_b)|x_b\rangle^*\,.\end{aligned} \tag{2.11}$$

For the amplitude (2.7) this implies

$$(x_b\,t_b|x_a\,t_a) = (x_a\,t_a|x_b\,t_b)^*\,. \tag{2.12}$$

2.2 Spectral Representation

Like any function of an operator, the time evolution amplitude has a spectral representation which turns out to be helpful for a lot of calculations at a later stage of this work. By multiplying equation (2.5) with a bra $\langle x_b|$ from the left and with a ket $|x_a\rangle$ from the right we obtain the Schrödinger equation

$$i\hbar\frac{\partial}{\partial t}(x_b\,t|x_a\,0) = \hat{H}(x_b,\hat{p}_b)(x_b\,t|x_a\,0)\,, \tag{2.13}$$

where

$$\hat{p}_b \equiv -i\hbar\frac{\partial}{\partial x_b}\,. \tag{2.14}$$

The initial condition is

$$(x_b\,0|x_a\,0) = \delta(x_b - x_a)\,, \tag{2.15}$$

which comes from equation (2.6) together with (2.9). Suppose now that we have found a complete and orthonormal set of eigenfunctions of the stationary Schrödinger equation

$$\hat{H}(x_b,\hat{p}_b)\Psi_n(x_b) = E_n\Psi_n(x_b)\,. \tag{2.16}$$

The completeness relation in this case reads

$$\sum_n \Psi_n^*(x_b)\Psi_n(x_a) = \delta(x_b - x_a)\,, \tag{2.17}$$

and the orthonormality property is

$$\int_{-\infty}^{+\infty} dx_b\Psi_n^*(x_b)\Psi_{n'}(x_b) = \delta_{n\,n'}\,. \tag{2.18}$$

Because of completeness, we can expand the time evolution amplitude $(x_b\,t|x_a\,0)$ in terms of the eigenfunctions $\Psi_n(x_b)$:

$$(x_b\,t|x_a\,0) = \sum_n c_n(t)\Psi_n(x_b)\,. \tag{2.19}$$

Inserting this ansatz into the Schrödinger equation (2.13), and using (2.16), we obtain

$$i\hbar\sum_n \dot{c}_n(t)\Psi_n(x_b) = \sum_n E_n c_n(t)\Psi_n(x_b)\,. \tag{2.20}$$

Multiplying (2.20) by $\Psi^*_{n'}(x_b)$ and integrating over x_b yields

$$i\hbar \sum_n \dot{c}_n(t) \int_{-\infty}^{+\infty} dx_b \Psi^*_{n'}(x_b)\Psi_n(x_b) = \sum_n E_n c_n(t) \int_{-\infty}^{+\infty} dx_b \Psi^*_{n'}(x_b)\Psi_n(x_b)\,, \tag{2.21}$$

which — employing the orthormality property (2.18) — transforms to

$$i\hbar \dot{c}_n(t) = E_n c_n(t)\,. \tag{2.22}$$

The solution to this differential equation simply is

$$c_n(t) = c_n(0) e^{-\frac{i}{\hbar}E_n t}\,. \tag{2.23}$$

Inserting (2.23) into the expansion (2.19), the real-time evolution amplitude becomes

$$(x_b\, t|x_a\, 0) = \sum_n c_n(0) e^{-\frac{i}{\hbar}E_n t}\Psi_n(x_b)\,. \tag{2.24}$$

The constants $c_n(0)$ are now fixed by applying the initial condition (2.15):

$$(x_b\, 0|x_a\, 0) = \sum_n c_n(0)\Psi_n(x_b) = \delta(x_b - x_a)\,. \tag{2.25}$$

Multiplication by $\Psi^*_{n'}(x_b)$ and integration over x_b leads to

$$c_{n'}(0) = \Psi^*_{n'}(x_a)\,. \tag{2.26}$$

So all in all we get for the real-time evolution amplitude

$$(x_b\, t|x_a\, 0) = \sum_n \Psi^*_n(x_a) e^{-\frac{i}{\hbar}E_n t}\Psi_n(x_b)\,, \tag{2.27}$$

which is its spectral representation.
Generally, every function of an operator $F(\hat{O})$ can be spectrally expanded as

$$F(\hat{O}) = \sum_n f(\lambda_n)\Psi_n\Psi^*_n\,, \tag{2.28}$$

where the λ_n are eigenvalues of the operator $\hat{O}$.

2.3 Imaginary-Time Evolution Amplitude

In order to make the transition from quantum mechanics to quantum statistics[1], we perform a so-called Wick rotation of the time:

$$t \to -i\tau \,. \tag{2.29}$$

Thus the *real*-time evolution amplitude $(x_b\, t_b|x_a\, t_a)$ turns into the *imaginary*-time evolution amplitude $(x_b\, \tau_b|x_a\, \tau_a)$. The imaginary-time evolution amplitude can also be expanded as

$$(x_b\, \tau_b|x_a\, \tau_a) = \langle x_b|\hat{U}(\tau_b, \tau_a)\, x_a\rangle \,, \tag{2.30}$$

where $\hat{U}(\tau_b, \tau_a)$ is the imaginary-time evolution operator

$$\hat{U}(\tau_b, \tau_a) \equiv e^{-(\tau_b - \tau_a)\hat{H}/\hbar} \,. \tag{2.31}$$

In contrast to the real-time evolution operator $\hat{U}(t_b, t_a)$, its imaginary counterpart $\hat{U}(\tau_b, \tau_a)$ is not unitary, but Hermitean:

$$\hat{U}^\dagger(\tau_b, \tau_a) = \hat{U}(\tau_b, \tau_a) \,. \tag{2.32}$$

That is why we get a slightly different time reversal behaviour for the imaginary-time evolution amplitude compared to the real one in (2.12). Defining $\beta \equiv 1/k_{\mathrm{B}}T$, we get

$$\begin{aligned}
(x_b\, \hbar\beta|x_a\, 0) &= \langle x_b|e^{-\beta\hat{H}}|x_a\rangle \\
&= \langle x_a|\left(e^{-\beta\hat{H}}\right)^\dagger|x_b\rangle^* \\
&= \langle x_a|e^{-\beta\hat{H}}|x_b\rangle^* \\
&= (x_a\, \hbar\beta|x_b\, 0)^* \,,
\end{aligned} \tag{2.33}$$

while it is known that the imaginary-time evolution amplitude is real for one-dimensional problems.
The imaginary-time evolution amplitude has a spectral representation which can easily be obtained from the spectral representation of the real-time evolution amplitude (2.27). We just have to replace real time by imaginary time according to the Wick rotation (2.29) in the spectral representation (2.27), yielding

$$(x_b\, \hbar\beta|x_a\, 0) = \sum_n \Psi_n^*(x_a) e^{-\beta E_n} \Psi_n(x_b) \,. \tag{2.34}$$

[1] We are considering equilibrium systems only.

2.4 Partition Function and Free Energy

Having defined the imaginary-time evolution amplitude, we now want to study one of the global quantities which can be derived from it, namely the partition function. The partition function Z is defined as the trace of the imaginary-time evolution amplitude,

$$Z \equiv \int_{-\infty}^{+\infty} dx (x\, \hbar\beta | x\, 0)\,. \tag{2.35}$$

The partition function is a useful quantity, as it defines the free energy via its logarithm

$$F = -\frac{1}{\beta} \log Z\,. \tag{2.36}$$

The derivatives of the free energy F lead to all the important thermo dynamical quantities, like e. g. pressure, entropy, or heat capacity.
From the spectral representation of the imaginary-time evolution amplitude (2.34) we see that the partition function Z also has a simple spectral representation, namely

$$Z = \sum_n \int_{-\infty}^{+\infty} dx_b \Psi_n^*(x_b) e^{-\beta E_n} \Psi_n(x_b) = \sum_n e^{-\beta E_n}\,, \tag{2.37}$$

which follows from the normalization integrals in equation (2.18).

2.5 Density Matrix

Let us now discuss an important local quantity which can be obtained from the imaginary-time evolution amplitude. The density matrix allows us to treat pure and mixed quantum mechanical states simultaneously. Often we have to deal with a statistical mixture of pure quantum states. For instance, the density matrix would be the appropriate formalism to deal with a continuous (not fully) polarized proton beam with proton spins pointing in various directions. The ensemble of the protons in the beam should be treated in a conventional statistical way, while a single proton obeys quantum mechanics.
Consider a time-independent base $|\Psi_n\rangle$ that is complete (2.17) and orthonormal (2.18). Then any state vector can be expanded in this base according to

$$|\Psi(t)\rangle = \sum_n c_n(t) |\Psi_n\rangle\,, \tag{2.38}$$

where normalization of $|\Psi(t)\rangle$ implies that

$$\sum_n |c_n(t)|^2 = 1\,. \tag{2.39}$$

The coefficients $c_n(t)$ are given by the scalar products

$$c_n(t) = \langle \Psi_n | \Psi(t) \rangle \,. \tag{2.40}$$

The time evolution is governed by the Schrödinger equation

$$\hat{H} |\Psi(t)\rangle = i\hbar \frac{d}{dt} |\Psi(t)\rangle \,. \tag{2.41}$$

Expanding the $|\Psi(t)\rangle$ according to (2.38) and multiplying from the left by $\langle \Psi_m|$ we get

$$\sum_n \langle \Psi_m | \hat{H} | \Psi_n \rangle c_n(t) = i\hbar \sum_n \langle \Psi_m | \Psi_n \rangle \dot{c}_n(t) = i\hbar \dot{c}_m(t) \,, \tag{2.42}$$

because the $|\Psi_n\rangle$ are orthonormal (2.18). Introducing the matrix elements of the Hamiltonian with respect to the base vectors $H_{mn} \equiv \langle \Psi_m | \hat{H} | \Psi_n \rangle$ we can rewrite equation (2.42) as

$$\sum_n H_{mn} c_n(t) = i\hbar \dot{c}_m(t) \,. \tag{2.43}$$

Since $\hat{H}$ is a Hermitean operator, the matrix elements H_{mn} form a Hermitean matrix:

$$H_{mn} = \langle \Psi_m | \hat{H} | \Psi_n \rangle = \langle \Psi_n | \hat{H}^\dagger | \Psi_m \rangle^* = \langle \Psi_n | \hat{H} | \Psi_m \rangle^* = H^*_{nm} \,. \tag{2.44}$$

We now introduce the density matrix for pure states by its matrix elements

$$\rho_{mn}(t) \equiv c_m(t) c^*_n(t) \,. \tag{2.45}$$

This quantity has the following properties:

(i) It has unit trace: $\mathrm{tr}\rho(t) = \sum_n \rho_{nn}(t) = \sum_n |c_n(t)|^2 = 1$.

(ii) It is Hermitean: $\rho^\dagger = \rho$.

(iii) The expectation value in the state $|\Psi(t)\rangle$ reads

$$\langle \Psi(t) | A \Psi(t) \rangle = \sum_{mn} A_{mn} c_n(t) c^*_m(t) = \sum_{mn} \rho_{mn}(t) A_{mn} = \mathrm{tr}[\rho(t) A] \,. \tag{2.46}$$

(iv) According to (2.43), it obeys an equation of motion:

$$\begin{aligned} i\hbar \dot{\rho}_{mn}(t) &= i\hbar \dot{c}_m(t) c^*_n(t) + i\hbar c_m(t) \dot{c}^*_n(t) \\ &= \sum_p H_{mp} c_p(t) c^*_n(t) - \sum_p H_{pn} c_m(t) c^*_p(t) \\ &= \sum_p (H_{mp} \rho_{pn}(t) - H_{pn} \rho_{mp}(t)) \\ &= [H, \rho(t)]_{mn} \,. \end{aligned} \tag{2.47}$$

This equation is known as the von Neumann equation.

(v) We have $\rho^2 = \rho$ for pure states.

With respect to the fourth property one should remark that $\rho(t)$ and H_{mn} are defined in the Schrödinger picture. One should not be deceived by the striking similarity to the Heisenberg equation $i\hbar\dot{\hat{F}} = [\hat{F}, \hat{H}]$ for $\partial\hat{F}/\partial t = 0$, where $\hat{F}, \hat{H}$ are operators in the Heisenberg picture. This is the reason why the density matrix $\rho(t)$ changes with the opposite sign with respect to the operator $\hat{F}$.
Once we know the initial value $\rho(0) \equiv \rho_0$, the von Neumann equation (2.47) enables us to calculate $\rho(t)$ for all times. For the time-independent Hamiltonian under consideration $\hat{H}$ the time evolution of the density matrix simply is

$$\rho(t) = e^{-\frac{i\hat{H}t}{\hbar}} \rho_0 e^{\frac{i\hat{H}t}{\hbar}} . \tag{2.48}$$

We now want to extend the definition of the density matrix to statistical mixtures of pure states. Therefore we define

$$\rho_{mn} \equiv \sum_\alpha p_\alpha c_m^{(\alpha)} c_n^{(\alpha)^*} , \tag{2.49}$$

with the real probabilities p_α obeying

$$\sum_\alpha p_\alpha = 1 , \tag{2.50}$$

and $p_\alpha \geq 0$.
The above properties of the density matrix for pure states remain the same except for its square: $\rho^2 \neq \rho$. This provides us with a convenient way to distinguish pure states from mixed quantum states.
In quantum statistics we only consider time-independent density matrices $\rho(t) = \rho$. This matrix is diagonal in the energy eigenstates $|\Psi_n\rangle$. The canonical density matrix can be represented as

$$\rho(x_b, x_a) = \frac{\sum_n \Psi_n^*(x_a) e^{-\beta E_n} \Psi_n(x_b)}{\sum_n e^{-\beta E_n}} , \tag{2.51}$$

which is the imaginary-time evolution amplitude (2.34), normalized by the partition function (2.37):

$$\rho(x_b, x_a) = \frac{(x_b\, \hbar\beta | x_a\, 0)}{Z} . \tag{2.52}$$

2.6 Correlation Function

Correlation functions of the path $x(\tau)$ carry important information of quantum statistical systems. They are defined as expectations of products of path positions at different times. For instance the two-point correlation function reads

$$\langle x(\tau_1)x(\tau_2)\rangle = \int_{-\infty}^{+\infty} dx \int_{-\infty}^{+\infty} dx_1 \int_{-\infty}^{+\infty} dx_2 (x\,\hbar\beta|x_2\,\tau_2)x_2(x_2\,\tau_2|x_1\,\tau_1)x_1(x_1\,\tau_1|x\,0)\,. \quad (2.53)$$

Correlation functions are observable in scattering experiments. All n-point correlation functions can be expanded according to Wick's rule. A generalization of that formalism can be found in Section 3.2.

2.7 Quantum Mechanical Limit $\beta \to \infty$

Quantum mechanical quantities can be reobtained from quantum statistics by letting the temperature go to zero or $\beta \to \infty$. In this limit the imaginary-time evolution amplitude becomes

$$(x_b\,\hbar\beta|x_a\,0) \sim \Psi_0^*(x_a)e^{-\beta E_0}\Psi_0(x_b) \quad (\beta \to \infty)\,, \quad (2.54)$$

because the term with the lowest energy in the summation in the spectral representation (2.34) — the ground state energy E_0 — is the one which decays slowest.
The low-temperature limit of the partition function (2.37) is of course

$$Z \sim e^{-\beta E_0} \quad (\beta \to \infty)\,, \quad (2.55)$$

such that the low temperature limit of the free energy (2.36) becomes

$$\lim_{\beta\to\infty} F = E_0\,. \quad (2.56)$$

The ground state wave function $\Psi_0(x)$ can be obtained from the diagonal elements of the density matrix $\rho(x,x)$ in a straight-forward way. According to (2.54) and (2.55) the low temperature limit of the diagonal elements of the density matrix (2.52) can be written as

$$\lim_{\beta\to\infty} \rho(x,x) = \lim_{\beta\to\infty} \frac{\Psi_0^*(x)e^{-\beta E_0}\Psi_0(x)}{e^{-\beta E_0}} = |\Psi_0(x)|^2\,. \quad (2.57)$$

So the ground state wave function simply is the square-root of the low-temperature limit of the diagonal elements of the density matrix

$$\Psi_0(x) = \sqrt{\lim_{\beta\to\infty} \rho(x,x)}\,, \quad (2.58)$$

for the one-dimensional wave function is real.

2.8 Classical Limit $\beta \to 0$

The classical limit is reached as the inverse temperature β goes to zero. In this limit, the non-diagonal elements of the density matrix $\rho(x_b, x_a)$ vanish

$$\lim_{\beta \to 0} \rho(x_b, x_a) = 0 \,, \; x_b \neq x_a \,, \tag{2.59}$$

and the diagonal elements approach the classical configuration space distribution $\rho_{\rm cl}(x)$:

$$\rho(x, x) \sim \rho_{\rm cl}(x) \quad (\beta \to 0) \,. \tag{2.60}$$

The latter is related to the classical phase space distribution

$$\rho_{\rm cl}(x, p) = \frac{1}{Z_{\rm cl}} \exp\left[-\beta H(x, p)\right] \,, \tag{2.61}$$

where $H(x, p)$ is the Hamilton function

$$H(x, p) = \frac{p^2}{2M} + V(x) \,. \tag{2.62}$$

The normalization of the phase space distribution (2.61) is ensured by the classical partition function $Z_{\rm cl}$ which fixes the integral over positions and momenta to be one. So the particle must be somewhere in phase space:

$$\int \frac{dx dp}{2\pi\hbar} \rho_{\rm cl}(x, p) = 1 \,. \tag{2.63}$$

Integrating over the momenta, we get the classical configuration space distribution

$$\rho_{\rm cl}(x) = \int_{-\infty}^{+\infty} \frac{dp}{2\pi\hbar} \rho_{\rm cl}(x, p) \,. \tag{2.64}$$

Inserting in the phase space distribution (2.61) with the Hamiltonian (2.62), we obtain

$$\rho_{\rm cl}(x) = \frac{e^{-\beta V(x)}}{Z_{\rm cl}} \,, \tag{2.65}$$

where the classical partition function reads

$$Z_{\rm cl} = \int_{-\infty}^{+\infty} \frac{dx}{\lambda_{\rm th}} e^{-\beta V(x)} \,, \tag{2.66}$$

with the thermal wavelength $\lambda_{\rm th} = \sqrt{2\pi\hbar^2 / M k_{\rm B} T}$.

Chapter 3

Imaginary-Time Evolution Amplitude

Feynman diagrams enable us to compute physical quantities of interacting theories in the form of perturbation series. In the beginning of this chapter we use this diagrammatic approach to calculate the imaginary-time evolution amplitude of the anharmonic oscillator to first perturbative order. For higher orders this approach becomes quite cumbersome. Therefore we develop a more efficient technique. We calculate the imaginary-time evolution amplitude recursively by choosing an ansatz which solves its Schrödinger equation. Thus we derive a set of recursive differential equations similar to the algebraic Bender-Wu recursion for quantum mechanical eigenfunctions and eigenvalues [1]. We then streamline the ansatz as well as the equations by proposing a strategy to exploit the symmetry (2.33) of the imaginary-time evolution amplitude. This way we reduce the number of recursive differential equations and transform most of them into algebraic ones. Finally we evaluate the equations up to seventh order with the help of a `Maple` programme.

3.1 Path Integral Representation

The path integral representation for the imaginary-time evolution amplitude of a particle of mass M moving in a one dimensional potential $V(x)$ reads [2]

$$(x_b\,\hbar\beta|x_a\,0) = \int_{x(0)=x_a}^{x(\hbar\beta)=x_b} \mathcal{D}x \exp\left\{-\frac{1}{\hbar}\int_0^{\hbar\beta} d\tau \left[\frac{M}{2}\dot{x}^2(\tau) + V(x(\tau))\right]\right\} . \tag{3.1}$$

For the anharmonic oscillator potential

$$V(x) = \frac{M}{2}\omega^2 x^2 + g x^4 \tag{3.2}$$

the imaginary-time evolution amplitude (3.1) can be expanded in powers of the coupling constant g. Thus we obtain the perturbation series

$$(x_b\,\hbar\beta|x_a\,0) = (x_b\,\hbar\beta|x_a\,0)_\omega \times\left[1-\frac{g}{\hbar}\int_0^{\hbar\beta}d\tau_1\langle x^4(\tau_1)\rangle_\omega+\frac{g^2}{2\hbar^2}\int_0^{\hbar\beta}d\tau_1\int_0^{\hbar\beta}d\tau_2\,\langle x^4(\tau_1)\,x^4(\tau_2)\rangle_\omega+\ldots\right], \tag{3.3}$$

where we have introduced the harmonic imaginary-time evolution amplitude

$$(x_b\,\hbar\beta|x_a\,0)_\omega \equiv \int_{x(0)=x_a}^{x(\hbar\beta)=x_b}\mathcal{D}x\exp\left\{-\frac{1}{\hbar}\int_0^{\hbar\beta}d\tau\left[\frac{M}{2}\dot{x}^2(\tau)+\frac{M}{2}\omega^2x^2(\tau)\right]\right\}, \tag{3.4}$$

and the harmonic expectation value for an arbitrary functional $F[x]$ of the path $x(\tau)$:

$$\begin{aligned}\langle F[x]\rangle_\omega \;\equiv\; & \frac{1}{(x_b\,\hbar\beta|x_a\,0)_\omega}\int_{x(0)=x_a}^{x(\hbar\beta)=x_b}\mathcal{D}x\,F[x]\\ & \times\exp\left\{-\frac{1}{\hbar}\int_0^{\hbar\beta}d\tau\left[\frac{M}{2}\dot{x}^2(\tau)+\frac{M}{2}\omega^2x^2(\tau)\right]\right\}.\end{aligned} \tag{3.5}$$

The latter is evaluated with the help of the generating functional for the harmonic oscillator, whose path integral representation reads

$$\begin{aligned}(x_b\,\hbar\beta|x_a\,0)_\omega[j] \;=\; & \int_{x(0)=x_a}^{x(\hbar\beta)=x_b}\mathcal{D}x\exp\left\{-\frac{1}{\hbar}\int_0^{\hbar\beta}d\tau\right.\\ & \left.\times\left[\frac{M}{2}\dot{x}^2(\tau)+\frac{M}{2}\omega^2x^2(\tau)-j(\tau)x(\tau)\right]\right\},\end{aligned} \tag{3.6}$$

leading to [2]

$$\begin{aligned}(x_b\,\hbar\beta|x_a\,0)_\omega[j] \;=\; & (x_b\,\hbar\beta|x_a\,0)_\omega\exp\left[\frac{1}{\hbar}\int_0^{\hbar\beta}d\tau_1\,x_{\rm cl}(\tau_1)j(\tau_1)\right.\\ & \left.+\frac{1}{2\hbar^2}\int_0^{\hbar\beta}d\tau_1\int_0^{\hbar\beta}d\tau_2\;G^{(\rm D)}(\tau_1,\tau_2)j(\tau_1)j(\tau_2)\right]\end{aligned} \tag{3.7}$$

with the harmonic imaginary-time evolution amplitude

$$(x_b\,\hbar\beta|x_a\,0)_\omega=\sqrt{\frac{M\omega}{2\pi\hbar\sinh\hbar\beta\omega}}\exp\left\{-\frac{M\omega}{2\hbar\sinh\hbar\beta\omega}[(x_a^2+x_b^2)\cosh\hbar\beta\omega-2x_ax_b]\right\}. \tag{3.8}$$

In equation (3.7) we have introduced the classical path

$$x_{\rm cl}(\tau)\equiv\frac{x_a\sinh(\hbar\beta-\tau)\omega+x_b\sinh\omega\tau}{\sinh\hbar\beta\omega}, \tag{3.9}$$

and the Dirichlet Green's function

$$G^{(\mathrm{D})}(\tau_1,\tau_2) \equiv \frac{\hbar}{M\omega}\frac{1}{\sinh\hbar\beta\omega}\left[\theta(\tau_1-\tau_2)\sinh(\hbar\beta-\tau_1)\omega\sinh\omega\tau_2 + \theta(\tau_2-\tau_1)\sinh(\hbar\beta-\tau_2)\omega\sinh\omega\tau_1\right], \tag{3.10}$$

whose properties are discussed in detail in Ref. [49].

3.2 Wick's Theorem

We follow Ref. [40, 50] and evaluate harmonic expectation values of polynomials in x arising from the generating functional (3.7) according to Wick's theorem. Let us illustrate the procedure to reduce the power of polynomials by the example of the harmonic expectation value $\langle x^n(\tau_1)\,x^m(\tau_2)\rangle_\omega$:

(i) Contracting $x(\tau_1)$ with $x^{n-1}(\tau_1)$ and $x^m(\tau_2)$ leads to Green's functions $G^{(\mathrm{D})}(\tau_1,\tau_1)$ and $G^{(\mathrm{D})}(\tau_1,\tau_2)$ with multiplicity $n-1$ and m, respectively. The rest of the polynomial remains within the harmonic expectation value, leading to $\langle x^{n-2}(\tau_1)\,x^m(\tau_2)\rangle_\omega$ and $\langle x^{n-1}(\tau_1)\,x^{m-1}(\tau_2)\rangle_\omega$.

(ii) If $n>1$, extract one $x(\tau_1)$ from the expectation value giving $x_{\mathrm{cl}}(\tau_1)$ multiplied by $\langle x^{n-1}(\tau_1)x^m(\tau_2)\rangle_\omega$.

(iii) Add the terms from (i) and (ii).

(iv) Repeat the previous steps until only products of expectation values $\langle x(\tau_1)\rangle_\omega = x_{\mathrm{cl}}(\tau_1)$ remain.

With the help of this procedure, the first-order harmonic expectation value $\langle x^4(\tau_1)\rangle_\omega$ is reduced to

$$\langle x^4(\tau_1)\rangle_\omega = x_{\mathrm{cl}}(\tau_1)\,\langle x^3(\tau_1)\rangle_\omega + 3\,G^{(\mathrm{D})}(\tau_1,\tau_1)\langle\, x^2(\tau_1)\rangle_\omega\,. \tag{3.11}$$

Furthermore, we find

$$\langle x^3(\tau_1)\rangle_\omega = x_{\mathrm{cl}}(\tau_1)\langle x^2(\tau_1)\rangle_\omega + 2G^{(\mathrm{D})}(\tau_1,\tau_1)\,x_{\mathrm{cl}}(\tau_1)\,, \tag{3.12}$$

and

$$\langle x^2(\tau_1)\rangle_\omega = x_{\mathrm{cl}}^2(\tau_1) + G^{(\mathrm{D})}(\tau_1,\tau_1)\,. \tag{3.13}$$

Combining equations (3.11)–(3.13) we obtain in first order

$$\langle x^4(\tau_1)\rangle_\omega = x_{\mathrm{cl}}^4(\tau_1) + 6\,x_{\mathrm{cl}}^2(\tau_1)\,G^{(\mathrm{D})}(\tau_1,\tau_1) + 3\,G^{(\mathrm{D})^2}(\tau_1,\tau_1)\,. \tag{3.14}$$

The second order harmonic expectation value requires considerably more effort and finally leads to

$$\begin{aligned}\langle x^4(\tau_1)\,x^4(\tau_2)\rangle_\omega &= x_{\rm cl}^4(\tau_1)\,x_{\rm cl}^4(\tau_2) + 16\,x_{\rm cl}^3(\tau_1)\,G^{(\rm D)}(\tau_1,\tau_2)\,x_{\rm cl}^3(\tau_2)\\ &+ 12\,x_{\rm cl}^2(\tau_1)\,G^{(\rm D)}(\tau_1,\tau_1)\,x_{\rm cl}^4(\tau_2) + 72\,x_{\rm cl}^2(\tau_1)\,G^{(\rm D)^2}(\tau_1,\tau_2)\,x_{\rm cl}^2(\tau_2)\\ &+ 36\,x_{\rm cl}^2(\tau_1)\,G^{(\rm D)}(\tau_1,\tau_1)\,G^{(\rm D)}(\tau_2,\tau_2)\,x_{\rm cl}^2(\tau_2) + 96\,x_{\rm cl}^3(\tau_1)\,G^{(\rm D)}(\tau_1,\tau_2)\,G^{(\rm D)}(\tau_2,\tau_2)\,x_{\rm cl}(\tau_2)\\ &+ 6\,G^{(\rm D)^2}(\tau_1,\tau_1)\,x_{\rm cl}^4(\tau_2) + 96\,x_{\rm cl}(\tau_1)\,G^{(\rm D)^3}(\tau_1,\tau_2)\,x_{\rm cl}(\tau_2)\\ &+ 144\,x_{\rm cl}(\tau_1)\,G^{(\rm D)}(\tau_1,\tau_1)\,G^{(\rm D)}(\tau_1,\tau_2)\,G^{(\rm D)}(\tau_2,\tau_2)\,x_{\rm cl}(\tau_2) + 9\,G^{(\rm D)^2}(\tau_1,\tau_1)\,G^{(\rm D)^2}(\tau_2,\tau_2)\\ &+ 36\,G^{(\rm D)^2}(\tau_1,\tau_1)\,x_{\rm cl}^2(\tau_2)\,G^{(\rm D)}(\tau_2,\tau_2) + 144\,x_{\rm cl}^2(\tau_1)\,G^{(\rm D)^2}(\tau_1,\tau_2)\,G^{(\rm D)}(\tau_2,\tau_2)\\ &+ 72\,G^{(\rm D)}(\tau_1,\tau_1)\,G^{(\rm D)^2}(\tau_1,\tau_2)\,G^{(\rm D)}(\tau_2,\tau_2) + 24\,G^{(\rm D)^4}(\tau_1,\tau_2)\,. \end{aligned} \tag{3.15}$$

3.3 Feynman Diagrams

These contractions can be illustrated by Feynman diagrams with the following rules: A vertex represents the integration over τ

(3.16)

a line denotes the Dirichlet Green's function

(3.17)

and a cross or a "current" pictures a classical path

(3.18)

Inserting the harmonic expectation values (3.14) and (3.15) into the perturbation expansion (3.3) leads in first order to the diagrams

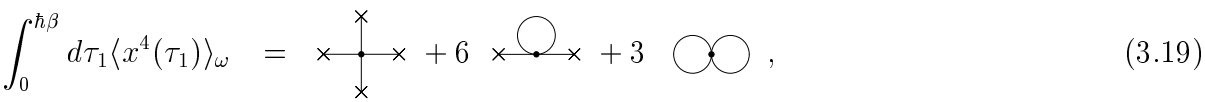

(3.19)

whereas the second-order terms are

$$\int_0^{\hbar\beta} d\tau_1 \int_0^{\hbar\beta} d\tau_2 \left\langle x^4(\tau_1)\, x^4(\tau_2)\right\rangle_\omega \quad =$$

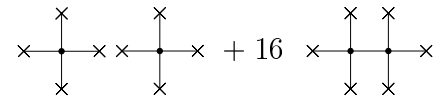

$$+ 16$$

$$+ 12$$

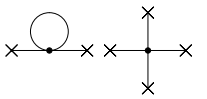

$$+ 72$$

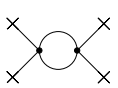

$$+ 36$$

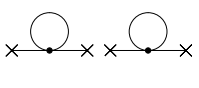

$$+ 96$$

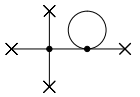

$$+ 6$$

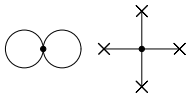

$$+ 96$$

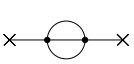

$$+ 144$$

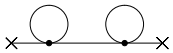

$$+ 36$$

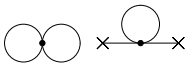

$$+ 144$$

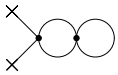

$$+ 72$$

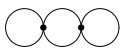

$$+ 24$$

$$+ 9$$

$$. \tag{3.20}$$

We now want to evaluate the first-order Feynman diagrams in (3.19) for finite temperatures and arbitrary x_a, x_b. Thus we will get a first-order result for the imaginary-time evolution amplitude in (3.3):

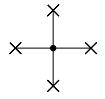

$$\begin{aligned}
&= \int_0^{\hbar\beta} d\tau x_{\mathrm{cl}}^4(\tau) \\
&= \frac{1}{\sinh^4 \hbar\beta\omega} \int_0^{\hbar\beta} d\tau \left[x_a \sinh(\hbar\beta - \tau)\omega + x_b \sinh \hbar\beta\omega\right]^4 \\
&= \frac{1}{32\omega \sinh^4 \hbar\beta\omega} \left[(x_a^4 + x_b^4)\left(\sinh 4\hbar\beta\omega - 8\sinh 2\hbar\beta\omega + 12\hbar\beta\omega\right)\right. \\
&\quad + (x_a^3 x_b + x_a x_b^3)\left(4\sinh 3\hbar\beta\omega + 36\sinh \hbar\beta\omega - 48\hbar\beta\omega\cosh \hbar\beta\omega\right) \\
&\quad \left. + x_a^2 x_b^2\left(-36\sinh 2\hbar\beta\omega + 48\hbar\beta\omega + 24\hbar\beta\omega\cosh 2\hbar\beta\omega\right)\right] .
\end{aligned} \tag{3.21}$$

The second diagram reduces to

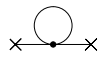

$$\begin{aligned}
&= \int_0^{\hbar\beta} d\tau x_{\mathrm{cl}}^2(\tau) G^{(\mathrm{D})}(\tau,\tau) \\
&= \frac{\hbar}{2M\omega \sinh^3 \hbar\beta\omega} \int_0^{\hbar\beta} d\tau \left[x_a \sinh(\hbar\beta - \tau)\omega + x_b \sinh \omega\tau\right]^2 \\
&\quad \left[\cosh \hbar\beta\omega - \cosh(\hbar\beta - 2\tau)\omega\right] \\
&= \frac{\hbar}{32M\omega^2 \sinh^3 \hbar\beta\omega} \left[(x_a^2 + x_b^2)\left(\sinh 3\hbar\beta\omega + 9\sinh \hbar\beta\omega - 12\hbar\beta\omega\cosh \hbar\beta\omega\right)\right. \\
&\quad \left. + x_a x_b\left(-12\sinh 2\hbar\beta\omega + 16\hbar\beta\omega + 8\hbar\beta\omega\cosh 2\hbar\beta\omega\right)\right] ,
\end{aligned} \tag{3.22}$$

whereas the last diagram turns out to be

$$\begin{aligned} &= \int_0^{\hbar\beta} d\tau G^{(\mathrm{D})^2}(\tau,\tau) \\ &= \frac{\hbar^2}{4M^2\omega^2\sinh^2\hbar\beta\omega}\int_0^{\hbar\beta} d\tau\,[\cosh\hbar\beta\omega-\cosh(\hbar\beta-2\tau)\omega]^2 \\ &= \frac{\hbar^2}{16M^2\omega^3\sinh^2\hbar\beta\omega}\left(-3\sinh 2\hbar\beta\omega+4\hbar\beta\omega+2\hbar\beta\omega\cosh 2\hbar\beta\omega\right). \end{aligned} \tag{3.23}$$

So all in all we get for the imaginary-time evolution amplitude

$$\begin{aligned} &(x_b\,\hbar\beta|x_a\,0) = (x_b\,\hbar\beta|x_a\,0)_\omega \\ &\times\left(1-\frac{g}{\hbar}\left\{\frac{\hbar^2}{M^2\omega^3\sinh^2\hbar\beta\omega}\left[-\frac{9}{16}\sinh 2\hbar\beta\omega+\frac{3}{4}\hbar\beta\omega+\frac{3}{8}\hbar\beta\omega\cosh 2\hbar\beta\omega\right]\right.\right. \\ &+\frac{\hbar}{M\omega^2\sinh^3\hbar\beta\omega}\left[(x_a^2+x_b^2)\left(\frac{3}{16}\sinh 3\hbar\beta\omega+\frac{27}{16}\sinh\hbar\beta\omega-\frac{9}{4}\hbar\beta\omega\cosh\hbar\beta\omega\right)\right. \\ &\left.+x_a x_b\left(-\frac{9}{4}\sinh 2\hbar\beta\omega+3\hbar\beta\omega+\frac{3}{2}\hbar\beta\omega\cosh 2\hbar\beta\omega\right)\right] \\ &+\frac{1}{\omega\sinh^4\hbar\beta\omega}\left[(x_a^4+x_b^4)\left(\frac{1}{32}\sinh 4\hbar\beta\omega-\frac{1}{4}\sinh 2\hbar\beta\omega+\frac{3}{8}\hbar\beta\omega\right)\right. \\ &+(x_a^3x_b+x_ax_b^3)\left(\frac{1}{8}\sinh 3\hbar\beta\omega+\frac{9}{8}\sinh\hbar\beta\omega-\frac{3}{2}\hbar\beta\omega\cosh\hbar\beta\omega\right) \\ &\left.\left.\left.+x_a^2x_b^2\left(-\frac{9}{8}\sinh 2\hbar\beta\omega+\frac{3}{2}\hbar\beta\omega+\frac{3}{4}\hbar\beta\omega\cosh 2\hbar\beta\omega\right)\right]\right\}+\ldots\right). \end{aligned} \tag{3.24}$$

As expected the imaginary-time evolution amplitude (3.24) has the time reversal behaviour (2.33) discussed in Section 2.3.

3.4 Partial Differential Equation

Consider the Schrödinger equation (2.13) for the real-time evolution amplitude

$$i\hbar\frac{\partial}{\partial t}(x_b\,t|x_a\,0) = -\frac{\hbar^2}{2M}\frac{\partial^2}{\partial x_b^2}(x_b\,t|x_a\,0)+V(x_b)\,(x_b\,t|x_a\,0)\,. \tag{3.25}$$

In order to get a corresponding quantum statistical Schrödinger equation we now have to change from real time to imaginary time, i.e. we have to perform the Wick rotation $t\to -i\tau$, as discussed earlier. Thus the Schrödinger equation (3.25) becomes

$$-\hbar\frac{\partial}{\partial\tau}(x_b\,\tau|x_a\,0) = -\frac{\hbar^2}{2M}\frac{\partial^2}{\partial x_b^2}(x_b\,\tau|x_a\,0)+V(x_b)\,(x_b\,\tau|x_a\,0)\,. \tag{3.26}$$

To solve that equation we need an initial condition. For both the real and the imaginary-time evolution amplitude this condition reads

$$(x_b\,0|x_a\,0) = \delta(x_b - x_a)\,. \tag{3.27}$$

Plugging the anharmonic oscillator potential (3.2) into the Schrödinger equation (3.26) we finally get

$$\left\{-\hbar\frac{\partial}{\partial\tau} + \frac{\hbar^2}{2M}\frac{\partial^2}{\partial x_b^2} - \frac{M}{2}\omega^2 x_b^2 - g x_b^4\right\}(x_b\,\tau|x_a\,0) = 0\,. \tag{3.28}$$

3.5 General Ansatz

Making the ansatz

$$(x_b\,\tau|x_a\,0) = (x_b\,\tau|x_a\,0)_\omega\, F(x_b, x_a, \tau)\,, \tag{3.29}$$

where $(x_b\,\tau|x_a\,0)_\omega$ is the harmonic imaginary-time evolution amplitude (3.8), we conclude from (3.28) a partial differential equation for $F(x_b, x_a, \tau)$:

$$\left\{\frac{\partial}{\partial\tau} - \frac{\hbar}{2M}\frac{\partial^2}{\partial x_b^2} + \omega\frac{x_b\cosh\omega\tau - x_a}{\sinh\omega\tau}\frac{\partial}{\partial x_b} + \frac{g}{\hbar}x_b^4\right\}F(x_b, x_a, \tau) = 0\,. \tag{3.30}$$

In order to solve equation (3.30) we expand at first $F(x_b, x_a, \tau)$ in powers of the coupling strength g:

$$F(x_b, x_a, \tau) = 1 + \sum_{n=1}^{\infty} g^n f^{(n)}(x_b, x_a, \tau)\,. \tag{3.31}$$

From our previous perturbative results we know that the nth order $f^{(n)}(x_b, x_a, \tau)$ can at most contain the powers $4n$ of x_a and x_b, respectively, for the corresponding diagram with the most currents consists of n cross diagrams:

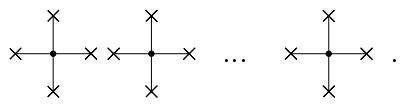

. (3.32)

So when expanding $f^{(n)}(x_b, x_a, \tau)$ in powers of x_b, the sum has to break off at $m = 4n$:

$$f^{(n)}(x_b, x_a, \tau) = \sum_{m=0}^{4n} C_m^{(n)}(x_a, \tau) x_b^m\,. \tag{3.33}$$

Thus our ansatz for $F(x_b, x_a, \tau)$ is a double expansion:

$$F(x_b, x_a, \tau) = 1 + \sum_{n=1}^{\infty}\sum_{m=0}^{4n} g^n\, C_m^{(n)}(x_a, \tau) x_b^m\,. \tag{3.34}$$

The initial condition (3.27) implies that the expansion coefficients $C_m^{(n)}(x_a,\tau)$ must not diverge in the limit $\tau \to 0$:

$$\lim_{\tau\to 0} \left| C_m^{(n)}(x_a,\tau) \right| < \infty \,. \tag{3.35}$$

3.6 First-Order Results

To first order in g the above ansatz (3.34) implies that $F(x_b,x_a,\tau)$ reads

$$\begin{aligned} F^{(1)}(x_b,x_a,\tau) &= 1 + g\left\{ C_0^{(1)}(x_a,\tau) + C_1^{(1)}(x_a,\tau)\, x_b + C_2^{(1)}(x_a,\tau)\, x_b^2 \right. \\ &\quad \left. + C_3^{(1)}(x_a,\tau)\, x_b^3 + C_4^{(1)}(x_a,\tau)\, x_b^4 \right\} . \end{aligned} \tag{3.36}$$

Inserting this into the partial differential equation (3.30) we get five recursive ordinary differential equations for the first-order coefficients $C_m^{(1)}(x_a,\tau)$ $(m = 0,...,4)$:

$$\frac{\partial C_4^{(1)}(x_a,\tau)}{\partial\tau} + 4\omega \coth\omega\tau\, C_4^{(1)}(x_a,\tau) = -\frac{1}{\hbar}\,, \tag{3.37}$$

$$\frac{\partial C_3^{(1)}(x_a,\tau)}{\partial\tau} + 3\omega \coth\omega\tau\, C_3^{(1)}(x_a,\tau) = \frac{4\omega x_a}{\sinh\omega\tau}\, C_4^{(1)}(x_a,\tau)\,, \tag{3.38}$$

$$\frac{\partial C_2^{(1)}(x_a,\tau)}{\partial\tau} + 2\omega \coth\omega\tau\, C_2^{(1)}(x_a,\tau) = \frac{6\hbar}{M}\, C_4^{(1)}(x_a,\tau) + \frac{3\omega x_a}{\sinh\omega\tau}\, C_3^{(1)}(x_a,\tau)\,, \tag{3.39}$$

$$\frac{\partial C_1^{(1)}(x_a,\tau)}{\partial\tau} + \omega \coth\omega\tau\, C_1^{(1)}(x_a,\tau) = \frac{3\hbar}{M}\, C_3^{(1)}(x_a,\tau) + \frac{2\omega x_a}{\sinh\omega\tau}\, C_2^{(1)}(x_a,\tau)\,, \tag{3.40}$$

$$\frac{\partial C_0^{(1)}(x_a,\tau)}{\partial\tau} = \frac{\hbar}{M}\, C_2^{(1)}(x_a,\tau) + \frac{\omega x_a}{\sinh\omega\tau}\, C_1^{(1)}(x_a,\tau)\,. \tag{3.41}$$

These equations are easy to solve by finding solutions to both the homogeneous set of equations and the inhomogeneous ones. We can give these equations an easier shape by making the following transformation:

$$C_m^{(1)}(x_a,\tau) = \frac{c_m^{(1)}(x_a,\tau)}{\sinh^m\omega\tau}\,, \tag{3.42}$$

where m runs from 0 to 4. Thus the five equations (3.37)–(3.41) become

$$\frac{\partial c_4^{(1)}(x_a,\tau)}{\partial\tau} = -\frac{1}{\hbar}\sinh^4\omega\tau\,, \tag{3.43}$$

$$\frac{\partial c_3^{(1)}(x_a,\tau)}{\partial\tau} = \frac{4\omega x_a}{\sinh^2\omega\tau}\,c_4^{(1)}(x_a,\tau)\,, \tag{3.44}$$

$$\frac{\partial c_2^{(1)}(x_a,\tau)}{\partial\tau} = \frac{3\omega x_a}{\sinh^2\omega\tau}\,c_3^{(1)}(x_a,\tau) + \frac{6\hbar}{M\sinh^2\omega\tau}\,c_4^{(1)}(x_a,\tau)\,, \tag{3.45}$$

$$\frac{\partial c_1^{(1)}(x_a,\tau)}{\partial\tau} = \frac{2\omega x_a}{\sinh^2\omega\tau}\,c_2^{(1)}(x_a,\tau)\frac{3\hbar}{M\sinh^2\omega\tau}\,c_3^{(1)}(x_a,\tau)\,, \tag{3.46}$$

$$\frac{\partial c_0^{(1)}(x_a,\tau)}{\partial\tau} = \frac{\omega x_a}{\sinh^2\omega\tau}\,c_1^{(1)}(x_a,\tau) + \frac{\hbar}{M\sinh^2\omega\tau}\,c_2^{(1)}(x_a,\tau)\,. \tag{3.47}$$

These new equations can easily be solved by direct integration. First we get from (3.43)

$$c_4^{(1)}(x_a,\tau) = -\frac{1}{\hbar}\int d\tau\sinh^4\omega\tau + d_4^{(1)}\,, \tag{3.48}$$

where $d_4^{(1)}$ denotes the integration constant as the integral chooses any stem function. Evaluating the integral and dividing by $\sinh^4\omega\tau$ according to equation (3.42) we find

$$\begin{aligned} C_4^{(1)}(x_a,\tau) &= \frac{1}{\hbar\omega\sinh^4\omega\tau}\left\{-\frac{1}{4}\sinh^3\omega\tau\cosh\omega\tau\right. \\ &\quad \left.+\frac{3}{8}\sinh\omega\tau\cosh\omega\tau - \frac{3}{8}\omega\tau + \hbar\omega d_4^{(1)}\right\}\,. \end{aligned} \tag{3.49}$$

Investigating the behaviour of this coefficient for $\tau\to 0$ we see that the constraint (3.35) fixes the integration constant $d_4^{(1)}$ to zero, so we obtain

$$C_4^{(1)}(x_a,\tau) = \frac{1}{\hbar\omega\sinh^4\omega\tau}\left\{-\frac{1}{32}\sinh 4\omega\tau + \frac{1}{4}\sinh 2\omega\tau - \frac{3}{8}\omega\tau\right\}\,. \tag{3.50}$$

Integrating the second differential equation (3.44) we get

$$\begin{aligned} c_3^{(1)}(x_a,\tau) &= 4\omega x_a\int d\tau\frac{c_4^{(1)}(x_a,\tau)}{\sinh^2\omega\tau} + d_3^{(1)} \\ &= \frac{4x_a}{\hbar}\int d\tau\left\{-\frac{1}{4}\sinh\omega\tau\cosh\omega\tau + \frac{3}{8}\coth\omega\tau - \frac{3}{8}\frac{\omega\tau}{\sinh^2\omega\tau}\right\} + d_3^{(1)} \\ &= \frac{x_a}{\hbar\omega}\left\{-\frac{1}{2}\sinh^2\omega\tau + \frac{3}{2}\omega\tau\coth\omega\tau\right\} + d_3^{(1)}\,. \end{aligned} \tag{3.51}$$

Dividing by $\sinh^3\omega\tau$ we derive from (3.42):

$$C_3^{(1)}(x_a,\tau) = \frac{x_a}{\hbar\omega\sinh^3\omega\tau}\left\{-\frac{1}{2}\sinh^2\omega\tau + \frac{3}{2}\omega\tau\coth\omega\tau + \frac{\hbar\omega d_3^{(1)}}{x_a}\right\}\,. \tag{3.52}$$

Taking the limit $\tau \to 0$ we see that the constraint (3.35) leads to

$$d_3^{(1)} = -\frac{3x_a}{2\hbar\omega}\,, \tag{3.53}$$

otherwise $C_3^{(1)}(x_a,\tau)$ would diverge for $\tau \to 0$. Thus from (3.52) and from (3.53) we obtain:

$$C_3^{(1)}(x_a,\tau) = \frac{x_a}{\hbar\omega\sinh^4\omega\tau}\left\{-\frac{1}{8}\sinh 3\omega\tau - \frac{9}{8}\sinh\omega\tau + \frac{3}{2}\omega\tau\cosh\omega\tau\right\}\,. \tag{3.54}$$

The same procedure is now applied to determine $c_2^{(1)}(x_a,\tau)$ and $C_2^{(1)}(x_a,\tau)$, respectively. It is a straightforward calculation which yields

$$\begin{aligned} C_2^{(1)}(x_a,\tau) &= \frac{1}{M\omega^2\sinh^3\omega\tau}\left\{-\frac{3}{16}\sinh 3\omega\tau - \frac{27}{16}\sinh\omega\tau + \frac{9}{4}\omega\tau\cosh\omega\tau\right\} \\ &\quad + \frac{x_a^2}{\hbar\omega\sinh^4\omega\tau}\left\{\frac{9}{8}\sinh 2\omega\tau - \frac{3}{2}\omega\tau - \frac{3}{4}\omega\tau\cosh 2\omega\tau\right\}\,. \end{aligned} \tag{3.55}$$

Correspondingly, the coefficient $C_1^{(1)}(x_a,\tau)$ reads

$$\begin{aligned} C_1^{(1)}(x_a,\tau) &= \frac{x_a}{M\omega^2\sinh^3\omega\tau}\left\{\frac{9}{4}\sinh 2\omega\tau - 3\omega\tau - \frac{3}{2}\omega\tau\cosh 2\omega\tau\right\} \\ &\quad + \frac{x_a^3}{\hbar\omega\sinh^4\omega\tau}\left\{-\frac{1}{8}\sinh 3\omega\tau - \frac{9}{8}\sinh\omega\tau + \frac{3}{2}\omega\tau\cosh\omega\tau\right\}\,. \end{aligned} \tag{3.56}$$

Finally we determine the last coefficient $C_0^{(1)}(x_a,\tau)$ to be

$$\begin{aligned} C_0^{(1)}(x_a,\tau) &= \frac{\hbar}{M^2\omega^3\sinh^2\omega\tau}\left\{\frac{9}{16}\sinh 2\omega\tau - \frac{3}{4}\omega\tau - \frac{3}{8}\omega\tau\cosh 2\omega\tau\right\} \\ &\quad + \frac{x_a^2}{M\omega^2\sinh^3\omega\tau}\left\{-\frac{3}{16}\sinh 3\omega\tau - \frac{27}{16}\sinh\omega\tau + \frac{9}{4}\omega\tau\cosh\omega\tau\right\} \\ &\quad + \frac{x_a^4}{\hbar\omega\sinh^4\omega\tau}\left\{-\frac{1}{32}\sinh 4\omega\tau + \frac{1}{4}\sinh 2\omega\tau - \frac{3}{8}\omega\tau\right\}\,. \end{aligned} \tag{3.57}$$

After having evaluated the integrals, we insert them into (3.36) and obtain a first-order perturbation expansion for the imaginary-time evolution amplitude (3.29). The result is seen to fully coincide with the earlier result (3.24) obtained from evaluating Feynman diagrams in the case that $\tau = \hbar\beta$.

3.7 Higher Orders

We now change our ansatz (3.34) for $F(x_b,x_a,\tau)$ slightly by introducing a third expansion in powers of x_a. Thus the expressions for the coefficients become smaller. Also we take out

the factor $\sinh^{-l}\omega\tau$ right from the beginning such that the ordinary differential equations for the expansion coefficients are simplified:

$$F(x_b, x_a, \tau) = \sum_{n=0}^{\infty}\sum_{k=0}^{2n}\sum_{l=0}^{2k} g^n \frac{c^{(n)}_{2k|l}(\tau)}{\sinh^l \omega\tau} x_a^{2k-l} x_b^l \,. \tag{3.58}$$

In order to obtain the unperturbed result $F(x_b, x_a, \tau) = 1$ for $g = 0$ we then need $c^{(0)}_{0|0}(\tau) = 1$. The superscript n in equation (3.58) still denotes the perturbative order, whereas $2k$ counts the (even) powers of the various products $x_a^i x_b^j$ and l can be identified with the index m in (3.34). Due to the time reversal behaviour (2.33), the coefficients $c^{(n)}_{2k|l}(\tau)$ show a symmetry, namely:

$$\frac{c^{(n)}_{2k|l}(\tau)}{\sinh^l \omega\tau} = \frac{c^{(n)}_{2k|2k-l}(\tau)}{\sinh^{2k-l} \omega\tau} \,. \tag{3.59}$$

Inserting the new ansatz (3.58) into the Schrödinger equation (3.30) we obtain:

$$\begin{aligned}
&\sum_{n=0}^{\infty}\sum_{k=0}^{2n}\sum_{l=0}^{2k} \left[-\omega l \coth\omega\tau c^{(n)}_{2k|l}(\tau) + \frac{\partial c^{(n)}_{2k|l}(\tau)}{\partial\tau} \right] g^n \frac{x_a^{2k-l} x_b^l}{\sinh^l \omega\tau} \qquad (3.60)\\
&- \frac{\hbar}{2M} \sum_{n=0}^{\infty}\sum_{k=0}^{2n}\sum_{l=2}^{2k} l(l-1) g^n \frac{c^{(n)}_{2k|l}(\tau)}{\sinh^l \omega\tau} x_a^{2k-l} x_b^{l-2} + \omega\coth\omega\tau \sum_{n=0}^{\infty}\sum_{k=0}^{2n}\sum_{l=1}^{2k} l g^n \frac{c^{(n)}_{2k|l}(\tau)}{\sinh^l \omega\tau} x_a^{2k-l} x_b^l\\
&- \frac{\omega}{\sinh\omega\tau} \sum_{n=0}^{\infty}\sum_{k=0}^{2n}\sum_{l=1}^{2k} l g^n \frac{c^{(n)}_{2k|l}(\tau)}{\sinh^l \omega\tau} x_a^{2k-l+1} x_b^{l-1} + \frac{1}{\hbar} \sum_{n=0}^{\infty}\sum_{k=0}^{2n}\sum_{l=0}^{2k} g^{n+1} \frac{c^{(n)}_{2k|l}(\tau)}{\sinh^l \omega\tau} x_a^{2k-l} x_b^{l+4} = 0 \,.
\end{aligned}$$

Note that the two terms containing $\coth\omega\tau$ cancel due to our choice of the $c^{(n)}_{2k|l}(\tau)$. Arranging the indices in such a way that each term is proportional to $x_a^{2k-l} x_b^l$ we get for the different powers of g and for $n > 0$:

$$\begin{aligned}
&\sum_{k=0}^{2n}\sum_{l=0}^{2k} \frac{x_a^{2k-l} x_b^l}{\sinh^l \omega\tau} \frac{\partial c^{(n)}_{2k|l}(\tau)}{\partial\tau} - \frac{\hbar}{2M} \sum_{k=-1}^{2n-1}\sum_{l=-2}^{2k-2} (l+2)(l+1) \frac{c^{(n)}_{2k+2|l+2}(\tau)}{\sinh^{l+2} \omega\tau} x_a^{2k-l} x_b^l\\
&\quad - \omega \sum_{k=0}^{2n}\sum_{l=-1}^{2k-1} (l+1) \frac{c^{(n)}_{2k|l+1}(\tau)}{\sinh^{l+2} \omega\tau} x_a^{2k-l} x_b^l + \frac{1}{\hbar} \sum_{k=2}^{2n}\sum_{l=4}^{2k+4} \frac{c^{(n-1)}_{2k-4|l-4}(\tau)}{\sinh^{l-4} \omega\tau} x_a^{2k-l} x_b^l = 0 \,.
\end{aligned} \tag{3.61}$$

Thus the sums over k and over l collapse and we determine the master equation for our coefficients $c^{(n)}_{2k|l}(\tau)$:

$$\begin{aligned}
\frac{\partial c^{(n)}_{2k|l}(\tau)}{\partial\tau} &= (l+2)(l+1)\frac{\hbar}{2M} \frac{c^{(n)}_{2k+2|l+2}(\tau)}{\sinh^2 \omega\tau} + (l+1)\omega \frac{c^{(n)}_{2k|l+1}(\tau)}{\sinh^2 \omega\tau}\\
&\quad - \frac{1}{\hbar} c^{(n-1)}_{2k-4|l-4}(\tau) \sinh^4 \omega\tau \,,
\end{aligned} \tag{3.62}$$

which is solved by

$$\begin{aligned} c^{(n)}_{2k|l}(\tau) &= (l+2)(l+1)\frac{\hbar}{2M}\int d\tau \frac{c^{(n)}_{2k+2|l+2}(\tau)}{\sinh^2\omega\tau} + (l+1)\omega\int d\tau \frac{c^{(n)}_{2k|l+1}(\tau)}{\sinh^2\omega\tau} \\ &\quad -\frac{1}{\hbar}\int d\tau c^{(n-1)}_{2k-4|l-4}(\tau)\,\sinh^4\omega\tau + d^{(n)}_{2k|l}\,. \end{aligned} \tag{3.63}$$

Here the $d^{(n)}_{2k|l}$ denote the integration constants which are fixed by applying the initial condition

$$\lim_{\tau\to 0}\left|\frac{c^{(n)}_{2k|l}(\tau)}{\sinh^l\omega\tau}\right| < \infty\,. \tag{3.64}$$

However the above master equation (3.63) is not valid for all k and l. Therefore we now introduce a set of empirical rules telling us which of the coefficients $c^{(n)}_{2k|l}(\tau)$ have to be dropped once we write down (3.63) for any order n:

(i) Drop all terms containing a $c^{(n)}_{2k|l}(\tau)$ where $2k > 4n$.

(ii) Drop all terms containing a $c^{(n)}_{2k|l}(\tau)$ with $l > 2k$.

(iii) Neglect all terms containing a $c^{(n)}_{2k|l}(\tau)$ with any negative indices k and l.

To convince the reader that equation (3.63) together with this procedure leads to the correct results we now reobtain our first-order results from Section 3.6. To that end we set $n = 1$, such that k runs from 0 to 2 and l from 0 to 4. Fixing $k = 2$ and counting down from $l = 4$ to $l = 0$ we get

$$c^{(1)}_{4|4}(\tau) = -\frac{1}{\hbar}\int d\tau c^{(0)}_{0|0}(\tau)\sinh^4\omega\tau + d^{(1)}_{4|4}\,, \tag{3.65}$$

$$c^{(1)}_{4|3}(\tau) = 4\omega\int d\tau\frac{c^{(1)}_{4|4}(\tau)}{\sinh^2\omega\tau} + d^{(1)}_{4|3}\,, \tag{3.66}$$

$$c^{(1)}_{4|2}(\tau) = 3\omega\int d\tau\frac{c^{(1)}_{4|3}(\tau)}{\sinh^2\omega\tau} + d^{(1)}_{4|2}\,, \tag{3.67}$$

$$c^{(1)}_{4|1}(\tau) = 2\omega\int d\tau\frac{c^{(1)}_{4|2}(\tau)}{\sinh^2\omega\tau} + d^{(1)}_{4|1}\,, \tag{3.68}$$

$$c^{(1)}_{4|0}(\tau) = \omega\int d\tau\frac{c^{(1)}_{4|1}(\tau)}{\sinh^2\omega\tau} + d^{(1)}_{4|0}\,. \tag{3.69}$$

Correspondingly, for $k = 1$ we obtain

$$c^{(1)}_{2|2}(\tau) = \frac{6\hbar}{M}\int d\tau \frac{c^{(1)}_{4|4}(\tau)}{\sinh^2 \omega\tau} + d^{(1)}_{2|2}\,, \tag{3.70}$$

$$c^{(1)}_{2|1}(\tau) = \frac{3\hbar}{M}\int d\tau \frac{c^{(1)}_{4|3}(\tau)}{\sinh^2 \omega\tau} + 2\omega\int d\tau \frac{c^{(1)}_{2|2}(\tau)}{\sinh^2(\tau)} + d^{(1)}_{2|1}\,, \tag{3.71}$$

$$c^{(1)}_{2|0}(\tau) = \frac{\hbar}{M}\int d\tau \frac{c^{(1)}_{4|2}(\tau)}{\sinh^2 \omega\tau} + \omega\int d\tau \frac{c^{(1)}_{2|1}(\tau)}{\sinh^2(\tau)} + d^{(1)}_{2|0}\,. \tag{3.72}$$

Finally for $k = 0$ we get the equation

$$c^{(1)}_{0|0}(\tau) = \frac{\hbar}{M}\int d\tau \frac{c^{(1)}_{2|2}(\tau)}{\sinh^2 \omega\tau} + d^{(1)}_{0|0}\,. \tag{3.73}$$

Performing the integrations in equations (3.65)–(3.73) and taking into account the initial condition (3.64), we get exactly the same result as in Section 3.6. The path of recursion which follows from this procedure is shown in Figure 3.1.

3.8 Exploiting the Symmetries — First-Order Results

As seen above we already have to solve nine ordinary differential equations for the first-order imaginary-time evolution amplitude. For any order n the number p of integrals to solve is

$$p = \sum_{j=1}^{2n+1}(2j-1) = 4n^2 + 4n + 1\,. \tag{3.74}$$

Exploiting the symmetry (3.59) we can cut down that number considerably. At first sight it is reduced to

$$p = \sum_{j=1}^{2n+1} j = 2n^2 + 3n + 1\,, \tag{3.75}$$

so there are only six integrals left for the first order. But we can go even further. Employing these symmetries we can eventually change almost all recursive *differential* equations into purely *algebraic* ones leaving only $(2n+1)$ integrations. So for the first order we are left with three integrations only, namely with equations (3.65), (3.70), and (3.73). These coefficients $c^{(1)}_{4|4}(\tau)$, $c^{(1)}_{2|2}(\tau)$, and $c^{(1)}_{0|0}(\tau)$ are integrated recursively. The other coefficients can then be obtained algebraically: Once we have $c^{(1)}_{4|4}(\tau)$ we also know $c^{(1)}_{4|0}(\tau)$ because of the symmetry (3.59). Comparing equation (3.62) for $k = 2, l = 4$ and $k = 2, l = 0$ we then obtain an algebraic equation for $c^{(1)}_{4|1}(\tau)$. The knowledge of $c^{(1)}_{4|1}(\tau)$ gives us $c^{(1)}_{4|3}(\tau)$ because of the

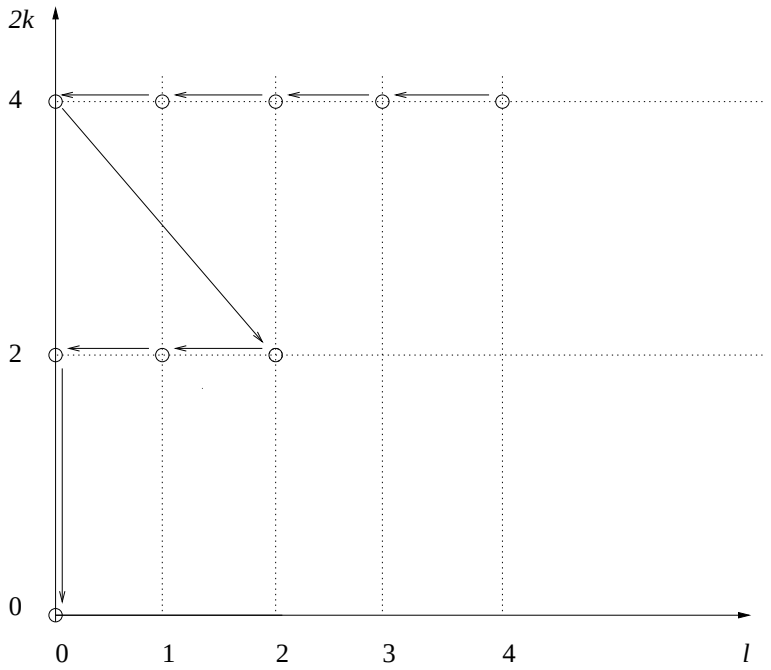

Figure 3.1: This diagram depicts the path of recursion for $n = 1$. We start in the top right hand side corner, which is to be identified with the coefficient $c^{(1)}_{4|4}$ and follow the arrows until reaching the bottom left hand side corner $c^{(1)}_{0|0}$.

symmetry (3.59) and by comparing (3.62) this time for $k = 2, l = 3$ on the one hand and $k = 2, l = 1$ on the other hand we are left with an algebraic equation for $c^{(1)}_{4|2}(\tau)$. Thus we get all the coefficients for $k = 2$ only by solving one differential equation, namely the one for $c^{(1)}_{4|4}(\tau)$. For $k = 1$ the procedure is similar, $k = 0$ only generates one coefficient anyway, namely $c^{(1)}_{0|0}(\tau)$, which still has to be solved by evaluating one integral. The new path of recursion is shown in Figure 3.2.
So finally three out of the nine first-order coefficients are obtained by integration, three more are clear for symmetry reasons and three come from an algebraic recursion.

3.9 Preparing the Algebraic Recursion Relation

We now generalize the algebraic part of our recursion. Consider again the symmetry property (3.59). Differentiation on both sides yields

$$\frac{\partial c^{(n)}_{2k|l}(\tau)}{\partial \tau} = \frac{1}{\sinh^{2k-2l}\omega\tau}\frac{\partial c^{(n)}_{2k|2k-l}(\tau)}{\partial \tau} - 2(k-l)\omega\cosh\omega\tau\frac{c^{(n)}_{2k|2k-l}(\tau)}{\sinh^{2k-2l+1}\omega\tau}\,. \tag{3.76}$$

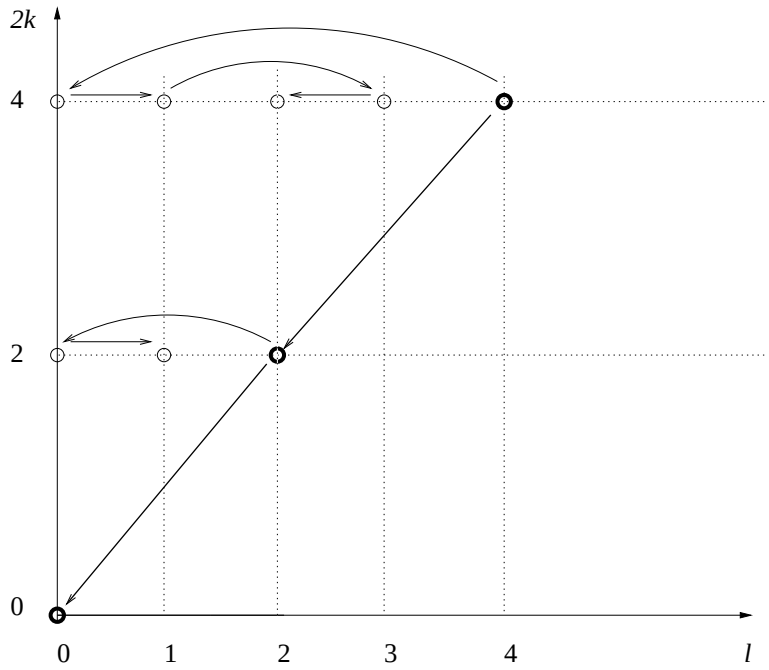

Figure 3.2: This diagram shows which of the first-order coefficients $c^{(1)}_{2k|l}(\tau)$ have to be integrated (bold) and which ones can be obtained by employing *symmetry and algebraic recursions* (light).

Now we substitute for the two partial derivatives according to equation (3.62) which yields

$$
\begin{aligned}
&(l+2)(l+1)\frac{\hbar}{2M}\frac{c^{(n)}_{2k+2|l+2}(\tau)}{\sinh^2\omega\tau}+(l+1)\omega\frac{c^{(n)}_{2k|l+1}(\tau)}{\sinh^2\omega\tau}-\frac{1}{\hbar}c^{(n-1)}_{2k-4|l-4}(\tau)\,\sinh^4\omega\tau\\
&=\frac{1}{\sinh^{2k-2l}\omega\tau}\left[(2k-l+2)(2k-l+1)\frac{\hbar}{2M}\frac{c^{(n)}_{2k+2|2k-l+2}(\tau)}{\sinh^2\omega\tau}+(2k-l+1)\omega\frac{c^{(n)}_{2k|2k-l+1}(\tau)}{\sinh^2\omega\tau}\right.\\
&\left.-\frac{1}{\hbar}c^{(n-1)}_{2k-4|2k-l-4}(\tau)\,\sinh^4\omega\tau\right]-2(k-l)\omega\cosh\omega\tau\frac{c^{(n)}_{2k|2k-l}(\tau)}{\sinh^{2k-2l+1}\omega\tau}\,. \qquad (3.77)
\end{aligned}
$$

Solving for the $(l+1)$-st coefficient and shifting the index l down by one we obtain

$$
\begin{aligned}
c^{(n)}_{2k|l}(\tau) \;=\;& -\frac{(l+1)\hbar}{2M\omega}c^{(n)}_{2k+2|l+1}(\tau)+\frac{c^{(n-1)}_{2k-4|l-5}(\tau)}{\hbar\omega l}\,\sinh^6\omega\tau\\
&+\frac{(2k-l+3)(2k-l+2)\hbar}{2M\omega l}\frac{c^{(n)}_{2k+2|2k-l+3}(\tau)}{\sinh^{2k-2l+2}\omega\tau}+\frac{2k-l+2}{l}\frac{c^{(n)}_{2k|2k-l+2}(\tau)}{\sinh^{2k-2l+2}\omega\tau}\\
&-\frac{1}{\hbar\omega l}\frac{c^{(n-1)}_{2k-4|2k-l-3}(\tau)}{\sinh^{2k-2l-4}\omega\tau}-\frac{(2k-2l+2)\cosh\omega\tau}{l}\frac{c^{(n)}_{2k|2k-l+1}(\tau)}{\sinh^{2k-2l+1}\omega\tau}\,, \qquad (3.78)
\end{aligned}
$$

which is the algebraic recursion relation for any non-diagonal coefficient $c^{(n)}_{2k|l}(\tau)$ with $0 < l \leq k$.[1] The diagonal coefficients $c^{(n)}_{2k|2k}(\tau)$ still have to be integrated.

3.10 Combined Differential and Algebraic Recursion

We now combine the differential recursion with the algebraic one. As only the diagonal coefficients have to be evaluated by integrating the differential recursive equation, we can even further simplify our master equation (3.63). We only need it for the diagonal coefficients, for which $l + 1 = 2k + 1$ is always greater than $2k$. And according to our index rule (ii), coefficients of the shape $c^{(n)}_{2k|2k+1}$ have to be neglected. We get

$$\begin{aligned} c^{(n)}_{2k|2k}(\tau) &= (2k+2)(2k+1)\frac{\hbar}{2M}\int d\tau \frac{c^{(n)}_{2k+2|2k+2}(\tau)}{\sinh^2 \omega\tau} \\ &\quad - \frac{1}{\hbar}\int d\tau c^{(n-1)}_{2k-4|2k-4}(\tau)\,\sinh^4 \omega\tau + d^{(n)}_{2k|2k}\,. \end{aligned} \tag{3.79}$$

Index rules (i) and (iii) still have to be applied, k runs from 0 to $2n$.
Let us quickly summarize the combined differential and algebraic recursion relation considering the first order as an example. Figure 3.2 shows all first-order coefficients for the imaginary time evolution amplitude. Each coefficient is represented by a little circle. Now the coefficients on the diagonal line $2k = l$ have to be obtained by referring to equation (3.79) together with rules (i) and (iii). These two rules tell us which of the coefficients either from the the same order n or from the previous order $n-1$ have to be integrated and which ones can be put to zero.
Once we have the diagonal coefficients $c^{(n)}_{2k|2k}(\tau)$ we can calculate the off-diagonal ones with $l \leq k$ with the help of equation (3.78). The coefficients with $k < l < 2k$ are then clear for symmetry reasons.

3.11 A Maple Programme

We now introduce a `Maple` programme[2] which analytically solves equation (3.79) for the initial condition (3.64), obeying the index rules from Section 3.7 and employing the symmetry (3.59). Thus we minimize the operating expense and obtain most of the coefficients by pure algebraic transformations, namely

$$p_{\text{alg}} = \sum_{j=1}^{2n+1}(2j-1) - (2n+1) = 4n^2 + 2n\,. \tag{3.80}$$

[1] The coefficients with $k < l < 2k$ are then clear for symmetry reasons.
[2] We used `Maple V R5` © and also release `R7`.

The number of coefficients which still has to be integrated is

$$p_{\text{diff}} = 2n + 1\,, \tag{3.81}$$

where of course $p_{\text{alg}} + p_{\text{diff}} = p$ is the total number of coefficients given by (3.74).
We first approach the diagonal coefficients, i.e. the ones which have to be integrated iteratively. The main problem here is the representation of the results, the integration itself is easy, as well as fixing the integration constants.
The algebraically obtained coefficients then have to be seamlessly embedded into this programme as the algebraic recursion also refers to the values of some of the diagonal coefficients. Again the representation of the results is subtle.
The expansion coefficients up to seventh order can be found at [51]. As we aimed at the most general recursion relation for the anharmonic oscillator, a recursion relation for its imaginary-time evolution amplitude, the expressions in [51] became very large. For further applications as e.g. for the evaluation of the free energy, some standard `Maple` commands like the "series"-command sometimes failed. Therefore we had to write our own versions of this command, relying only on the most basic `Maple` scripts.

Part II

Variational Perturbation Theory — Applications

Chapter 4

Variational Perturbation Theory for the Free Energy

In this chapter we obtain perturbative results for the partition function by integrating the diagonal elements of our perturbative expression for the imaginary-time evolution amplitude from the previous chapter. From the partition function we then compute the free energy perturbatively. Then we apply variational perturbation theory to this quantity up to the fifth order which is three orders more than what has been achieved in previous work [18]. By doing so we study in detail the convergence behaviour of the variational resummation.

4.1 Partition Function and Free Energy Revisited

As discussed in Chapter 2 the partition function can be obtained from the imaginary-time evolution amplitude as follows:

$$Z = \int_{-\infty}^{+\infty} dx (x\, \hbar\beta | x\, 0)\,. \tag{4.1}$$

So we just have to substitute $x \equiv x_a = x_b$ into the perturbation expansion for $(x_b\, \hbar\beta | x_a\, 0)$ as obtained with the help of a computer algebra program, introduced in Chapter 3. Then we integrate over x. As the free energy reads

$$F = -\frac{1}{\beta} \log Z\,, \tag{4.2}$$

we then have to expand the logarithm in order to obtain a perturbation expansion for the free energy F. The Taylor series for the logarithm is

$$\log(1+x) = x - \frac{1}{2}x^2 + \frac{1}{3}x^3 - \frac{1}{4}x^4 \pm \ldots\,. \tag{4.3}$$

For the first order we insert (3.24) together with (3.8) into (4.1) and evaluate the integral. By taking the logarithm we get with (4.2) and with (4.3) for the free energy to first order

$$F^{(1)}(\beta) = \frac{1}{\beta} \log 2 \sinh \frac{\hbar\beta\omega}{2} + \frac{3g\hbar^2}{4M^2\omega^2} \coth^2 \frac{\hbar\beta\omega}{2} \,. \tag{4.4}$$

For the second order we follow the same procedure, taking into account the higher-order results from [51] for the coefficients $c^{(n)}_{2k|l}(\tau)$ and plugging them into the ansatz (3.58). We obtain

$$\begin{aligned} F^{(2)}(\beta) &= \frac{1}{\beta} \log 2 \sinh \frac{\hbar\beta\omega}{2} + \frac{3g\hbar^2}{4M^2\omega^2} \coth^2 \frac{\hbar\beta\omega}{2} \\ &\quad - \frac{g^2\hbar^3}{64M^4\omega^5} \frac{54\hbar\beta\omega + 36\hbar\beta\omega\cosh\hbar\beta\omega + 60\sinh\hbar\beta\omega + 21\sinh 2\hbar\beta\omega}{\sinh^4 \frac{\hbar\beta\omega}{2}} \,. \end{aligned} \tag{4.5}$$

The higher orders are omitted for the sake of keeping the type face clear.

4.2 A Diagrammatical Check

It is possible to check the perturbative results for the partition function and the free energy for all temperatures. Namely, we can expand Z in terms of harmonic expectations in a similar way as for the imaginary-time evolution amplitude in (3.3). To that end we need the generating functional

$$Z[j(\tau)] = \int_{-\infty}^{+\infty} dx (x\,\hbar\beta|x\,0)_\omega[j] \tag{4.6}$$

which we get from (3.7)-(3.10). It is of the form

$$Z[j(\tau)] = Z[0] \exp\left[\frac{1}{2\hbar^2} \int_0^{\hbar\beta} d\tau_1 \int_0^{\hbar\beta} d\tau_2 G^{(\mathrm{p})}(\tau_1,\tau_2) j(\tau_1) j(\tau_2)\right] , \tag{4.7}$$

where the harmonic partition function reads

$$Z[0] = \frac{1}{2\sinh\frac{\hbar\beta\omega}{2}} \tag{4.8}$$

and

$$G^{(\mathrm{p})}(\tau_1,\tau_2) = \frac{\hbar}{2M\omega} \frac{\cosh\left(\frac{\hbar\beta\omega}{2} - |\tau_1-\tau_2|\omega\right)}{\sinh\frac{\hbar\beta\omega}{2}} \tag{4.9}$$

denotes the periodic Green's function of the harmonic oscillator. The different properties of the periodic Green's function (4.9) and the Dirichlet-Green's function (3.10) are discussed

in detail in Ref. [49]. We now obtain the partition function Z of the anharmonic oscillator from the generating functional $Z[j(\tau)]$ by differentiating with respect to the current $j(\tau)$ while setting $j(\tau) = 0$ afterwards:

$$Z = \exp\left\{-\frac{1}{\hbar}\int_0^{\hbar\beta} d\tau\, g\left[\frac{\hbar\delta}{\delta j(\tau)}\right]^4\right\} Z[j(\tau)]\Bigg|_{j=0} . \tag{4.10}$$

Thus we get

$$\begin{aligned} Z &= Z[0]\left\{1 - \frac{3g}{\hbar}\int_0^{\hbar\beta} d\tau_1 G^{(\mathrm{p})^2}(\tau_1,\tau_1)\right. \\ &\quad + \frac{g^2}{2\hbar^2}\int_0^{\hbar\beta} d\tau_1 \int_0^{\hbar\beta} d\tau_2 \left[9G^{(\mathrm{p})^2}(\tau_1,\tau_1)G^{(\mathrm{p})^2}(\tau_2,\tau_2)\right. \\ &\quad \left.\left. + 72G^{(\mathrm{p})}(\tau_1,\tau_1)G^{(\mathrm{p})^2}(\tau_1,\tau_2)G^{(\mathrm{p})}(\tau_2,\tau_2) + 24G^{(\mathrm{p})^4}(\tau_1,\tau_2)\right] + ...\right\} . \end{aligned} \tag{4.11}$$

In terms of Feynman diagrams this reads

$$\begin{aligned} Z &= Z[0]\left[1 + \frac{3g}{\hbar}\right. \quad + \frac{g^2}{2\hbar^2}\Big(9 \quad \quad \\ &\quad \left. + 72 \quad + 24 \quad \Big) + ...\right] \\ &= \exp\left[\frac{1}{2} \quad + \frac{3}{\hbar} \quad + \frac{g^2}{2\hbar^2}\Big(72 \quad + 24 \quad \Big) + ...\right] , \end{aligned} \tag{4.12}$$

where we have introduced the symbol

$$\frac{1}{2} \quad \equiv \log Z[0] . \tag{4.13}$$

Once we rewrite the partition function Z in the form of the cumulant expansion as on the right hand side of equation (4.12), the disconnected Feynman diagrams disappear [2]. Now we can easily take the logarithm. Following (4.2) we obtain for the free energy

$$F = -\frac{1}{\beta}\left[\frac{1}{2} \quad + \frac{3g}{\hbar} \quad + \frac{g^2}{2\hbar^2}\Big(72 \quad + 24 \quad \Big) + ...\right] . \tag{4.14}$$

The above Feynman diagrams are of course constructed with the help of the same rules as for the imaginary-time evolution amplitude (3.16), (3.17), and (3.18), but instead of the Dirichlet's Green's function (3.10) we have to use the periodic Green's function (4.9). We now want to evaluate the four diagrams in (4.14) so that we get a second-order expression for the free energy for finite temperatures. According to (4.8) and (4.13) we get for the zeroth-order contribution

$$\frac{1}{2} \quad = \log\left[\frac{1}{2\sinh\frac{\hbar\beta\omega}{2}}\right] , \tag{4.15}$$

whereas the first-order diagram becomes

$$= \int_0^{\hbar\beta} d\tau G^{(\mathrm{p})^2}(\tau,\tau) = \frac{\hbar^3\beta}{4M^2\omega^2}\coth^2\frac{\hbar\beta\omega}{2}\,. \tag{4.16}$$

The integration in (4.16) is trivial, because $G^{(\mathrm{p})}(\tau,\tau)$ does not depend on τ any more according to (4.9). For the second order the integrations become more sophisticated:

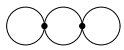

$$\begin{aligned} &= \int_0^{\hbar\beta} d\tau_1 \int_0^{\hbar\beta} d\tau_2 G^{(\mathrm{p})}(\tau_1,\tau_1) G^{(\mathrm{p})^2}(\tau_1,\tau_2) G^{(\mathrm{p})}(\tau_2,\tau_2) \\ &= \frac{\hbar^5\beta\coth^2\frac{\hbar\beta\omega}{2}}{32M^4\omega^5\sinh^2\frac{\hbar\beta\omega}{2}}(\hbar\beta\omega+\sinh\hbar\beta\omega)\,. \end{aligned} \tag{4.17}$$

The other contribution to the second order yields

$$\begin{aligned} &= \int_0^{\hbar\beta} d\tau_1 \int_0^{\hbar\beta} d\tau_2 G^{(\mathrm{p})^4}(\tau_1,\tau_2) \\ &= \frac{\hbar^5\beta}{256M^4\omega^5\sinh^4\frac{\hbar\beta\omega}{2}}(\sinh 2\hbar\beta\omega+8\sinh\hbar\beta\omega+6\hbar\beta\omega)\,. \end{aligned} \tag{4.18}$$

So all in all we get for the free energy (4.14) up to second order in the coupling constant g the result (4.5). It shows the correct low temperature behaviour

$$\lim_{\beta\to\infty} F^{(2)}(\beta) = \frac{\hbar\omega}{2} + \frac{3g\hbar^2}{4M^2\omega^2} - \frac{21g^2\hbar^3}{8M^4\omega^5}\,, \tag{4.19}$$

which can be found for instance in [2].

4.3 Variational Perturbation Theory

Variational perturbation theory[1] is a method that enables us to resum divergent perturbation series in such a way that they converge even in the case that the perturbation couples infinitely strong. To this end we add and subtract a trial harmonic oscillator with trial frequency Ω to our anharmonic oscillator (3.2):

$$V(x) = \frac{M}{2}\Omega^2x^2 + g\frac{M}{2}\frac{\omega^2-\Omega^2}{g}x^2 + gx^4\,. \tag{4.20}$$

Now we treat the second term as if it was of the order of the coupling constant g. The result is obtained most simply by substituting for the frequency ω in the original anharmonic oscillator potential (3.2) according to Kleinert's square-root trick [2]

$$\omega \to \Omega\sqrt{1+gr}\,, \tag{4.21}$$

[1] In Section 4.6 the reader can find the most general description of the substitutions coming along with variational perturbation theory that eventually lead to the strong-coupling results.

where

$$r \equiv \frac{\omega^2 - \Omega^2}{g\Omega^2}\,. \tag{4.22}$$

These substitutions are not the most general ones. The square root is just a special case for the anharmonic oscillator. We will discuss its origin at the end of this chapter in Section 4.6.
We now apply the trick (4.21) to our first-order series representation for the free energy F (4.4). Substituting for the frequency ω according to (4.21), expanding for fixed r up to the first order in g and resubstituting for r according to (4.22) we get

$$F^{(1)}(\beta,\Omega) = -\frac{1}{\beta}\log\frac{1}{2\sinh\frac{\hbar\beta\Omega}{2}} + \frac{3g\hbar^2}{4M^2\Omega^2}\coth^2\frac{\hbar\beta\Omega}{2} + \frac{\hbar\Omega}{4}\left(\frac{\omega^2}{\Omega^2}-1\right)\coth\frac{\hbar\beta\Omega}{2}\,. \tag{4.23}$$

So the free energy (4.23) now depends on the trial frequency Ω which is of no physical relevance. In order to get rid of it, we have to minimize its effect by employing the principle of least sensitivity [48]. This principle suggests to search for local extrema of $F(\beta,\Omega)$ with respect to Ω:[2]

$$\frac{\partial F^{(1)}(\beta,\Omega)}{\partial\Omega} = 0\,. \tag{4.24}$$

For the first order $F^{(1)}(\beta,\Omega)$ it turns out that there are several extrema for each β. As we seek a curve $\Omega^{(1)}(\beta)$ that is as smooth as possible the choice is easy — we take the lowest branch for the others are not bounded (see Figure 4.1). Moreover the other branches lead to diverging results.
To second order, we proceed in a similar way and we find that there are no extrema at all for $F^{(2)}(\beta,\Omega)$. In accordance with the principle of least sensitivity we look for inflection points instead, i.e. we look for solutions to the equation

$$\frac{\partial^2 F^{(2)}(\beta,\Omega)}{\partial\Omega^2} = 0\,. \tag{4.25}$$

In general we try to solve the equation

$$\frac{\partial^n F^{(N)}(\beta,\Omega)}{\partial\Omega^n} = 0 \tag{4.26}$$

for the smallest possible n. Plugging $\Omega^{(N)}(\beta)$ into $F^{(N)}(\beta,\Omega)$, we finally get back a resummed expression for the physical quantity $F(\beta)$. The results for the first three orders are given in Figure 4.2. In order to check our results we have to compare them to the numerically evaluated free energy $F^{(N)}_{\text{num}}(\beta)$ which is discussed in the upcoming section.

[2] Actually P. M. Stevenson restricted this principle to minima of the variational parameter. H. Kleinert suggested to minimize its influence by taking into account extrema, inflection points, and higher derivatives.

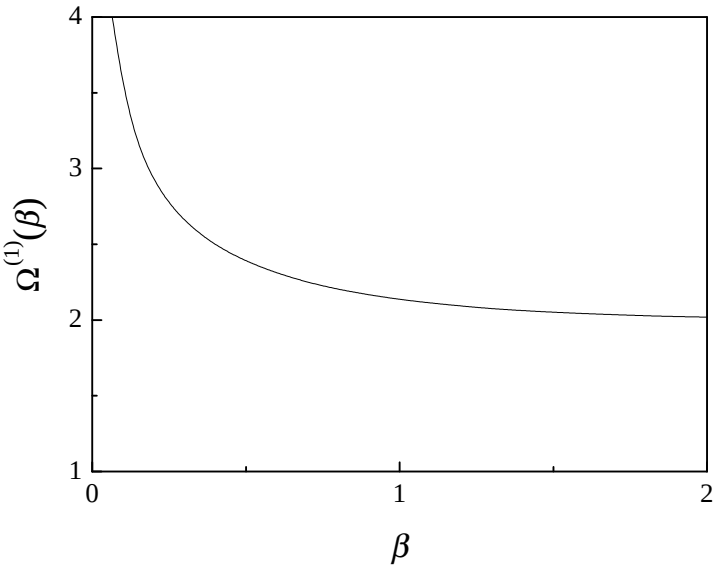

Figure 4.1: Branch of the variational parameter $\Omega^{(1)}(\beta)$ which we chose. The coupling strength is $g = 1$. Other branches not shown in this figure lead to highly diverging results. Throughout this chapter all results are presented in natural units $\hbar = M = k_{\rm B} \equiv 1$ and, additionally, we have set $\omega \equiv 1$.

4.4 Checking Our Results

The spectral representation of the partition function reads

$$Z = \sum_{n=0}^{\infty} e^{-\beta E_n} \,, \tag{4.27}$$

where the E_n are the energy eigenvalues. Let us define the numerical approximants

$$Z_{\rm num}^{(N)} = \sum_{n=0}^{N} e^{-\beta E_n} \tag{4.28}$$

and

$$F_{\rm num}^{(N)} = -\frac{1}{\beta} \log Z^{(N)} \,, \tag{4.29}$$

respectively. One possibility to obtain numerical results for the eigenvalues E_n is provided for by the so called "shooting method". We integrate the Schrödinger equation numerically for the potential (3.2) and for a particular value of the coupling strength g. If the energy E which we plug into the program does not coincide with one of the energy eigenvalues E_n, the solution to the Schrödinger equation explodes already for relatively small values of the coordinate x. If the energy eigenvalue is close to the exact answer, we have $|\Psi(x)| < \infty$ also

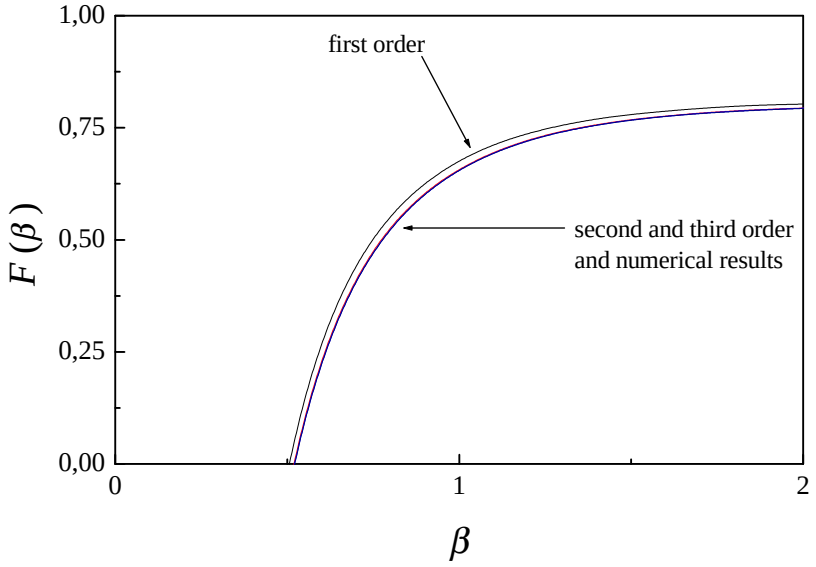

Figure 4.2: Free energy of the anharmonic oscillator up to third order for intermediate coupling $g = 1$. The black line represents the exact result $F^{(9)}_{\text{num}}(\beta)$, obtained by approximating the partition function (4.28) with the help of the first ten energy eigenvalues. The other lines are variational perturbative results: The blue line shows the first order, the red line shows the second order, and the navy blue line represents the third order. Note that the second and third order are hardly distinguishable from the exact results. Higher orders for special values of the inverse temperature β can be found in Figure 4.5.

n	E_n	n	E_n
0	0.8037701932	5	14.203064494
1	2.7378891484	6	17.633934116
2	5.1792814619	7	21.236268598
3	7.9423804544	8	24.994705012
4	10.963538555	9	28.896941521

Table 4.1: The first ten energy eigenvalues E_n of the anharmonic oscillator for intermediate coupling $g = 1$. They were obtained by numerically integrating the Schrödinger equation with the initial condition that $\Psi(0) = 1$, $\Psi'(0) = 0$, and $|\Psi(x)| < \infty$ for large x.

for larger values of x. This method yields the unnormalized eigenfunctions (the wave functions which still have to be normalized) and the energy eigenvalues to very high accuracy. Renormalization is necessary, for the computer algebra program[3] needs an initial value $\Psi(0)$ which we set to one. Plugging the first ten numeric energy eigenvalues into equation (4.28) and evaluating (4.29) up to $N = 9$, we obtain a function $F^{(N)}_{\text{num}}(\beta)$. So let us first check how fast the numerically obtained free energy $F^{(N)}_{\text{num}}(\beta)$ from (4.29) converges. To that end we set $g = 1$ and we plot $F^{(N)}_{\text{num}}(\beta)$ for N from 0 to 9 in Figure 4.3 on the interval $[0, 2]$. As one

[3]This time we used `Mathematica` 3.1 ©.

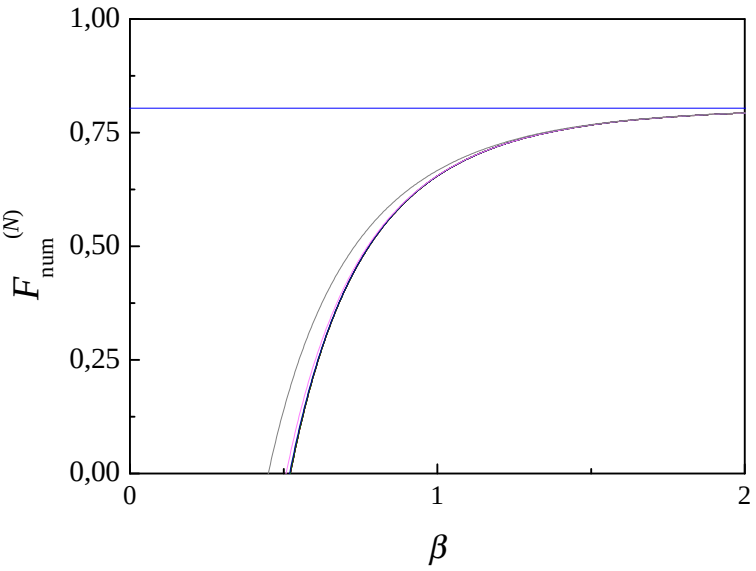

Figure 4.3: Convergence of the spectral representation of the partition function (4.27). This figure shows the approximants of the free energy $F_{\mathrm{num}}^{(N)}(\beta)$ from (4.29) for the first ten orders. One can see that the low temperature behaviour is correct even for the roughest approximant $F_{\mathrm{num}}^{(0)}(\beta)$ (blue line). All the curves converge to the ground state energy E_0. For high temperatures more and more energy eigenvalues have to be taken into account to get realistic results. Alternatively one can compare the results with the classical expressions (4.31) (see also Figure 4.4). The colour code is: $N = 1$: blue, $N = 2$: gray, $N = 3$: violet, $N = 4$: navy, $N = 5$: olive, $N = 6$: whine, $N = 7$: light blue, $N = 8$: orange, $N = 9$: black.

can see $F_{\mathrm{num}}^{(N)}(\beta)$ converges rapidly. For low temperatures T, corresponding to high values of β, even the roughest approximant $F_{\mathrm{num}}^{(0)}(\beta)$ reproduces the correct curve. This should not surprise us as we know that $\lim_{\beta\to\infty} F^{(0)}(\beta) = E_0$. It turns out that the first ten energy eigenvalues E_n are sufficient. So we can probe our perturbative results by comparison to $F_{\mathrm{num}}^{(9)}(\beta)$.
For high temperatures we have another cross check for our results. High temperatures correspond to classical statistical distributions such that we can evaluate the partition function (2.66) according to

$$Z_{\mathrm{cl}} = \int_{-\infty}^{+\infty} \frac{dx}{\lambda_{\mathrm{th}}} \exp\left[-\beta V(x)\right] , \tag{4.30}$$

with the potential (3.2) and $\lambda_{\mathrm{th}} = \sqrt{2\pi\hbar^2/Mk_{\mathrm{B}}T}$. This integral can be solved according to [52]:

$$Z_{\mathrm{cl}} = \frac{1}{2\lambda_{\mathrm{th}}}\sqrt{\frac{M\omega^2}{2g}} \exp\left(\frac{\beta M^2\omega^4}{32g}\right) K_{1/4}\left(\frac{\beta M^2\omega^4}{32g}\right) , \tag{4.31}$$

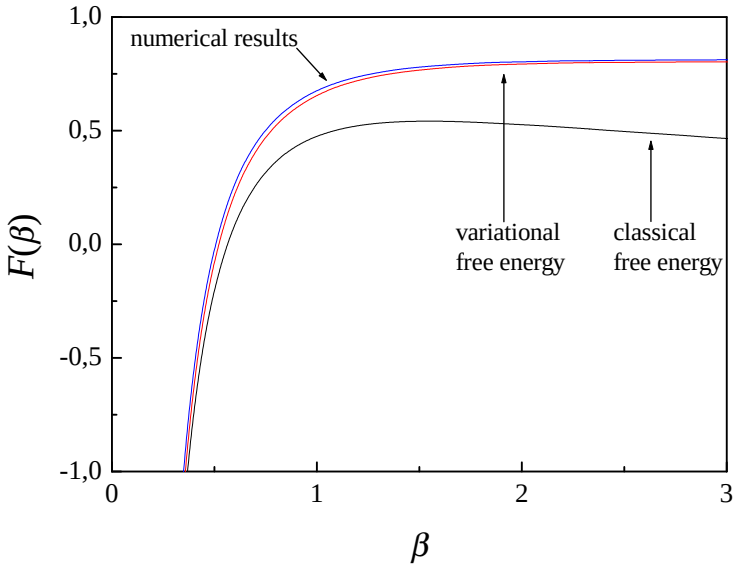

Figure 4.4: Third-order variational perturbative results for the free energy, $F^{(3)}(\beta)$ (red line). The blue line represents the numerical free energy $F^{(9)}_{\mathrm{num}}(\beta)$, whereas the black line shows the classical free energy. For small values of the inverse temperature β the classical calculations coincide with the other results. Lower temperatures, corresponding to higher values of β, reveal differences between the classical approach (4.31) and quantum statistics.

where $K_{1/4}(z)$ is a modified Bessel function. The classical partition function (4.31) can be evaluated for high temperatures which corresponds to small values of β. Consequently, when we test our variational perturbative results, we compare values $\beta < 1/4$ to the classical partition function (4.31), whereas we consider the numerical free energy $F^{(9)}_{\mathrm{num}}(\beta)$ for higher values of the inverse temperature β.
In natural units $\hbar = M = \omega = k_{\mathrm{B}} = 1$ a value of $\beta = 1/4$ corresponds to a temperature of $T = 4$. In these units the temperature scales like $T = 3.16 \times 10^5$K.

4.5 Higher-Order Variational Perturbation Theory

We now evaluate the convergence behaviour for the variational perturbative results for the free energy $F^{(N)}(\beta)$ up to the fifth order. However, in order to reduce the computational operating expense we restrict ourselves to certain values of the inverse temperature β. Results are shown in Figure 4.5. For odd variational perturbation orders we optimized the free energy according to (4.24), i.e. we determined Ω by setting the first derivative of $F^{(N)}(\beta)$ with respect to Ω (4.24) to zero. For even orders we had to go for inflection points, instead. So we had to solve equation (4.25). This pattern is repeated in the convergence behaviour of the free energy. Odd and even orders oscillate about an exponential best fit curve. Thus, for each value of the inverse temperature β, we get an interval of convergence which we check against the numerical results $F^{(9)}_{\mathrm{num}}(\beta)$ and against the classical result (4.31) if the

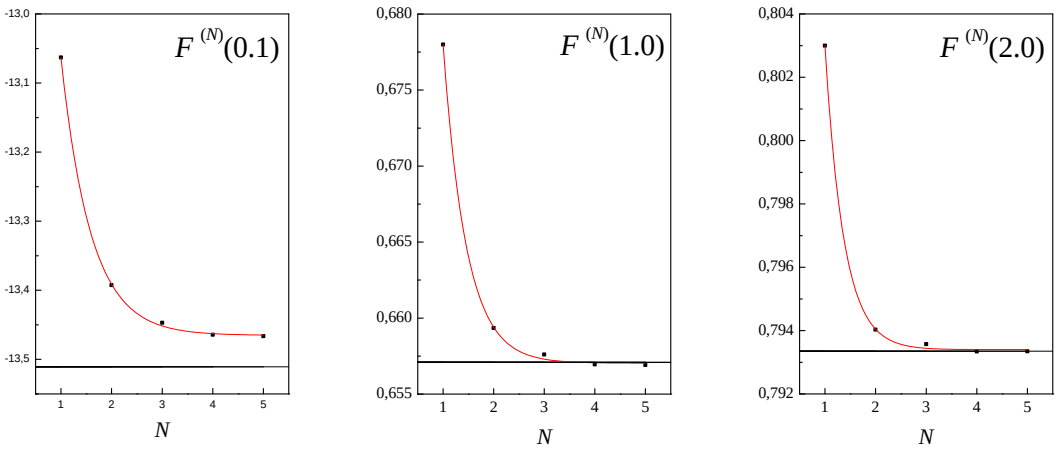

Figure 4.5: The free energy of the anharmonic oscillator for intermediate coupling $g = 1$ for $\beta = 0.1$, $\beta = 1$, and for $\beta = 2$ up to fifth variational perturbative order. The values converge exponentially towards the numerical values $F^{(9)}_{\rm num}(\beta)$. In the case of high temperatures ($\beta = 0.1$) the solid line represents the classical results (4.31) as a cross check, as the function $F^{(9)}_{\rm num}(\beta)$ becomes rather inaccurate for such high temperatures.

temperature is high enough. For $\beta = 0.1$, $\beta = 1$, and $\beta = 2$ the exact results always turn out to lie within the interval of convergence, as shown in Figure 4.5. Clearly the variational perturbative results converge exponentially. For $\beta = 0.1$ the interval is $[-13.49, -13.46]$ which contains the exact classical value $F_{\rm cl}(0.1) = -13.511$ if we consider the threefold standard deviation. For $\beta = 1.0$ we obtain the interval $[0.6572, 0.6585]$ which includes the numerical result $F^{(9)}_{\rm num}(1.0) = 0.6571$. And finally for very low temperatures $\beta = 2.0$ the interval reads $[0.7928, 0.7935]$ containing $F^{(9)}_{\rm num}(2.0) = 0.79335$.

4.6 On the Square-Root Trick

As mentioned at the beginning of this chapter, the square root (4.21) substituted into the free energy is only a special case for the anharmonic oscillator potential. Here we quickly go through the general case [2, 8]. Consider the truncated weak-coupling series of some quantity f as a function of some coupling constant g

$$f_N(g) = \sum_{n=0}^{N} f_n g^n \,. \tag{4.32}$$

Let us now rewrite this weak-coupling expansion by introducing an auxiliary scaling parameter κ [8, 38]

$$f_N(g) = \kappa^p \sum_{n=0}^{N} f_n \left(\frac{g}{\kappa^q}\right)^n , \tag{4.33}$$

which we later set to one. The generalized square root trick now reads

$$\kappa \to \sqrt{K^2 + \kappa^2 - K^2} = K\sqrt{1+gr}\,, \tag{4.34}$$

where K is a "dummy" scaling parameter generalizing the trial frequency Ω and

$$r = \frac{1}{g}\left(\frac{\kappa^2}{K^2} - 1\right) . \tag{4.35}$$

Substituting (4.34) into the truncated weak-coupling series (4.33) we obtain

$$f_N(g,K) = \sum_{n=0}^{N} f_n K^{p-nq}(1+gr)^{(p-nq)/2} g^n . \tag{4.36}$$

The factor $(1+gr)^\alpha$ (with $\alpha \equiv (p-nq)/2$) can be expanded by means of generalized binomials according to

$$\begin{aligned}(1+gr)^\alpha &= \sum_{k=0}^{N-n} \binom{\alpha}{k} (gr)^k g^n \\ &= \sum_{k=0}^{N-n} \binom{\alpha}{k} \left(\frac{1}{K^2} - 1\right)^k g^n ,\end{aligned} \tag{4.37}$$

where we have used (4.35) and finally have set $\kappa \equiv 1$. The binomial is defined as

$$\binom{\alpha}{k} \equiv \frac{\Gamma(\alpha+1)}{\Gamma(k+1)\Gamma(\alpha+k+1)} . \tag{4.38}$$

So we read off that the function $f_N(g,K)$ can now be written as

$$f_N(g,K) = \sum_{n=0}^{N} \left[\sum_{k=0}^{N-n} \binom{\frac{1}{2}(p-jq)}{k} \left(\frac{1}{K^2} - 1\right)^k K^{p-nq}\right] f_n g^n . \tag{4.39}$$

To first order this expression reduces to

$$f_1(g,K) = \left(1 - \frac{p}{2}\right) f_0 K^p + \frac{p}{2} f_0 K^{p-2} + f_1 g K^{p-q} . \tag{4.40}$$

Applying the principle of least sensitivity [48] leaves us with

$$\frac{\partial f_1(g,K)}{\partial K} \sim p\left(1-\frac{p}{2}\right) f_0 + \frac{p(p-2)}{2} f_0 K^{-2} + (p-q) f_1 g K^{-q} \equiv 0\,. \tag{4.41}$$

Making the strong-coupling ansatz

$$K^{(1)}(g) = g^{1/q}\left(k_0 + k_1 g^{-2/q} + ...\right)\,, \tag{4.42}$$

we obtain the following equation from (4.41):

$$p\left(1-\frac{p}{2}\right) f_0 + \frac{p(p-2)}{2} f_0 (k_0^{(1)} g^{1/q})^{-2} + (p-q) f_1 g (g^{1/q} k_0^{(1)})^{-q} = 0\,. \tag{4.43}$$

The second term is a subleading contribution in the limit as the coupling g goes to infinity which we can neglect. Solving for $k_0^{(1)}$ we get

$$k_0^{(1)} = \left(\frac{2f_1}{f_0}\frac{p-q}{p(p-2)}\right)^{1/q}\,. \tag{4.44}$$

Assuming that the ansatz (4.42) for the variational parameter $K(g)$ also holds for higher orders we obtain from the function $f_N(g,K)$ in (4.39)

$$f_N(g) = g^{\frac{p}{q}}\left[b_0^{(N)}(k_0^{(N)}) + b_1^{(N)}(k_0^{(N)})\left(\frac{g}{\kappa^q}\right)^{-\frac{2}{q}} + ...\right]\,, \tag{4.45}$$

where the leading strong-coupling coefficient $b_0^{(N)}(k_0^{(N)})$ is given by

$$b_0^{(N)}(k_0^{(N)}) = \sum_{n=0}^{N}\sum_{k=0}^{N-n}\binom{\frac{1}{2}(p-iq)}{k}(-1)^k f_n (k_0^{(N)})^{p-nq}\,. \tag{4.46}$$

The inner sum can be further simplified according to [52], yielding

$$\sum_{k=0}^{m}(-1)^k\binom{n}{k} = (-1)^m\binom{n-1}{m}\,. \tag{4.47}$$

Thus the strong-coupling coefficient (4.46) reduces to

$$b_0^{(N)}(k_0^{(N)}) = \sum_{n=0}^{N}(-1)^{N-n}\binom{\frac{1}{2}(p-nq)-1}{N-n} f_n (k_0^{(N)})^{p-nq}\,. \tag{4.48}$$

So looking at equation (4.45) we see that the fraction p/q tells us the leading power behaviour in g and $2/q$ indicates the approach to scaling.

4.7 Scaling Behaviour

For the ground state energy of the anharmonic oscillator we can derive the values of p and q from the scaling behaviour of its ground state wave function. Consider the time-independent real Schrödinger equation for the ground state wave function of the anharmonic oscillator (3.2):

$$\left(-\frac{\hbar^2}{2M}\frac{\partial^2}{\partial x^2}+\frac{M}{2}\omega^2 x^2+gx^4\right)\Psi_0(x)=E\Psi_0(x)\,. \tag{4.49}$$

We now rescale the coordinate x according to

$$x=\alpha x'\,, \tag{4.50}$$

such that the new derivative reads

$$\frac{\partial}{\partial x}=\frac{1}{\alpha}\frac{\partial}{\partial x'}\,. \tag{4.51}$$

The ground state wave function transforms like

$$\Psi_0'(x')=\Psi_0(\alpha x')\,. \tag{4.52}$$

Thus the transformed time-independent Schrödinger equation reads

$$\left(\frac{\hbar^2}{2M}\frac{\partial^2}{\partial x'^2}+\frac{M}{2}\omega^2\alpha^4 x'^2+g\alpha^6 x'^4\right)\Psi_0'(x')=\alpha^2 E_0\Psi_0'(x')\,. \tag{4.53}$$

We now impose that the factor in front of the anharmonicity x'^4 is equal to one, so we obtain for α

$$\alpha=g^{-1/6}\,. \tag{4.54}$$

Consequently α^2 is proportional to $g^{-1/3}$. In order to get the units right, we now need

$$E_0^{(0)}(g)=g^{1/3}\epsilon_0\,. \tag{4.55}$$

The superscript indicates that equation (4.55) only is a zeroth-order approximation. Taking into account higher order corrections we get for the ground state energy

$$E_0(g)=g^{1/3}\left(\epsilon_0+g^{-2/3}\epsilon_1+g^{-4/3}\epsilon_2+...\right)\,. \tag{4.56}$$

Corresponding considerations for the wave function yield the expansion

$$\Psi_0'(x')=\phi_0(x')+g^{-2/3}\phi_1(x')+...\,, \tag{4.57}$$

such that the leading power behaviour of the ground state energy is $p/q = 1/3$ and the approach to scaling is $2/q = 2/3$ which lies well in the range

$$\frac{1}{2} < \frac{2}{q} < 1\,, \tag{4.58}$$

for which the convergence proof in Ref. [8] holds. So all in all for the anharmonic oscillator we have

$$p = 1\,, \quad q = 3\,. \tag{4.59}$$

The differential equation for the zeroth-order expansion coefficient of the ground state wave function (4.57) reads

$$-\frac{\hbar^2}{2M}\phi_0''(x') + x'^4\phi_0''(x') = \epsilon_0\phi_0(x')\,. \tag{4.60}$$

The derivation of the numbers p and q was originally invented for the ground state energy [2, 27]. In this chapter we studied the free energy. As the low-temperature limit of the free energy is just the ground state energy, we can assume that the numbers p and q can be extended to our finite temperature calculation.

Chapter 5

Variational Perturbation Theory for Ground State Wave Function

In this chapter we improve the first-order variational calculations for the ground state wave function carried out by T. Hatsuda, T. Tanaka, and T. Kunihiro [41] and our second-order results [40]. First we use our perturbative results for the imaginary-time evolution amplitude to drive the perturbation expression for the ground state wave function up to seventh order, so that we reobtain results from the original Bender-Wu recursion [1]. Then we apply variational perturbation theory up to this order and we study the asymptotic behaviour of the ground state wave function in order to investigate the convergence of our variational results.

5.1 Perturbative Results

As discussed before in Section 2.5 the density matrix is defined as

$$\rho(x_b, x_a) \equiv \frac{(x_b\, \hbar\beta | x_a\, 0)}{Z} \tag{5.1}$$

and the ground state wave function follows from the low temperature limit of its diagonal elements:

$$\Psi_0(x) = \sqrt{\lim_{\beta\to\infty} \rho(x,x)}\,. \tag{5.2}$$

Evaluating the ansatz (3.29) for the first-order result (3.24) together with the harmonic imaginary-time evolution amplitude (3.8), we get the diagonal elements of the imaginary-time evolution amplitude (3.29) in the low temperature limit

$$\begin{aligned}\lim_{\beta\to\infty} (x\, \hbar\beta | x\, 0)^{(1)} &= \lim_{\beta\to\infty} \sqrt{\frac{M\omega}{\pi\hbar}} \exp\left(-\frac{M\omega}{\hbar}x^2 + \frac{\hbar\beta\omega}{2}\right)\left[1 - \frac{g}{\hbar}\left(\frac{9\hbar^2}{8M^2\omega^3}\right.\right.\\ &\quad \left.\left. - \frac{3\hbar^3\beta}{4M^2\omega^2} - \frac{3\hbar}{2M\omega^2}x^2 - \frac{1}{2\omega}x^4\right)\right]. \end{aligned} \tag{5.3}$$

The trace of this first-order expression yields the partition function in the low temperature limit [40]

$$\lim_{\beta\to\infty} Z^{(1)} = \int_{-\infty}^{+\infty} dx \lim_{\beta\to\infty} (x\,\hbar\beta|0\,x)^{(1)} = \lim_{\beta\to\infty} \exp\left(-\frac{\hbar\beta\omega}{2} - \frac{3g\hbar^2\beta}{4M^2\omega^2}\right) . \tag{5.4}$$

So the diagonal elements of the density matrix (5.1) up to first order read

$$\lim_{\beta\to\infty} \rho^{(1)}(x,x) = \sqrt{\frac{M\omega}{\pi\hbar}} \exp\left(-\frac{M\omega}{\hbar}x^2\right) \left[1 - \frac{g}{\hbar}\left(\frac{9\hbar^2}{8M^2\omega^3} - \frac{3\hbar}{2M\omega^2}x^2 - \frac{1}{2\omega}x^4\right)\right] . \tag{5.5}$$

Now the ground state wave function can easily be computed according to (5.2). We obtain

$$\begin{aligned} \Psi_0^{(1)}(x) &= \left(\frac{M\omega}{\hbar\pi}\right)^{1/4} \exp\left(-\frac{M\omega}{2\hbar}x^2\right) \\ &\quad \times \left[1 - \frac{g}{\hbar}\left(-\frac{9\hbar^2}{16M^2\omega^3} + \frac{3\hbar}{4M\omega^2}x^2 + \frac{1}{4\omega}x^4\right)\right] . \end{aligned} \tag{5.6}$$

To first order this leads to the cumulant expansion

$$\Psi_0^{(1)}(x) = \left(\frac{M\omega}{\hbar\pi}\right)^{1/4} \exp\left[-\frac{M\omega}{2\hbar}x^2 + \frac{g}{\hbar}\left(\frac{9\hbar^2}{16M^2\omega^3} - \frac{3\hbar}{4M\omega^2}x^2 - \frac{1}{4\omega}x^4\right)\right] . \tag{5.7}$$

The higher orders can be obtained in the same way: From the seventh-order imaginary-time evolution amplitude [51] we get the partition function up to seventh order following definition (2.35). Then we compute the density matrix according to (5.1), take the low-temperature limit and the square-root, yielding a perturbation expression for the seventh-order ground state wave function which is then transformed into the cumulant expansion:

$$\begin{aligned} \Psi_0^{(7)}(x) = \left(\frac{M\omega}{\hbar\pi}\right)^{1/4} \exp\Bigg[& -\frac{M\omega}{2\hbar}x^2 + \frac{g}{\hbar}\left(\frac{9\hbar^2}{16M^2\omega^3} - \frac{3\hbar}{4M\omega^2}x^2 - \frac{1}{4\omega}x^4\right) \\ & + \frac{g^2}{\hbar^2}\left(-\frac{205\hbar^4}{64M^4\omega^6} + \frac{21\hbar^3}{8M^3\omega^5}x^2 + \frac{11\hbar^2}{16M^2\omega^4}x^4 + \frac{\hbar}{12M\omega^3}x^6\right) \\ & + \frac{g^3}{\hbar^3}\left(\frac{8049\hbar^6}{256M^6\omega^9} - \frac{333\hbar^5}{16M^5\omega^8}x^2 - \frac{45\hbar^4}{8M^4\omega^7}x^4 - \frac{7\hbar^3}{8M^3\omega^6}x^6 - \frac{\hbar^2}{16M^2\omega^5}x^8\right) \\ & + \frac{g^4}{\hbar^4}\Bigg(- \frac{849887\hbar^8}{2048M^8\omega^{12}} + \frac{30885\hbar^7}{128M^7\omega^{11}}x^2 + \frac{8669\hbar^6}{128M^6\omega^{10}}x^4 \end{aligned}$$

$$
\begin{aligned}
&+\frac{1159\hbar^5}{96M^5\omega^9}x^6+\frac{163\hbar^4}{128M^4\omega^8}x^8+\frac{\hbar^3}{16M^3\omega^7}x^{10}\Bigg)\\
&+\frac{g^5}{\hbar^5}\Bigg(\frac{68941527\hbar^{10}}{10240M^{10}\omega^{15}}-\frac{916731\hbar^9}{256M^9\omega^{14}}x^2-\frac{33171\hbar^8}{32M^8\omega^{13}}x^4\\
&-\frac{6453\hbar^7}{32M^7\omega^{12}}x^6-\frac{823\hbar^6}{32M^6\omega^{11}}x^8-\frac{319\hbar^5}{160M^5\omega^{10}}x^{10}-\frac{7\hbar^4}{96M^4\omega^9}x^{12}\Bigg)\\
&+\frac{g^6}{\hbar^6}\Bigg(-\frac{3156181949\hbar^{12}}{24576M^{12}\omega^{18}}+\frac{65518401\hbar^{11}}{1024M^{11}\omega^{17}}x^2+\frac{19425763\hbar^{10}}{1024M^{10}\omega^{16}}x^4+\frac{752825\hbar^9}{192M^9\omega^{15}}x^6\\
&+\frac{143783\hbar^8}{256M^8\omega^{14}}x^8+\frac{3481\hbar^7}{64M^7\omega^{13}}x^{10}+\frac{1255\hbar^6}{384M^6\omega^{12}}x^{12}+\frac{3\hbar^5}{32M^5\omega^{11}}x^{14}\Bigg)\\
&+\frac{g^7}{\hbar^7}\Bigg(\frac{1287421536711\hbar^{14}}{458752M^{14}\omega^{21}}-\frac{2723294673\hbar^{13}}{2048M^{13}\omega^{20}}x^2-\frac{411277893\hbar^{12}}{1024M^{12}\omega^{19}}x^4\\
&-\frac{44413183\hbar^{11}}{512M^{11}\omega^{18}}x^6-\frac{3440609\hbar^{10}}{256M^{10}\omega^{17}}x^8-\frac{190735\hbar^9}{128M^9\omega^{16}}x^{10}\\
&-\frac{7317\hbar^8}{64M^8\omega^{15}}x^{12}-\frac{2477\hbar^7}{448M^7\omega^{14}}x^{14}-\frac{33\hbar^6}{256M^6\omega^{13}}x^{16}\Bigg)\Bigg]\,. \qquad (5.8)
\end{aligned}
$$

We now check our results against the well known Bender-Wu results [1].

5.2 Checking Our Results — Bender-Wu Recursion

In 1969, C. Bender and T. Wu developed an algebraic recursion formula for energy eigenfunctions and energy eigenvalues of the anharmonic oscillator [1]. In this section we want to sketch their method for the ground state wave function.
Consider the stationary Schrödinger equation for the ground state wave function of the anharmonic oscillator:

$$\left(-\frac{\hbar^2}{2M}\frac{\partial^2}{\partial x^2}+\frac{M}{2}\omega^2x^2+gx^4\right)\Psi_0(x)=E_0\Psi_0(x)\,. \qquad (5.9)$$

The unnormalized solution to the harmonic problem $g=0$ reads

$$\Psi_0(x)=e^{-\frac{M\omega}{2\hbar}x^2}H_0(x)\,, \qquad (5.10)$$

where H_0 is the zeroth Hermite polynomial

$$H_0(x)=1\,. \qquad (5.11)$$

For the solution to the anharmonic problem (5.9) we choose the ansatz [2]

$$\Psi_0(x)=e^{-\frac{M\omega}{2\hbar}x^2}\sum_{k=0}^{\infty}(-g)^k\Phi_k^{(0)}(x) \qquad (5.12)$$

and

$$E_0 = \sum_{k=0}^{\infty} g^k E_k^{(0)} \,. \tag{5.13}$$

In order to clarify the type face we now drop the superscripts. Plugging our ansatz (5.12) and (5.13) into the Schrödinger equation (5.9) we obtain

$$\left(\frac{\hbar\omega}{2} + gx^4\right) \sum_{k=0}^{\infty} (-g)^k \Phi_k(x) + \hbar\omega x \sum_{k=0}^{\infty} \Phi_k'(x) \\ -\frac{\hbar^2}{2M} \sum_{k=0}^{\infty} (-g)^k \Phi_k''(x) - \sum_{k'=0}^{\infty} \sum_{k=0}^{\infty} g^{k'} (-g)^k E_{k'} \Phi_k(x) = 0 \,. \tag{5.14}$$

For the different powers of g we get

$$\frac{\hbar\omega}{2} \Phi_k(x) - x^4 \Phi_{k-1}(x) + \hbar\omega x \Phi_k'(x) - \frac{\hbar^2}{2M} \Phi_k''(x) = \sum_{k'=0}^{k} (-1)^{k'} E_{k'} \Phi_{k-k'}(x) \,. \tag{5.15}$$

We know that the $(k' = 0)$-term on the right hand side is $E_0 = \hbar\omega/2$, so we can absorb the first term on the left hand side into the summation, thereby obtaining

$$\hbar\omega x \Phi_k'(x) = x^4 \Phi_{k-1}(x) + \frac{\hbar^2}{2M} \Phi_k''(x) + \sum_{k'=1}^{k} (-1)^{k'} E_{k'} \Phi_{k-k'}(x) \,, \tag{5.16}$$

where $\Phi_k(x) = 0$ for $k < 0$. For the kth-order contribution to the ground state wave function (5.12) we can assume the shape of a power series with contributions from even powers only, for the potential (3.2) is even. Moreover the power series breaks off at $4k$. A similar break off has already been discussed in Section 3.5 for the imaginary-time evolution amplitude. Thus our ansatz for $\Phi_k(x)$ reads

$$\Phi_k(x) = \sum_{p=0}^{2k} A_k^{(2p)} x^{2p} \,, \tag{5.17}$$

where $\Phi_k(0) = A_k^{(0)}$ is subject to the normalization

$$\int_{-\infty}^{+\infty} dx |\Psi_0(x)|^2 \equiv 1 \,. \tag{5.18}$$

Performing the Gaussian integration to zeroth order we can fix $A_0^{(0)}$ to

$$A_0^{(0)} = \left(\frac{M\omega}{\pi\hbar}\right)^{1/4} \,. \tag{5.19}$$

Inserting the power series ansatz (5.17) into equation (5.16) we get for the different even powers of x to first order:

$$\begin{aligned} \frac{\hbar^2}{M} A_1^{(2)} &= E_1 A_0^{(0)} , \\ 2\hbar\omega A_1^{(2)} &= \frac{6\hbar^2}{M} A_1^{(4)} , \\ 4\hbar\omega A_1^{(4)} &= A_0^{(0)} . \end{aligned} \tag{5.20}$$

This set of recursive algebraic equations can easily be solved:

$$\begin{aligned} A_1^{(2)} &= \frac{1}{4\hbar\omega} A_0^{(0)} , \\ A_1^{(4)} &= \frac{3}{4M\omega^2} A_0^{(0)} , \\ E_1 &= \frac{3\hbar^2}{4M^2\omega^2} , \end{aligned} \tag{5.21}$$

where $A_0^{(0)}$ is given by (5.19). Again the coefficient $A_1^{(0)}$ has to be fixed by first-order normalization of the wave function according to (5.18) and leads to

$$A_0^{(1)} = -\frac{9\hbar^2}{16M^2\omega^3} A_0^{(0)} . \tag{5.22}$$

Inserting all the coefficients $A_1^{(2p)}$, $p = 0, 1, 2$, from (5.21) and (5.22) into equation (5.17) and then plugging $\Phi_k(x)$ into the ground state wave function (5.12), we finally reobtain (5.6) by pulling out the overall factor $A_0^{(0)}$.
More generally, for any order k, plugging the ansatz (5.17) into the differential equation (5.16) leads to

$$\begin{aligned} 2\hbar\omega \sum_{p=1}^{2k} p A_k^{(2p)} x^{2p} &= \sum_{p=0}^{2k-2} A_{k-1}^{(2p)} x^{2p+4} + \frac{\hbar^2}{M} \sum_{p=1}^{2k} p(2p-1) A_k^{(2p)} x^{2p-2} \\ &\quad + \sum_{k'=1}^{k} (-1)^{k'} E_{k'} \sum_{p=0}^{2(k-k')} A_{k-k'}^{(2p)} x^{2p} . \end{aligned} \tag{5.23}$$

Shifting the summation indices in such a way that all terms are proportional to x^{2p}, we can write down the equations for each (even) power x^{2p}:

$$2\hbar\omega p A_k^{(2p)} = A_{k-1}^{(2p-4)} + \frac{\hbar^2}{2M}(2p+2)(2p+1) A_k^{(2p+2)} + \sum_{k'=1}^{k} (-1)^{k'} A_{k-k'}^{(2p)} , \tag{5.24}$$

where $A_k^{(2p)} \equiv 0$ for $p < 0$ and for $p > 2k$. This is the Bender-Wu recursion. With the help of a `Maple` programme we compared the results for the ground state wave function of our combined differential and algebraic recursion relation in (5.8) to the Bender-Wu results. Up to seventh order no deviations could be found.

5.3 First-Order Variational Results

In this section we apply variational perturbation theory to the ground state wave function. To that end, as seen in the previous chapter on the free energy, we execute Kleinert's square root trick (4.21) together with (4.22) in the cumulant expansion of the ground state wave function (5.7). Then we expand the result in powers of g for fixed r up to the first order and finally we resubstitute for r according to (4.22). Thus we obtain an expression for the ground state wave function which now additionally depends on the trial frequency Ω. In the first order we get

$$\Psi_0^{(1)}(x,\Omega) = \exp[W_0^{(1)}(x,\Omega)]\,, \tag{5.25}$$

where the cumulant is

$$\begin{aligned} W_0^{(1)}(x,\Omega) &= \frac{1}{4}\log\left(\frac{M\Omega}{\hbar\pi}\right) - \frac{1}{8} + \frac{\omega^2}{8\Omega^2} - \frac{M\Omega}{4\hbar}\left(1+\frac{\omega^2}{\Omega^2}\right)x^2 \\ &\quad + \frac{g}{\hbar}\left(\frac{9\hbar^2}{16M^2\Omega^3} - \frac{3\hbar}{4M\Omega^2}x^2 - \frac{1}{4\Omega}x^4\right)\,. \end{aligned} \tag{5.26}$$

Analogously to the procedure in Chapter 4 we now eliminate the Ω-dependence by applying the principle of least sensitivity [48]. To that end we look for extrema of the cumulant $W_0^{(1)}(x,\Omega)$ with respect to Ω. To first order we find that the equation

$$\frac{\partial W_0^{(1)}(x,\Omega)}{\partial\Omega} = 0 \tag{5.27}$$

has two branches of solutions, separated by a gap in the domain of $\Omega(x)$ [40, 41]. As suggested by H. Kleinert, in accordance with the principle of least sensitivity [48], in the gap we search for inflection points instead [40]:

$$\frac{\partial^2 W_0^{(1)}(x,\Omega)}{\partial\Omega^2} = 0\,. \tag{5.28}$$

Figure 5.1 shows the different branches and our final choice for the variational parameter $\Omega(x)$ on the various intervals. Plugging $\Omega(x)$ into (5.26), we gain an expression for the ground state wave function which is at first not normalized. This normalization can be reassured according to

$$\Psi_0^{(1)}(x) = \frac{\Psi_0^{(1)}(x,\Omega(x))}{\displaystyle\int_{-\infty}^{+\infty} dx' \left|\Psi_0^{(1)}(x',\Omega(x'))\right|^2}\,. \tag{5.29}$$

The results for three different coupling strengths g can be found in Figure 5.2. A comparison of these variational results to numerical calculations obtained with the "shooting method" from Section 4.4 shows no visible deviations. Indeed, the standard deviation for intermediate coupling $g = 1/2$ is 1.1×10^{-5}, which is already very small.

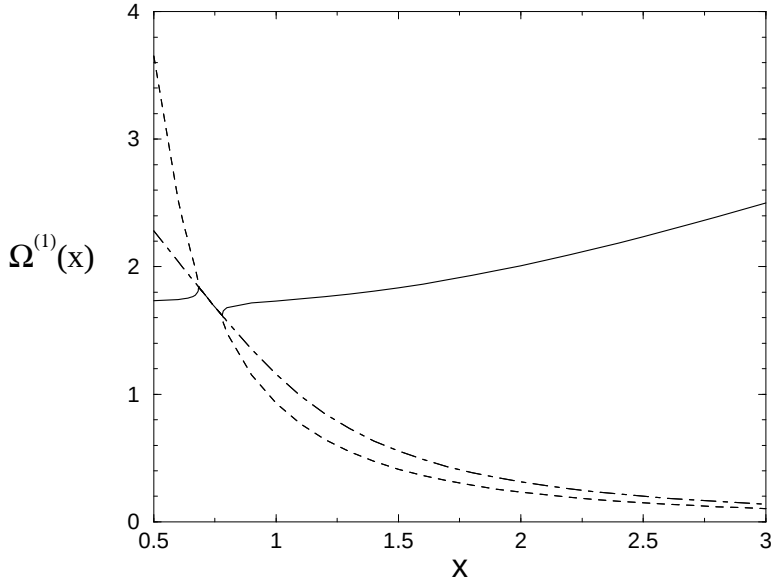

Figure 5.1: The variational parameter $\Omega(x)$ to first order for intermediate coupling $g = 1/2$. The branches for $x < 0.684$ and $x > 0.780$ (solid line and dashed line) are solutions to the equation $\partial\Psi_0^{(1)}(x,\Omega)/\partial\Omega = 0$. For $0.684 < x < 0.780$ there are no real positive solutions to that equation. That is why we look for inflection points on that interval instead, i.e. we look for real positive solutions to the equation $\partial^2\Psi_0^{(1)}(x,\Omega)/\partial\Omega^2 = 0$. The curve for the inflection points lies between the two other branches and it neatly fills the gap. So we choose those branches $\Omega^{(1)}(x)$ which provide us with the smoothest curve on the entire interval, which is the solid line.

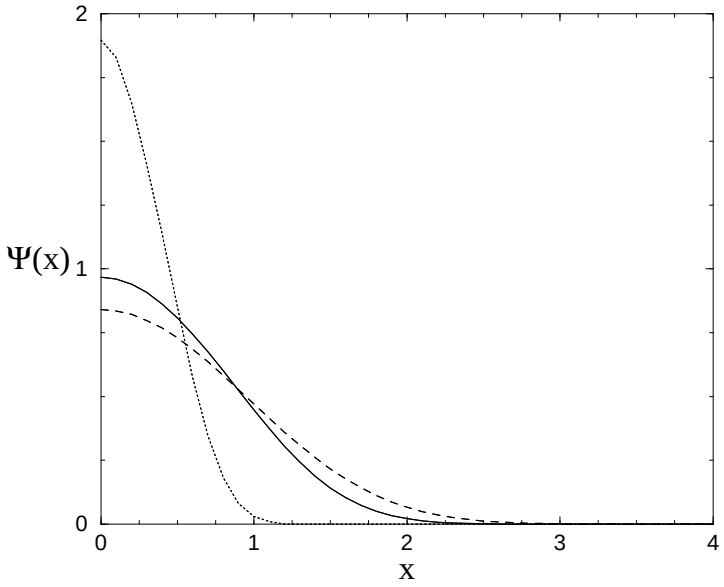

Figure 5.2: The normalized first-order results for the ground state wave function $\Psi_0(x)$ of the anharmonic oscillator for weak coupling (dashed line, $g = 0.1$), for intermediate coupling (solid line, $g = 1/2$), and for strong coupling (dotted line, $g = 50$).

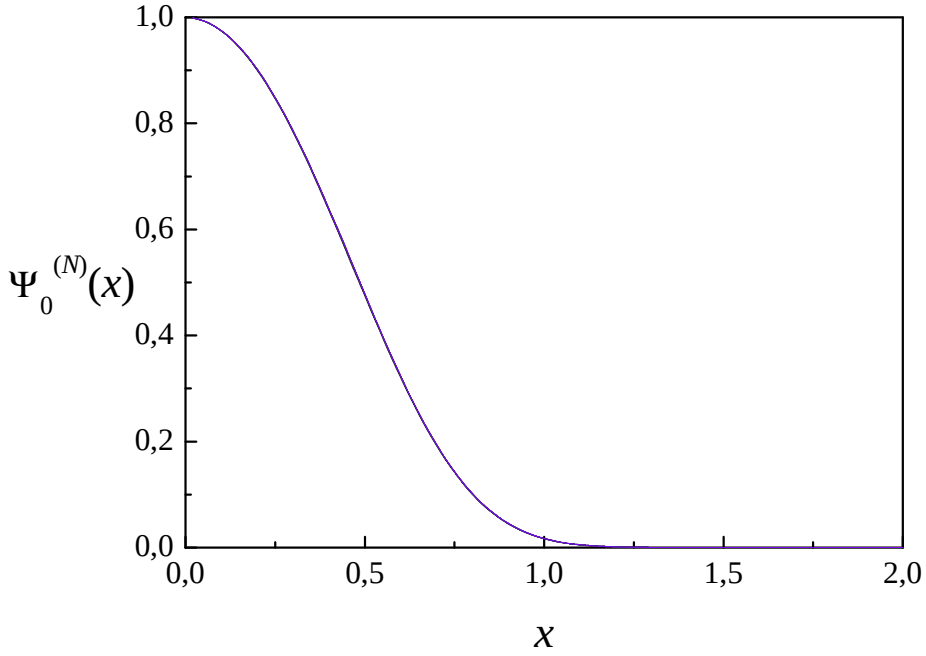

Figure 5.3: The first seven orders of the unnormalized ground state wave function $\Psi^{(N)}(x)$ for strong coupling $g = 50$. N=1: black, N=2: red, N=3: blue, N=4: navy, N=5: purple, N=6: olive, N=7: violet. The curves are hardly distinguishable. For simplicity the ground state wave function is now normalized according to $\Psi_0^{(N)}(0) = 1$.

5.4 Higher-Order Variational Results

Order by order we now apply variational perturbation theory to the cumulant expansion (5.8) of the wave function. As variational perturbation theory especially allows for strong coupling, we concentrate on the example $g = 50$ in this section. The first-order ground state wave function for that coupling strength has already been shown in Figure 5.2. All seventh-order results are depicted in Figure 5.3. The curves are hardly distinguishable. More interesting is the collection of the physical branches of the variational parameter $\Omega^{(N)}(x)$ for N from one to seven (see Figure 5.4). In Table 5.1 pointwise convergence of the wave function is discussed for $x = 0.5$ and $x = 1.0$. The orders exponentially converge to the correct limiting values. However, odd and even order can best be fitted separately (see Figure 5.5). It turns out that the equation

$$\frac{\partial W^{(N)}(x)}{\partial \Omega} = 0 \tag{5.30}$$

has real positive solutions for odd N only. For even values of N we have to go for inflection points:

$$\frac{\partial^2 W^{(N)}(x)}{\partial \Omega^2} = 0\,, \tag{5.31}$$

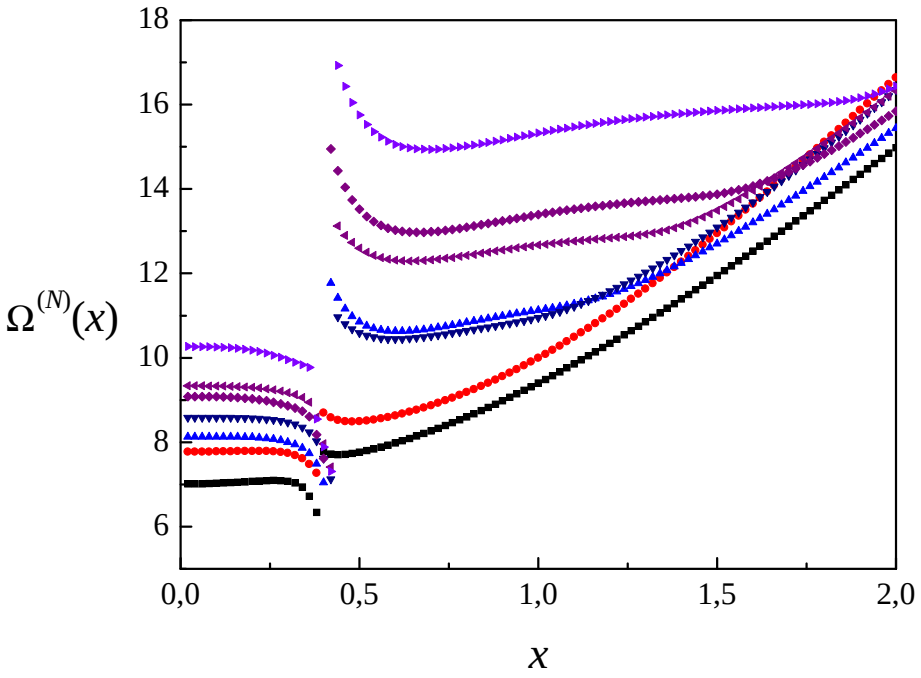

Figure 5.4: The physical branches of the variational parameter $\Omega^{(N)}(x)$ for the first seven orders for the ground state wave function of the anharmonic oscillator for strong coupling $g = 50$. N=1: black/squares, N=2: red/dots, N=3: blue/triangles, N=4: navy/triangles upside down, N=5: purple/hashes, N=6: olive/triangles left, N=7: violet/triangles right. For $N = 1, 3, 5, 7$ the parameter $\Omega^{(N)}(x)$ can be obtained from the first derivative (5.30). For even $N = 2, 4, 6$ we have to search for inflection points (5.31) instead.

	$x = 0.5$	$x = 1.0$
$\Psi_0^{(1)}(x)$	0.474293	0.016468
$\Psi_0^{(2)}(x)$	0.477367	0.017073
$\Psi_0^{(3)}(x)$	0.477825	0.017050
$\Psi_0^{(4)}(x)$	0.477384	0.017013
$\Psi_0^{(5)}(x)$	0.477923	0.017038
$\Psi_0^{(6)}(x)$	0.477385	0.017002
$\Psi_0^{(7)}(x)$	0.477928	0.017029
$\Psi_0^{(\mathrm{num})}(x)$	0.478128	0.016997

Table 5.1: Pointwise convergence of the unnormalized ground state wave function at $x = 0.5$ and at $x = 1.0$ for $g = 50$. Clearly, the convergence of odd and even orders of variational perturbation theory are varying (see Figure 5.5). Fitting odd and even orders separately yields intervals of convergence for the respective value of x. The best fits are exponentials. Exact results for the ground state wave function, $\Psi_0^{(\mathrm{num})}(x)$, obtained numerically with the shooting method (compare Section 4.4), lie within these intervals (see Figure 5.5). The normalization is done according to $\Psi_0^{(N)}(0) = 1$ in this example.

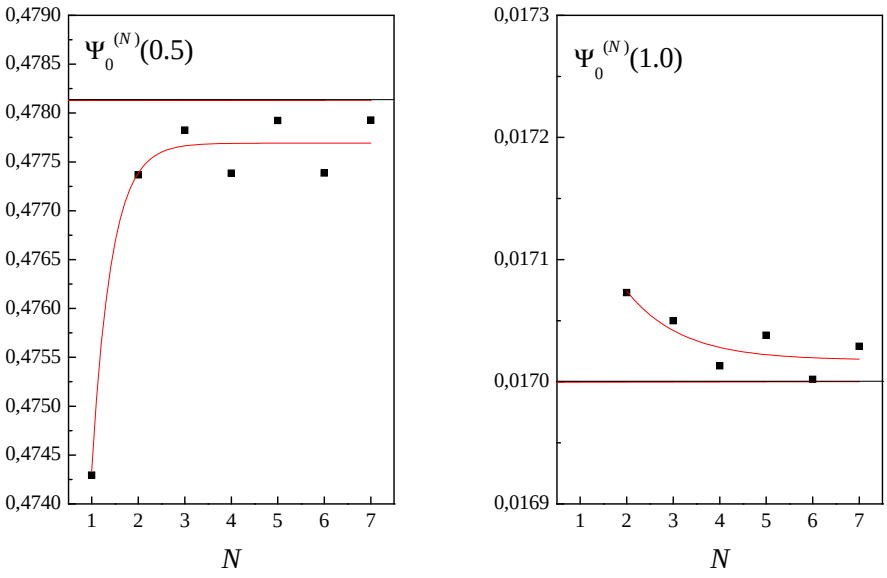

Figure 5.5: Odd and even orders of variational perturbation theory separately converge to the limiting value. The figures show the best fit curves for all orders. Fitting separately, however, yields the following intervals of convergence. For $x = 0.5$ we get: $\Psi_0^{(\infty)}(0.5) \in [0.47793, 0.492]$. The upper boundary cannot be determined more accurately, for we can only consider three points. For $x = 1.0$ we get: $\Psi_0^{(\infty)}(1.0) \in [0.1698, 0.1702]$. Again the statistical errors prevent us from a more accurate evaluation of the intervals. However, for both cases the exact numerical results $\Psi_0^{(\mathrm{num})}(x)$ lie within the respective intervals.

as in the case of the free energy in Chapter 4. This phenomenon has been observed before [2], namely for the ground state energy. It is already reflected in the convergence behaviour of the ground state wave function. As shown in Figure 5.5, odd and even orders can best be fitted separately. Extrapolation to infinity for both odd and even orders thus yields an interval of convergence instead of just one limiting value with a purely statistical deviation. Comparing to numerical results obtained using the "shooting method" (compare Section 4.4), we find that the exact results lie within that interval for all orders.
In the upcoming section we analyze the asymptotic ground state wave function, i.e. the ground state wave function in the limit as x goes to infinity.

5.5 Asymptotic Limit

We now check whether variational perturbation theory preserves the asymptotic behaviour of the ground state wave function. The asymptotic behaviour is of special interest as variational perturbation theory is most likely to converge rather slowly at $|x| \to \infty$. In order to find the asymptotic behaviour of the ground state wave function we have to consider the time-independent Schrödinger equation (4.49) in the limit $|x| \to \infty$. In this limit the harmonic

term, proportional to x^2, and the energy eigenvalue are negligible, so we obtain

$$-\frac{\hbar^2}{2M}\Psi_0''(x) + gx^4\Psi_0(x) = 0\,. \tag{5.32}$$

In the limit $|x| \to \infty$ the wave function behaves like

$$\Psi_0(x) \sim \exp\left(-C|x|^\alpha\right) \quad (|x| \to \infty)\,, \tag{5.33}$$

where C is some constant depending on the coupling strength g. The absolute value of the coordinate x reflects the symmetry of the anharmonic oscillator potential (3.2). As the potential is symmetric, the wave function can either be symmetric or antisymmetric. As we only consider the ground state wave function, we have to choose the one with the lowest energy which is the symmetric one. Differentiating the asymptotic wave function (5.33) twice with respect to the coordinate x and plugging it into the asymptotic Schrödinger equation (5.32) yields

$$-\frac{\hbar^2}{2M}\left[-C\alpha(\alpha-1)x^{\alpha-2} + C^2\alpha^2x^{2\alpha-2}\right]\Psi_0(x) + gx^4\Psi_0(x) = 0\,. \tag{5.34}$$

In the limit $|x| \to \infty$ only the second term in the square brackets survives, so we can neglect the first one. Comparing the powers of x we see that there is a constraint on the value of α

$$2\alpha - 2 = 4\,, \tag{5.35}$$

which fixes the power α to be $\alpha = 3$. With this value for α the time-independent asymptotic Schrödinger equation (5.32) becomes

$$\left(-\frac{9\hbar^2}{2M}C^2 + g\right)\Psi_0(x) = 0\,, \tag{5.36}$$

so we get for the constant C in equation (5.33)

$$C = \sqrt{\frac{2Mg}{9\hbar^2}}\,. \tag{5.37}$$

Thus the strong-coupling asymptotic wave function looks like

$$\Psi_0(x) \sim \exp\left(-\sqrt{\frac{2Mg}{9\hbar^2}}|x|^3\right) \quad (|x| \to \infty)\,, \tag{5.38}$$

which is the same as in Ref. [41].[1] Now we check which asymptotic behaviour is generated by variational perturbation theory. According to the principle of least sensitivity [48] we

[1] Please note that Tanaka et al. use a different definition for the coupling constant, such that the numbers in the square root look a bit different.

differentiate $W_0^{(1)}(x,\Omega)$ from (5.26) with respect to Ω and look for zeros:

$$\frac{\partial W_0^{(1)}(x,\Omega)}{\partial\Omega} = \frac{1}{4\Omega} - \frac{1}{4\Omega^3} - \frac{M}{4\hbar}x^2 + g\left(-\frac{27\hbar}{16M^2\Omega^4} + \frac{3}{2M\Omega^3}x^2 + \frac{1}{4\hbar\Omega^2}x^4\right) = 0\,. \quad (5.39)$$

As the harmonic ground state wave function

$$\Psi_0(x) = \exp\left(-\frac{M\Omega}{2\hbar}x^2\right) \quad (5.40)$$

has to turn into (5.38) in the limit $|x| \to \infty$, we assume for Ω

$$\Omega(x) = \tilde{C}g^{1/2}|x| \quad (5.41)$$

as an ansatz. Taking into account this ansatz in (5.39), we can drop a lot of terms, as $|x|$ goes to infinity. We obtain

$$\frac{M}{4\hbar}x^2 - \frac{g}{4\hbar\Omega^2}x^4 - \frac{M}{4\hbar}x^2 - \frac{1}{4\hbar\tilde{C}^2}x^2 = 0\,. \quad (5.42)$$

All other terms do not contribute, for they vanish in the limit $|x| \to \infty$. Solving equation (5.42) for $\tilde{C}$ we get

$$\tilde{C} = M^{-1/2}\,. \quad (5.43)$$

In order to obtain the asymptotic ground state wave function we plug $\tilde{C}$ back into the ansatz (5.41). Then we evaluate the cumulant (5.26) for that function for $\Omega^{(1)}(x)$ in the limit $|x| \to \infty$, which yields

$$W_0^{(1)}(x) = -\frac{M}{4\hbar}M^{-1/2}g^{1/2}|x|^3 - \frac{g}{4\hbar}M^{1/2}g^{-1/2}|x|^3 = -C^{(1)}|x|^3\,, \quad (5.44)$$

where of course the constant $C^{(1)}$ is

$$C^{(1)} = \frac{1}{2}\sqrt{\frac{Mg}{\hbar^2}}\,. \quad (5.45)$$

This is a very good first-order approximation for the exact value (5.37), which is

$$C = 0.471404520... \times \sqrt{\frac{Mg}{\hbar^2}}\,. \quad (5.46)$$

The higher orders can be found in Table 5.2. The numbers are converging to the correct limiting value (5.46). However they do not converge algebraically, for Richardson extrapolations [53] oscillate wildly around the correct value. The convergence is exponentially as can

N	$C^{(N)}$
1	0.5
2	0.4871392898
3	0.4791666667
4	0.4776822078
5	0.4752604167
6	0.4749049495
7	0.4737955740
C	0.471404520

Table 5.2: The coefficients $C^{(N)}$ which determine the asymptotic behaviour of the ground state wave function for strong coupling. The numbers converge to the correct limiting value $C = \sqrt{2/9}$.

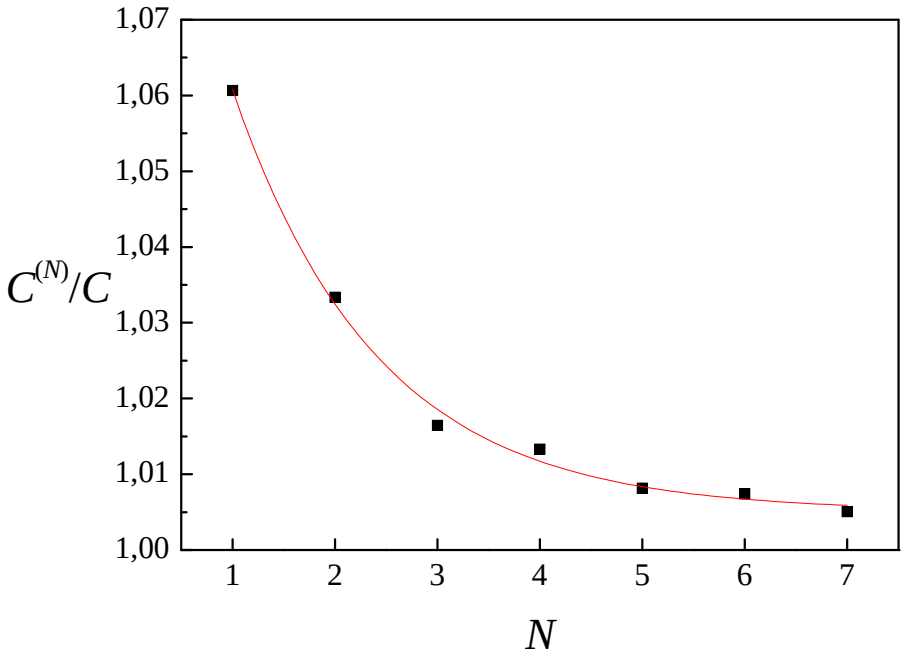

Figure 5.6: Asymptotic ground state wave function showing exponential convergence. The correct limiting value is in good accordance with the exponential fitted to the seven numbers from Table 5.2. Fitting odd and even orders separately we get an interval of convergence: $C^{(\infty)}/C = [1.00496, 1.00505]$. This does not exclude the correct limiting value, for the statistical errors associated with these extrapolations are still very large.

be seen in Figure 5.6. As in the case of the ground state wave function for $g = 50$ discussed in the previous section, odd and even orders scatter a bit around the best fit curve which is an exponential. Taking into account all the seven orders we get for the ratio of extrapolated

constant $C^{(\infty)}$ to the exact value $C = \sqrt{2/9}$ from (5.37)

$$\frac{C^{(\infty)}}{\sqrt{2/9}} = 1.005 \pm 0.002\,, \tag{5.47}$$

where the deviation is purely statistical. Extrapolating odd and even orders separately we get the interval

$$\frac{C^{(\infty)}}{\sqrt{2/9}} \in [1.00496, 1.00505]\,. \tag{5.48}$$

This seems to exclude the correct limiting value (5.37). However, the statistical errors associated with the upper and lower boundary of this interval are very large. Going to higher orders will certainly correct for that, and include the correct result (5.37)

Chapter 6

Boundary-Layer Theory, Strong-Coupling Series, and Large-Order Behaviour

In this chapter we report some progress in understanding (albeit not a complete solution to) a general class of problems in mathematical physics. We consider here the conversion of a continuum problem into a discrete problem by the insertion of a lattice spacing parameter a, the perturbative solution of the continuum problem on the lattice, and the subsequent extremely subtle continuum limit $a \to 0$.
Almost every continuum physics problem is singular as a function of the parameters in the problem. As a result, only rarely does the perturbation series take the form of a Taylor series having a nonzero radius of convergence. As an elementary example, consider the algebraic polynomial equation

$$\epsilon x^3 + x - 1 = 0. \tag{6.1}$$

This problem is singular in the limit $\epsilon \to 0$. In this limit, the degree of the polynomial changes from three to one and thus two of the roots abruptly disappear. As a consequence, a perturbative solution to this problem (expressing the roots $x(\epsilon)$ as series in powers of ϵ) yields expressions that are more complicated than Taylor series:

$$x(\epsilon) = \epsilon^{-1/2} x_{-1} + x_0 + \epsilon^{1/2} x_2 + \epsilon x_3 + \epsilon^{3/2} x_4 + ... \tag{6.2}$$

would be the real root to the problem (6.1) expressed as a series in ϵ.
A more elaborate example of a singular problem is the time-independent Schrödinger equation

$$-\frac{\hbar^2}{2M}\nabla^2\Psi(\mathbf{x}) + [V(\mathbf{x}) - E]\Psi(\mathbf{x}) = 0. \tag{6.3}$$

In the classical limit $\hbar \to 0$ this differential equation abruptly becomes an *algebraic* equation, and thus the general solution no longer contains any arbitrary constants or functions and, as

a result, it can no longer satisfy the initial conditions. We know that for small $\hbar$ the solution is not Taylor-like but rather is a singular exponential in WKB form:

$$\Psi(\mathbf{x}) \sim e^{iS(\mathbf{x})/\hbar} \quad (\hbar \to 0). \tag{6.4}$$

In the study of quantum field theory, it is well known that infinities appear in the perturbative expansion in powers of the coupling constant. There are two kinds of infinities. The first kind, which is due to the point-like nature of the interaction, requires the use of renormalization. The second kind, which is due to singularities in the complex-coupling-constant plane, forces the perturbation series to have a zero radius of convergence.
A quantum field theory can be regulated by introducing a lattice spacing. The resulting discrete theory is completely finite and can be studied numerically by using various kinds of numerical methods such as Monte Carlo integration. However, the underlying singular nature of the continuum quantum field theory resurfaces in the continuum limit $a \to 0$. The introduction of a lattice spacing and the singular nature of the continuum limit was investigated in a series of papers by Bender et al. [54, 55, 56, 57, 58, 59, 60, 61, 62].
A quantum field theory is just one instance in which discretization regulates and eliminates the singular nature of the problem. Another example is provided by a boundary-layer problem, which is a singular perturbation problem, as introducing a lattice spacing converts it into a regular perturbation problem [63, 64, 65]. A *boundary-layer problem* is a differential-equation-boundary-value problem in which the highest derivative of the differential equation is multiplied by a small parameter ϵ. Consider as an example

$$\epsilon y''(x) + a(x)y'(x) + b(x)y(x) = c(x)\,, \tag{6.5}$$

where the boundary conditions on the function $y(x)$ typically have a form such as

$$y(0) = A, \qquad y(1) = B. \tag{6.6}$$

This boundary-value problem is singular because in the limit $\epsilon \to 0$ one of the solutions abruptly disappears and the limiting solution is not able to satisfy the two boundary conditions in (6.6). The usual way to solve the boundary-value problem (6.5) – (6.6) is to decompose the interval $0 \leq x \leq 1$ into two regions, an *outer region*, in which the solution varies slowly as a function of x, and an *inner region* or *boundary-layer region*, in which the solution varies rapidly as a function of x. The boundary-layer region is a narrow region whose thickness is typically of order ϵ or some power of ϵ [53].
An important example of a boundary-layer problem is the instanton equation

$$\epsilon^2 f''(x) + f(x) - f^3(x) = 0\,, \tag{6.7}$$

with the associated boundary conditions

$$f(0) = 0, \qquad f(\infty) = 1\,. \tag{6.8}$$

The exact solution to this instanton problem is

$$f(x) = \tanh \frac{x}{\epsilon\sqrt{2}} \,. \tag{6.9}$$

Note that the solution $f(x)$ varies rapidly at the origin $x = 0$ over a region of thickness ϵ; this is the boundary-layer region. The solution varies slowly (it is approximately 1) outside of this region. The outer region consists of those x not near the origin.
A novel way to solve the instanton problem is to discretize it by introducing a lattice. On the lattice, the differential equation becomes a difference equation that can easily be solved perturbatively. In the continuum limit, as the lattice spacing vanishes, we then obtain a strong-coupling expansion that must be evaluated by means of a Padé or a variational perturbation theory method. To illustrate the approach our objective will be to calculate the slope of the instanton at $x = 0$, which from (6.9) has the value

$$f'(0) = \frac{1}{\epsilon\sqrt{2}} \,. \tag{6.10}$$

We introduce a lattice with lattice spacing a so that the real axis is discretized in steps of width a. The spatial coordinate reads $x_n = na$, where the function $f(x)$ assumes the value $f_n = f(x_n)$. On the lattice the second spatial derivative in (6.7) becomes

$$f''(x) \;\rightarrow\; \frac{f_{n+1} - 2f_n + f_{n-1}}{a^2} \,. \tag{6.11}$$

Thus, from the instanton equation (6.7) we obtain the difference equation

$$\frac{\epsilon^2}{a^2}(f_{n+1} - 2f_n + f_{n-1}) + f_n - f_n^3 = 0 \,, \tag{6.12}$$

where the boundary values follow from (6.8):

$$f_0 = 0 \,, \qquad f_\infty = 1 \,. \tag{6.13}$$

The natural expansion parameter in (6.12) is ϵ^2/a^2, to which we assign the name δ:

$$\delta \equiv \frac{\epsilon^2}{a^2} \,. \tag{6.14}$$

The singular perturbation problem in the continuum (whose solution $f(x)$ in (6.9) does not possess a Taylor expansion in powers of ϵ), has become a *regular* perturbation problem. That is, we can now expand the solution f_n to the difference equation (6.12) as a Taylor series in powers of δ:

$$f_n = a_{n,0} + a_{n,1}\delta + a_{n,2}\delta^2 + \ldots \,. \tag{6.15}$$

We impose the boundary values (6.13) by requiring that

$$a_{0,0} \equiv 0 \quad \text{and} \quad a_{n,0} \equiv 1 \ (n \geq 1). \tag{6.16}$$

Inserting the ansatz (6.15) into the difference equation (6.12), we get the recursion relation [63]

$$a_{n,j} = \frac{1}{2}a_{n+1,j-1} + a_{n,j-1} + \frac{1}{2}a_{n-1,j-1} - \sum_{k=1}^{j-1} a_{n,k}a_{n,j-k} - \frac{1}{2}\sum_{k=1}^{j-1}\sum_{l=1}^{j-k} a_{n,k}a_{n,l}a_{n,j-k-l}. \tag{6.17}$$

For the first derivative at the origin $x = 0$ this leads to the series

$$\begin{aligned} f'(0) &= \lim_{a\to 0}\frac{f_1 - f_0}{a} = \lim_{a\to 0}\frac{f_1}{a} = \lim_{a\to 0}\frac{1}{a}\sum_{j=0}^{\infty} a_{1,j}\delta^j \\ &= \lim_{a\to 0}\frac{1}{a}\left(1 - \frac{\delta}{2} + \frac{\delta^2}{8} + \frac{11\delta^4}{128} + ...\right). \end{aligned} \tag{6.18}$$

We have calculated the coefficients $a_{n,j}$ with the help of `Maple V R7` up to order $j = 200$. A complete list of these coefficients can be found on the webpage of the author FW [66]. The first 20 numbers are given in Table 6.1. Note that the expansion parameter δ in (6.18) is not small but rather tends to infinity in the limit as the lattice spacing a approaches zero. Using the parameter δ defined in (6.14) we rewrite the series (6.18) as

$$f'(0) = \frac{1}{\epsilon}\lim_{\delta\to\infty}\sqrt{\delta}\left(1 - \frac{\delta}{2} + \frac{\delta^2}{8} + \frac{11\delta^4}{128} + ...\right). \tag{6.19}$$

Taking into account the exact result (6.10), we obtain the identity

$$\frac{1}{\sqrt{2}} = \lim_{\delta\to\infty}\sqrt{\delta}\left(1 - \frac{\delta}{2} + \frac{\delta^2}{8} + \frac{11\delta^4}{128} + ...\right). \tag{6.20}$$

The purpose of this chapter is to examine equations like (6.20). This equation shows that the singular nature of the instanton problem has resurfaced in the continuum limit $\delta \to \infty$ of the lattice expansion. The expression on the right side of (6.20) should have the value $1/\sqrt{2} = 0.7071067812\ldots$, but it is not at all obvious why this is so, and the objective of this chapter is to analyze this difficult and subtle limit.

This chapter is organized as follows. In Section 6.1 we use Padé techniques [63] to perform the limit in (6.20). We will see that while the results are not bad (the accuracy is about 1%), better methods are needed. We perform the Padé analysis to much higher order than has ever been done before and we discover a new qualitative behaviour that has not yet been observed. In Section 6.2 we use of the variational perturbation theory techniques introduced by H. Kleinert to perform the sum in (6.20). These techniques increase the accuracy by a factor of about 10, but they still do not give the exact result. While variational perturbation

j	$a_{1,j}$	j	$a_{1,j}$
1	$-\frac{1}{8}$	11	$-\frac{2887747}{262144}$
2	$\frac{1}{8}$	12	$\frac{99392471}{4194304}$
3	0	13	$-\frac{215798295}{4194304}$
4	$\frac{11}{128}$	14	$\frac{3781670831}{33554432}$
5	$-\frac{23}{128}$	15	$-\frac{8349041385}{33554432}$
6	$\frac{295}{1024}$	16	$\frac{1188129285795}{2147483648}$
7	$-\frac{589}{1024}$	17	$-\frac{2659104132291}{2147483648}$
8	$\frac{39203}{32768}$	18	$\frac{47890245452569}{17179869184}$
9	$-\frac{80723}{32786}$	19	$-\frac{108383753179167}{17179869184}$
10	$\frac{1354949}{262144}$	20	$\frac{39433620359113981}{274877906944}$

Table 6.1: The first 20 weak-coupling coefficients $a_{1,j}$ for the instanton problem (6.16) and (6.17).

theory works very well in summing the strong-coupling series for the ground state energy of the anharmonic oscillator [2], and for critical exponents of second-order phase transitions [8], we show that the series in (6.20) is at the very edge of validity for Kleinert's methods. We then examine the large-order behaviour of the terms of the sum in (6.20) in Section 6.3. We show definitively that the Taylor expansion has a nonzero radius of convergence and thus, on the lattice, the instanton problem is a regular perturbation problem.
In Section 6.4 we turn to a more difficult singular perturbation problem; namely, the Blasius equation of fluid dynamics. We use the same approach as for the instanton equation. In Sections 6.5, 6.6, and 6.7 we study the summation of the lattice perturbation expansion using Padé and variational methods and we examine the large-order behaviour of the lattice perturbation series. We find that Padé methods give good but not excellent results and that variational perturbation theory is better than Padé. Again, the series that we need to evaluate in the continuum limit lies at the very edge of validity for Kleinert's methods. We also find that, unlike the lattice perturbation expansion coefficients for the instanton problem, the sign pattern of the Blasius weak-coupling series does not alternate. Rather, it is governed by a cosine function with a frequency different from π.

6.1 Padé Resummation for the Instanton Equation

In this section we examine what happens if we attempt to evaluate the right side of (6.20) by using Padé techniques. Padé resummation has already been applied to the instanton problem up to 50th order [63]. However, we have been able to perform the procedures to

N	S_N	N	S_N
1	1	11	0.709998411
2	0.840896415	12	0.708235422
3	0.781934407	13	0.706789935
4	0.757237797	14	0.705659505
5	0.740759114	15	0.704734605
6	0.731210449	16	0.704006945
7	0.723927185	17	0.703419862
8	0.719045188	18	0.702964717
9	0.715146335	19	0.702610220
10	0.712308458	20	0.702349024

Table 6.2: The first 20 Padé approximants for the solution to the instanton problem (6.20).

much higher order. We have discovered that remarkable and unsuspected new phenomena occur just a few orders beyond what has been computed previously.
The procedure is as follows. Consider the formal Frobenius series

$$S(\delta) = \delta^M \sum_{n=0}^{\infty} a_n \delta^n, \tag{6.21}$$

where M is a non-negative number. Raising this series to the power $1/M$, inverting the right hand side and re-expanding, we obtain

$$S^{1/M}(\delta) = \frac{\delta}{\sum_{n=0}^{\infty} b_n \delta^n}, \tag{6.22}$$

with new expansion coefficients b_n. Assuming we know the first $N+1$ terms of the original power series in (6.21), we raise equation (6.22) to the power N. We then truncate the summation at $n = N$, finally getting

$$S^{N/M}(\delta) = \frac{\delta^N}{\sum_{n=0}^{N} c_n^{(N)} \delta^n}, \tag{6.23}$$

where we have re-expanded and obtained new expansion coefficients $c_n^{(N)}$. In the limit $\delta \to \infty$, only the Nth term in the denominator survives and we obtain the approximant

$$(S_N)^{N/M} \equiv \lim_{\delta\to\infty} S^{N/M}(\delta) = \lim_{\delta\to\infty} \frac{\delta^N}{\sum_{n=0}^{N} c_n^{(N)} \delta^n} = \frac{1}{c_N^{(N)}}. \tag{6.24}$$

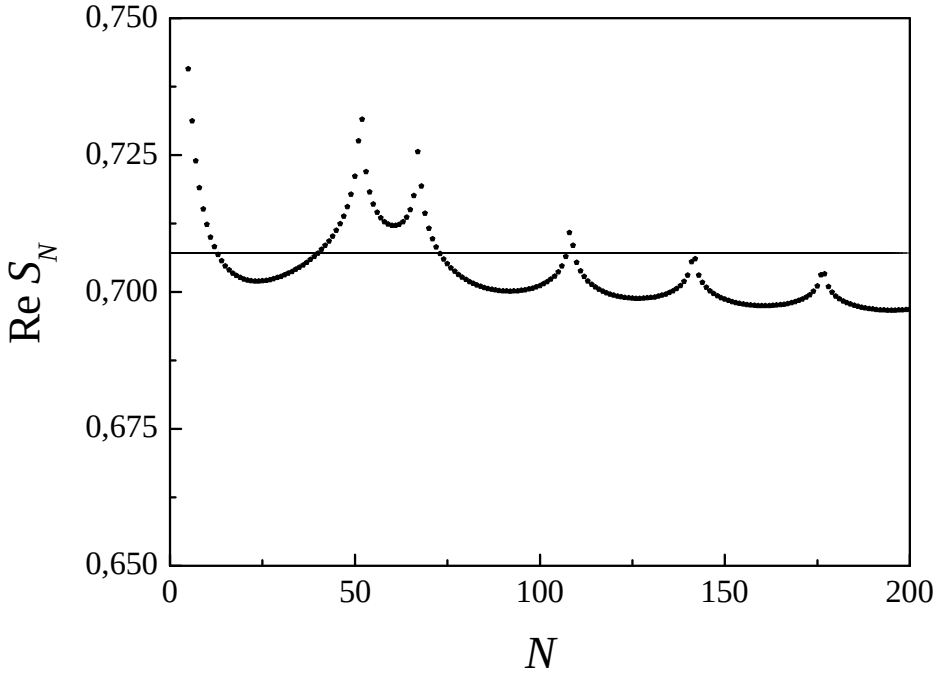

Figure 6.1: The real part of the Padé approximants S_N up to 200th order. Note that the approximants do not converge to the exact solution, which is represented by the horizontal solid line. The phases where the approximants become complex are marked by spikes.

The approximant $S_N = \left(c_N^{(N)}\right)^{-M/N}$ is the zeroth-order survivor of the limiting process. Also, taking into account the first-order correction we observe that, as in the case of variational perturbation theory (see Section 6.2), there is an approach to scaling. In the limit $\delta \to \infty$ the Frobenius series $S(\delta)$ in equation (6.21) converges to a constant C. Additionally, the approach to scaling, following from the Padé resummation (6.24), reveals how fast it converges:

$$S(\delta) \sim C + C'\delta^{-1} \quad (\delta \to \infty). \tag{6.25}$$

We now apply this procedure to the boundary-layer problem (6.12). (Recall that the weak-coupling coefficients for the first 20 coefficients $a_{1,j}$ obtained from (6.17) are shown in Table 6.1 and that more can be found in [66].) Resumming the series (6.15) for $n = 1$,

$$f_1 = \sum_{j=0}^{N} a_{1,j}\delta^j, \tag{6.26}$$

according to the Padé procedure (6.24) with $M = 1/2$ as follows from (6.20) and evaluating the approximants $S_N = \left(c_N^{(N)}\right)^{-M/N}$, we get the numbers listed in Table 6.2.

Compared with the numerical solution $1/\sqrt{2} \approx 0.7171067812...$, this strong-coupling expansion seems to converge quite well. However, when we go to higher orders, we find that the numbers drop below the exact solution and assume a minimum at $N = 24$, where the approximant has the value $S_{24} \approx 0.70198319$. The approximants then rise again, cross the exact solution at $N = 41$ and become complex at $N = 52$. The appearance of complex numbers is a consequence of taking the Nth root in equation (6.24) when the coefficients $c_N^{(N)}$ become negative. This phenomenon has not been observed before in the course of using this Padé procedure. The imaginary part then becomes smaller and smaller as N rises. Abruptly, at $N = 68$, the approximants become real again. As one can see from the spikes in Figure 6.1 this pattern is repeated for higher N. Note that the figure only shows the real part of the Padé approximant S_N.
Apparently, the sequence of approximants S_N does not converge. The singular nature of the instanton equation has the effect of making the Padé approximants behave like the partial sums of a divergent (asymptotic) series; at first the partial sums appear to converge to a limit, and then they veer off. In the case of the Padé's shown in Figure 6.1 the approximants approach to within 1% of the correct limit before veering off. It appears that another more powerful resummation technique is needed to treat the expression in (6.20). In the next section we apply a technique due to Kleinert.

6.2 Variational Perturbation Theory for the Instanton Equation

As seen in Chapter 4 where we discussed the free energy of the anharmonic oscillator we now have to derive the numbers p and q again in order to fix the leading power behaviour p/q and the approach to scaling $2/q$ according to [2]:

$$\sum_{j=0}^{\infty} a_j \delta^j \sim \delta^{p/q} \left(b_0 + b_1 \delta^{-2/q} + ... \right) \quad (\delta \to \infty). \tag{6.27}$$

For the instanton equation we do this by re-obtaining the differential equation (6.7) from the difference equation (6.12). The positive real axis is discretized in steps of width a, so that we let $x_n \equiv na$. The power series expansion for the discrete function $f_n = f(x_n)$ has the form

$$f_{n\pm1} = f(x_n) \pm f'(x_n)a + \frac{1}{2} f''(x_n)a^2 \pm \frac{1}{6} f'''(x_n)a^3 + \frac{1}{24} f''''(x_n)a^4 \pm \dots . \tag{6.28}$$

Thus, the numerator of the second derivative (6.11) becomes

$$f_{n+1} - 2f_n + f_{n-1} = f_n'' a^2 + \frac{1}{12} f_n'''' a^4 + \dots , \tag{6.29}$$

N	$b_0^{(N)}$	N	$b_0^{(N)}$
180	0.707530492	190	0.707471024
181	0.707524250	191	0.707465419
182	0.707518076	192	0.707459872
183	0.707511970	193	0.707454384
184	0.707505930	194	0.707448952
185	0.707499955	195	0.707443575
186	0.707494044	196	0.707438253
187	0.707488197	197	0.707432986
188	0.707482412	198	0.707427771
189	0.707476687	199	0.707422609

Table 6.3: The last 20 variational strong-coupling coefficients $b_0^{(N)}$ from equation (6.40).

order	value for $b_0^{(N)}$	convergence
1	0.70640049	decreasing
2	0.70639983200	increasing
3	0.706399832082	increasing
4	0.7063998320858658	increasing
5	0.706399832085884411	increasing
6	0.7063998320858844 98	increasing

Table 6.4: Six orders of Richardson extrapolations for the strong-coupling coefficient $b_0^{(N)}(k_0)$ up to $N = 200$ for the instanton problem. The last value is only 0.099% away from the correct limiting value $1/\sqrt{2} = 0.7071067812\ldots$.

so the zeroth-, first-, and third-order contributions cancel. Translating the lattice result for f_n back to the continuous function $f(x_n) = f_n$, the difference equation (6.12) reads

$$\epsilon^2 \left[f''(x) + \frac{1}{12} f''''(x) a^2 + \ldots \right] + f(x) - f^3(x) = 0 \,. \tag{6.30}$$

Writing out the power series

$$f(x) = f_0(x) + a^2 f_1(x) + a^4 f_2(x) + \ldots \,, \tag{6.31}$$

and comparing even powers of a, we get from equation (6.30) for a^0

$$\epsilon^2 f_0''(x) + f_0(x) - f_0^3(x) = 0 \,, \tag{6.32}$$

which is just the original instanton equation (6.7), whereas for a^2 we have

$$\epsilon^2 f_1''(x) + f_1(x) \left(1 - 3 f_0^2(x)\right) = -\frac{1}{12} \epsilon^2 f_0''''(x) \,. \tag{6.33}$$

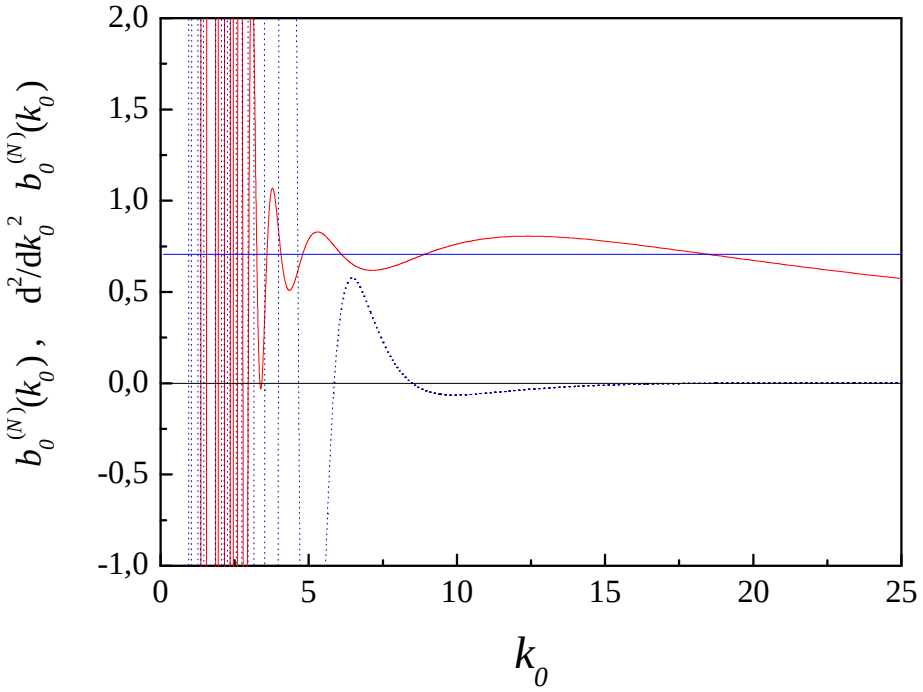

Figure 6.2: The function $b_0^{(N)}(k_0^{(N)})$ from (6.40) for $N = 200$ (solid line) and its second derivative with respect to $k_0^{(N)}$ (dotted line). The upper horizontal line equals $1/\sqrt{2}$, the correct limiting value of the instanton problem. All extrema of $b_0^{(N)}(k_0^{(N)})$ are far from this value. Only the inflection point on the right-hand side comes close. The value for $k_0^{(N)}$, for which the second derivative vanishes, is $k_0^{(N)} = 18.42510$. Substituting that number into the function $b_0^{(N)}(k_0^{(N)})$, we obtain $b_0^{(200)} = 0.707417$. The corresponding Richardson extrapolations can be found in Table 6.4.

The boundary values read

$$f_0(0) = 0\,, \qquad f_0(\infty) = 1\,, \tag{6.34}$$

and

$$f_1(0) = f_1(\infty) = 0\,, \tag{6.35}$$

respectively. The solution to equation (6.32) with the boundary values (6.34) is of course

$$f_0(x) = \tanh \frac{x}{\epsilon\sqrt{2}}\,. \tag{6.36}$$

So, finally from (6.31) we get for the derivative at the origin $x = 0$:

$$f'(0) = f_0'(0) + \frac{\epsilon^2}{\delta} f_1'(0) + \ldots = \frac{1}{\epsilon\sqrt{2}} + \frac{\epsilon^2}{\delta} f_1'(0) + \ldots\,. \tag{6.37}$$

Comparing equation (6.37) with (6.19), we resum the weak-coupling series in (6.19) as

$$1 - \frac{\delta}{2} + \frac{\delta^2}{8} + ... = \delta^{-1/2} \left[\frac{1}{\sqrt{2}} + \epsilon^3 f_1'(0) \delta^{-1} + ... \right] . \tag{6.38}$$

Also, comparing with (6.27), we conclude that the leading power and the approach to scaling are given by

$$\frac{p}{q} = -\frac{1}{2}, \qquad \frac{2}{q} = 1 \, , \tag{6.39}$$

respectively. So we read off $p = -1$ and $q = 2$.
We now evaluate the leading strong-coupling coefficient b_0 from (6.27) according to (4.48),

$$b_0^{(N)}(k_0^{(N)}) = \sum_{n=0}^{N} (-1)^{N-m} \binom{\frac{1}{2}(p - nq) - 1}{N - n} f_n (k_0^{(N)})^{p-iq}, \tag{6.40}$$

with $p = -1$ and $q = 2$. To that end we substitute our 200 weak-coupling coefficients into the formula using a computer algebra program. Now we are confronted with the following problem: The principle of least sensitivity cannot be unambiguously applied. Optimizing with respect to extrema, inflection points, or higher derivatives does yield converging results for the strong-coupling limit. However, all these strong-coupling series converge to the wrong values.
There is one very unpleasant case: The second derivative with respect to $k_0^{(N)}$ for the largest $k_0^{(N)}$ where this derivative exists (see Figure 6.2) gives a convergent strong-coupling series. The numbers come extremely close to $1/\sqrt{2}$ as one can see from the 20 numbers in Table 6.3. The 200th leading strong-coupling coefficient is $b_0^{(200)} = 0.707417....$ However, a Richardson extrapolation [53] based on the first 200 orders then unfortunately shows that variational perturbation theory produces a value slightly smaller than $1/\sqrt{2}$. The first six orders of Richardson extrapolations are presented in Table 6.4. Hence, the strong-coupling series $b_0^{(N)}$ does converge, but it converges to the wrong number, only one part per 1000 away from the true value:

$$f_1^{(\mathrm{VPT})} \approx \lim_{\delta \to \infty} \sum_{n=0}^{200} a_{1,n} \delta^n = b_0^{(\infty)} = 0.7063998320858845 \pm 0.0000000000000001 \tag{6.41}$$

compared with $f'(0) = 1/\sqrt{2} = 0.7071067812...$. The deviation is just 0.099%, but $1/\sqrt{2}$ can unfortunately be ruled out.
Given $p = -1$ and $q = 2$, the failure of variational perturbation theory is not surprising. According to Ref. [8] the fraction $2/q$ must lie within the open interval $(1/2, 1)$. Otherwise, one cannot prove that variational perturbation theory converges. Thus, this problem lies exactly on the boundary of the region in which the summation method is known to work.
We can understand the upper edge of the range of the parameter $2/q$ that describes the approach to scaling $2/q$ by looking at the standard deviation from the actual limiting value.

order	value for A	convergence
1	-1.4998	increasing
2	-1.500017	decreasing
3	-1.5000011	decreasing
4	-1.49999874	increasing
5	-1.5000004	decreasing
6	-1.499999893	increasing

Table 6.5: Six orders of Richardson extrapolations for the exponent A of the large-order instanton weak-coupling coefficients, based on the first 200 weak-coupling coefficients. The value $A = -3/2$ is quite plausible.

It turns out [8] that the deviation in the limit as the perturbative order N goes to infinity assumes the shape

$$\left| \frac{b_0^{(N)} - b_0}{b_0} \right| \sim \exp\left(-CN^{1-2/q}\right) \quad (N \to \infty)\,, \tag{6.42}$$

where C is a constant. So, to obtain exponential convergence for the sequence formed by the $b_0^{(N)}$, we need $1 - 2/q > 0$. In other words, the approach to scaling $2/q$ is bounded and it must be smaller than one. The lower edge is more subtle and is discussed in Ref. [8].
In conclusion, we have applied variational perturbation theory to a case that lies at the very edge of its applicability. We see that variational perturbation theory gives better results by about a factor of 10 than the Padé approximations examined in Section 6.1. However, we have not yet found a systematic method for resumming (6.20) that enables us to perform the continuum limit of the discrete lattice theory up to an arbitrary accuracy. Therefore, we now lay the foundation for further investigations by analyzing the large-order behaviour of the instanton series.

6.3 Large-Order Behaviour for the Instanton Equation

It can be seen from the numerical results in [66] that the instanton weak-coupling series is of Borel type. That is, it exhibits an alternating sign pattern. From the ratio test we can see that the coefficients $a_{n,j}$ do not grow factorially fast. The large-order behaviour of $a_{n,j}$ has the general form

$$a_{n,j} \sim (-1)^{n+j+1} K_n^j j^{A_n} B_n \quad (j \to \infty). \tag{6.43}$$

The constant A_n can be obtained by evaluating the limit

$$A_n = \lim_{j\to\infty} \frac{\log \dfrac{a_{n,j+2}\, a_{n,j}}{(a_{n,j+1})^2}}{\log \dfrac{j(j+2)}{(j+1)^2}}\,, \tag{6.44}$$

order	value for K	convergence
1	2.46692	decreasing
2	2.4668283	increasing
3	2.46682911	decreasing
4	2.466829065	decreasing
5	2.4668290597	increasing
6	2.4668290635	decreasing

Table 6.6: Six orders of Richardson extrapolations for the inverse radius of convergence K of the large-order instanton weak-coupling coefficients, based on the first 200 weak-coupling coefficients under the assumption that $A = -3/2$.

order	value for B_1	convergence
1	0.0170837	increasing
2	0.0170864	increasing
3	0.017087	increasing
4	0.0170893	increasing
5	0.0170908	increasing
6	0.0170922	increasing

Table 6.7: Six orders of Richardson extrapolations for the overall factor B_1 of the large-order instanton weak-coupling coefficients, based on the first 200 weak-coupling coefficients and under the assumption that $K = 2.4482906$ and $A = -3/2$. The value of B_1 strongly depends on the numerical values for A and K. Changing K in the sixth decimal place influences the third significant figure of B_1. Also, all the Richardson extrapolations are increasing so, strictly speaking, we only have a lower boundary for B_1. Thus, the accuracy of B_1 may not be very good.

and the reciprocal of the radius of convergence is

$$K_n = -\lim_{j\to\infty} \frac{a_{n,j+1}}{a_{n,j}} \left(\frac{j}{j+1}\right)^{A_n} . \tag{6.45}$$

Also, the overall factor B_n is determined from

$$B_n = \lim_{j\to\infty} \frac{|a_{n,j}|}{K_n^j j^{A_n}} . \tag{6.46}$$

Using the 200 weak-coupling coefficients, we find that the exponent A_n and the reciprocal radius of convergence K_n are independent of n. The value of $K_2 = 2.46682906$ coincides with $K_1 = 2.46682906$ for all significant digits. The same is true for $A_1 = -1.500000$ and $A_2 = -1.500000$. Thus, it appears that we may omit the subscripts n for K_n and A_n. In contrast, the data suggests that B_n strongly depends on n. B_n is the numerical value associated with the largest uncertainty. In fact, equation (6.46) suggests that small

order	value for B_2	convergence
1	0.119069	increasing
2	0.119083	increasing
3	0.119093	increasing
4	0.119054095	increasing
5	0.119054125	increasing
6	0.119054146	increasing

Table 6.8: Six orders of Richardson extrapolations for the overall factor B_2 of the large-order instanton weak-coupling coefficients based on the first 200 weak-coupling coefficients under the same assumptions as in the case of B_1 (see Table 6.7). The value of B_2 depends strongly on A and K.

deviations in K and A lead to dramatic changes in the value of B_n. Therefore $B_n = B$ cannot be ruled out completely. We calculated A, K, B_1, and B_2 up to 200th order with the help of `Maple V R7`. We then extrapolated these 200 orders to infinity using Richardson extrapolation [53]. We obtained

$$\begin{aligned} A &= -1.500000 \pm 0.000001\,, \\ K &= 2.46682906 \pm 0.0000001\,, \\ B_1 &= 0.0171 \pm 0.0001\,, \\ B_2 &= 0.1190 \pm 0.0001\,. \end{aligned} \tag{6.47}$$

Detailed numerical results for the first three Richardson extrapolations for the exponent A, the inverse radius of convergence K, and the overall factors B_1, B_2 can be found in Tables 6.5, 6.6, 6.7, and 6.8. The calculation of B_1 and B_2 is extremely delicate; changing the inverse radius of convergence in the sixth decimal place influences the third significant figure of B_1.

Unfortunately, there is no way to derive these values by applying an asymptotic analysis to the recursion relation (6.17). The problem is that the double summation in this equation includes small j, so we cannot let j go to infinity and use the large-order behaviour (6.43). Substituting the ansatz (6.43) into equation (6.17) and taking the limit leads to contradictory results. For $n = 1$ we get

$$\begin{aligned} K j^A B_1 &= \frac{1}{2}(j-1)^A B_2 + (j-1)^A B_1 - \frac{3}{2} B_1^2 K \sum_{k=1}^{j-1} k^A (j-k)^A \\ &\quad - \frac{1}{2} B_1^3 K \sum_{k=1}^{j-1} \sum_{l=1}^{j-k} k^A l^A (j-k-l)^A\,. \end{aligned} \tag{6.48}$$

Pulling out some factors and letting $x \equiv k/j$, we obtain for the first summation

$$\lim_{j\to\infty} \sum_{k=1}^{j} \left(\frac{k}{j}\right)^A \left(1 - \frac{k}{j}\right)^A = \int_0^1 dx\, [x(1-x)]^A = \frac{\Gamma^2(A+1)}{\Gamma(2A+2)}\,, \tag{6.49}$$

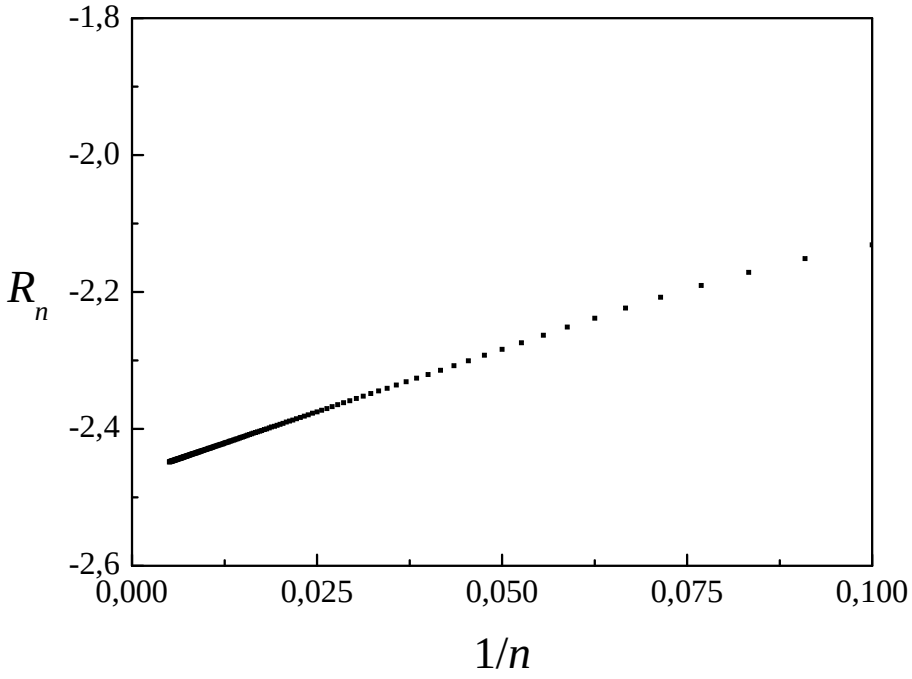

Figure 6.3: One can obtain the inverse ratio of convergence K by applying methods normally used for critical exponents. Plotting the ratio $R_n = a_{1,n+1}/a_{1,n}$ versus $1/n$ gives K as the offset of the linear regression and its slope is the exponent α, according to (6.55).

if and only if $A > -1$. For $A < -1$ which is strongly favored by the data we obtain

$$\int_0^1 dx\,[x(1-x)]^A = 2\zeta\,(-A)\;. \tag{6.50}$$

The double summation reduces to

$$\lim_{j\to\infty}\sum_{k=1}^{j}\sum_{l=1}^{j-k}\frac{k^A l^A}{j^{2A}}\left(1-\frac{k}{j}-\frac{l}{j}\right) = \int_0^1 dx\int_0^1 dy\,[xy(1-x-y)]^A = \frac{\Gamma^3(A+1)}{\Gamma(3A+3)}\,, \tag{6.51}$$

where $y \equiv l/j$ and $A > -1$. For $A < -1$ the result is

$$\int_0^1 dx\int_0^1 dy\,[xy(1-x-y)]^A = 3\zeta^2\,(-A)\;. \tag{6.52}$$

Substituting the results in (6.50) and (6.52) into (6.48) leads to a contradiction: The inverse radius of convergence then turns out to be

$$K = \frac{1+\frac{B_2}{2B_1}}{1+3\zeta\left(\frac{3}{2}\right)B_1+\frac{3}{2}\zeta^2\left(\frac{3}{2}\right)B_1^2}\,, \tag{6.53}$$

which would imply that, given $B_1 = 0.0171$ and $B_2 = 0.1190$, the value of K would be

$$K = 3.940\,. \tag{6.54}$$

This result can be ruled out because of the numerical result (6.47). Also, (6.53) does not contain the exponent A because all the factors j^A in (6.48) cancel. So A cannot be determined analytically using this asymptotic analysis.
The inverse radius of convergence K can also be obtained in a different manner from that usually employed for critical phenomena. According to Ref. [8], the ratio $R_j \equiv a_{j+1}/a_j$ approaches the inverse radius of convergence as

$$R_j = -K\left(1 + \frac{1}{j}\right)^{\alpha}\,, \tag{6.55}$$

where α is some exponent. So, if we plot R_n versus $1/n$, then the slope of the linear regression is α and the offset is K, as one can see in Figure 6.3. We get

$$K = 2.46656 \pm 0.00001 \quad \text{and} \quad \alpha = 3.6598 \pm 0.0007\,. \tag{6.56}$$

This value for K differs from the number in (6.47) in the fifth digit. The difference is due to not taking into account the factor j^A as in (6.43) and (6.45).

6.4 Boundary-Layers on the Lattice — Blasius Equation

The Blasius equation [67] arises in the study of fluid dynamics. It is a special limiting case of the Navier-Stokes equation and determines the flow of an incompressible fluid across a semi-infinite flat plate. The Blasius equation reads

$$2\epsilon y'''(x) + y(x)y''(x) = 0\,. \tag{6.57}$$

Assuming that the tangential velocity $y'(x)$ at the outer limit of the boundary layer is constant, the boundary conditions read [68]

$$y(0) = y'(0) = 0\,, \qquad y'(\infty) = 1\,. \tag{6.58}$$

Our objective here is to calculate the second derivative $y''(0)$, which represents the stress on the plate. We discretize the Blasius equation (6.57) by introducing a lattice spacing a:

$$2\delta(f_{n+1} - 3f_n + 3f_{n-1} - f_{n-2}) + f_n(f_{n+1} - 2f_n + f_{n-1}) = 0\,, \tag{6.59}$$

where we define $f_n \equiv y(na)/a$ and $\delta \equiv \epsilon/a^2$. The boundary conditions (6.58) now read

$$f_0 = f_{-1} = 0\,, \qquad f_n \sim n \quad (n \to \infty)\,. \tag{6.60}$$

Expanding f_n as a series in powers of δ as in equation (6.15), we obtain the recursion relation [63]

$$\begin{aligned} a_{n+1,j} - 2a_{n,j} + a_{n-1,j} &= -\frac{2}{n}\left(a_{n+1,j-1} - 3a_{n,j-1} + 3a_{n-1,j-1} - a_{n-2,j-1}\right) \\ &\quad -\frac{1}{n}\sum_{k=1}^{j-1} a_{n,k}\left(a_{n+1,j-k} - 2a_{n,j-k} + a_{n-1,j-k}\right) . \end{aligned} \tag{6.61}$$

The boundary values are

$$\begin{aligned} a_{n,0} &= n \ (n \geq 0) , \\ a_{-1,0} &= 0 , \\ a_{-n-1,j} &= a_{n,j} \ (n \geq 0) . \end{aligned} \tag{6.62}$$

Equations (6.61) and (6.62) can be solved order by order by using a computer algebra program. Table 6.9 shows the first 20 weak-coupling coefficients $a_{1,j}$. All coefficients up to the 300th order can be found at [69].

6.5 Padé Resummation for the Blasius Equation

We now resum the weak-coupling coefficients using the Padé method (6.24) with $M = -1/2$. This value of M will be derived in Section 6.6 in equation (6.69). The exact solution [63] to the Blasius equation (6.57), obtained numerically up to five digits, is $y''(0) = 0.33206$. Unfortunately, the sequence formed by the approximants S_N appears to converge, but not to the correct value. According to Table 6.10 the sequence becomes very flat and Richardson extrapolation [53] shows that the S_N approach the wrong limiting value (see Table 6.11). A third-order Richardson gives $S_\infty = 0.3430$, based on the first 70 weak-coupling coefficients. This value is significantly higher than the correct value $y''(0) = 0.33206$.
The failure of the Padé resummation is not surprising because the Padé method assumes the approach to scaling δ^{-1} according to (6.25). However, in the case of the Blasius equation the approach to scaling is $\delta^{-1/2}$, as we will see in equation (6.69) in the next section.

6.6 Variational Perturbation Theory for the Blasius Equation

Variational perturbation theory for the Blasius equation fails to converge to the correct answer in the same way as for the instanton problem. We determined the leading strong-coupling term (6.40) up to 300th order and again it was impossible to find extrema, inflection points, or higher derivatives that yield the correct result. By determining the values of p and q we show why variational perturbation is likely to fail for this problem.

j	$a_{1,j}$	j	$a_{1,j}$
1	-2	11	$\frac{30868632383}{5457375}$
2	2	12	$\frac{6325029622}{637875}$
3	$\frac{8}{3}$	13	$-\frac{487693745019181}{13408770375}$
4	-6	14	$-\frac{4774319527974167}{37819608750}$
5	$-\frac{184}{15}$	15	$\frac{430321251088745734}{2212447111875}$
6	$\frac{136}{9}$	16	$\frac{796235344548876790517}{603998061541875}$
7	$\frac{11062}{105}$	17	$-\frac{22499880545067641745840 49}{6776858250499837500}$
8	$-\frac{8162}{225}$	18	$-\frac{178060537619150189817796}{14237097164915625}$
9	$-\frac{10557416}{14175}$	19	$-\frac{132248961522197296674980 38639}{1301909768346024337500}$
10	$-\frac{57628622}{99225}$	20	$\frac{121756993154067534451733120837029}{1153217968487557347375000}$

Table 6.9: The first 20 weak-coupling coefficients for the Blasius recursion relation (6.61) and (6.62). Observe that the coefficients $a_{1,j}$ are not of Borel type (they do not alternate in sign). A cosine function with a frequency different from π governs the sign pattern (see Section 6.7).

Consider again the Taylor expansions for $f_{n\pm1}$ in (6.28) together with the Taylor series for $f_{n-2} = f(x_n - 2a)$, namely

$$f_{n-2} = f(x_n) - 2f'(x_n)a + 2f''(x_n)a^2 - \frac{4}{3}f'''(x_n)a^3 + \frac{2}{3}f''''(x_n)a^4 \pm \dots . \tag{6.63}$$

Inserting these expressions into the difference equation for the Blasius problem (6.59) and translating back to the continuous function $f(x_n) = f_n$, we get

$$2\epsilon\left(f'''(x)a - \frac{1}{2}f''''(x)a^2 + \dots\right) + f(x)\left(f''(x)a^2 + \frac{1}{2}f''''(x)a^4 + \dots\right) = 0 . \tag{6.64}$$

Next we transform back to the function $y(x) = af(x)$ and assume the Taylor series

$$y(x) = y_0(x) + ay_1(x) + a^2y_2(x) + \dots . \tag{6.65}$$

To zeroth order in a we obtain

$$2\epsilon y_0'''(x) + y_0(x)y_0''(x) = 0 , \tag{6.66}$$

which is just the Blasius equation (6.57). The small parameter a, which is the lattice spacing, relates ϵ and δ by $a = \sqrt{\epsilon/\delta}$. Thus, if we evaluate the Taylor series (6.65) for the second

N	S_N	N	S_N
1	0.5	11	0.3574632121
2	0.4204482076	12	0.3563326651
3	0.3948201830	13	0.3553848048
4	0.3819443732	14	0.3545795944
5	0.3742062309	15	0.3538882842
6	0.3690504811	16	0.3532891509
7	0.3653779673	17	0.3527655813
8	0.3626359060	18	0.3523046588
9	0.3605155915	19	0.3518961929
10	0.3588309707	20	0.3515320399

Table 6.10: The first 20 Padé approximants for the solution to the Blasius equation (6.61). The sequence formed by the S_N converges extremely slowly.

order	value of $y''(0)$	convergence
1	0.3445	decreasing
2	0.3436	decreasing
3	0.3430	oscillating

Table 6.11: Three orders of Richardson extrapolations for the Blasius equation (6.57), based on the first 70 Padé approximants S_N.

derivative at the origin, we see that

$$y''(0) = y_0''(0) + a y_1''(0) + ... = \frac{0.33206}{\sqrt{\epsilon}} + \sqrt{\frac{\epsilon}{\delta}} y_1''(0) + ... \,. \tag{6.67}$$

Comparing this series to the original weak-coupling series

$$y''(0) = \sqrt{\frac{\delta}{\epsilon}} \left(1 - 2\delta + 2\delta^2 + ...\right) \,, \tag{6.68}$$

we can now determine the leading power p/q and the approach to scaling $2/q$:

$$1 - 2\delta + 2\delta^2 + ... = \delta^{-1/2} \left(0.33206 + \delta^{-1/2} \epsilon y_1''(0) + ...\right) \,, \tag{6.69}$$

so we obtain $p = -2$ and $q = 4$.
Again we find that the approach to scaling $2/q = 1/2$ lies just on the boundary of the open interval $(1/2, 1)$, for which the proof of convergence [8] holds. This situation here is the opposite of the instanton case in that it sits at the *lower* boundary of the open interval in which variational perturbation theory works. Table 6.12 shows some variational results for (6.27) in the Blasius case. The numbers were obtained by searching for extrema. Unfortunately they do not aim at the correct limiting value, as one can see from the Richardson

N	$b_0^{(N)}$	N	$b_0^{(N)}$
180	0.33696017793094	190	0.33695971119646
181	0.33696012777085	191	0.33695966849139
182	0.33696007843082	192	0.33695962644843
183	0.33696002989308	193	0.33695958505396
184	0.33695998214034	194	0.33695954429471
185	0.33695993515575	195	0.33695950415774
186	0.33695988892292	196	0.33695946463046
187	0.33695984342591	197	0.33695942570058
188	0.33695979864918	198	0.33695938735612
189	0.33695975457760	199	0.33695934958540

Table 6.12: The last 20 variational strong-coupling coefficients $b_0^{(N)}$ for the Blasius equation. The very last coefficient is $b_0^{(200)} = 0.33695931237713$, as opposed to the correct value $y''(0) = 0.33206$.

order	value for $b_0^{(N)}$	convergence
1	0.3369518	increasing
2	0.336955563	increasing
3	0.336955600539	increasing
4	0.3369556008803	increasing
5	0.336955600883462	increasing
6	0.33695560088349232	increasing

Table 6.13: Six orders of Richardson extrapolations for the strong-coupling coefficient $b_0^{(N)}(k_0)$ up to $N = 200$ for the Blasius equation. The last value is 1.5% away from the correct limiting value $y''(0) = 33206$.

extrapolations in Table 6.13.
Still the accuracy of the variational perturbative calculations is considerably higher than the one of the Padé resummation. The latter one is 5.9% away from the correct result whereas variational perturbation theory only deviates by 1.5%.

6.7 Large-Order Behaviour for the Blasius Equation

The Blasius equation exhibits a large-order behaviour which is a more subtle than for the instanton problem (6.43). As one can see from Table 6.9, the Blasius weak-coupling coefficients are not of Borel type; that is, the sign pattern is not alternating. Rather, the sign structure is governed by a cosine function with a frequency that is significantly different from π. Remarkably, it turns out that a pure cosine $\cos(an)$ cannot reproduce all signs correctly. Up to 300th order the sign structure given by $\cos(an)$ is broken twice: The signs at $n = 62$ and at $n = 212$ are not correct. So we must consider an additional phase shift $\cos(an + b)$.

a	b
1.3941	3.09
1.3939	3.11
7.67830	3.031
7.67686	3.130

Table 6.14: Examples of the parameters a and b that give the first 300 signs of the Blasius weak-coupling coefficients correctly, assuming that the sign structure of the underlying large-order behaviour is of the form $\cos(an+b)$. The last two values for a can be obtained approximately by summing 2π to the first two values.

The parameter b turns out to be slightly smaller than π, but it reproduces all 300 signs correctly.
In order to determine the numerical values of a and b we define

$$f(a,b) \equiv \sum_{n=1}^{N} \frac{\cos(an+b)}{|\cos(an+b)|} \frac{a_{1,n}}{|a_{1,n}|} \,. \tag{6.70}$$

The sum ends at $N = 300$ because this is as high as we can calculate using `Maple`; we know the first 300 weak-coupling coefficients $a_{1,j}$ [69]. For the correct values of a and b the function $f(a,b)$ must be equal to 300. We then plot the function $f(a,b)$ over the a–b plane and search for peaks. A careful study of the peaks yields values for a and b which allow the function $f(a,b)$ to assume its maximum at 300. These numbers are given in Table 6.14.
The large-order behaviour of the Blasius weak-coupling coefficients (unlike the large-order behaviour of the instanton coefficients) has an additional overall factor $\cos(an+b)$, and we can now see that the remaining structure differs from the structure of the instanton weak-coupling coefficients. Dividing by the cosine, we observe that the coefficients

$$a'_j \equiv \frac{a_{1,j}}{\cos(aj+b)} \tag{6.71}$$

grow factorially fast. Thus, we also divide by $j!$:

$$b_j \equiv \frac{a_{1,j}}{\cos(aj+b)j!} \,. \tag{6.72}$$

The coefficients b_j are unstable under a ratio test. That is, the ratio b_{j+1}/b_j decreases and then begins to oscillate. This reflects the inaccuracy that results from the delicate sign pattern of the first 300 coefficients $a_{1,j}$.

Chapter 7

Discussion

Having gone through the recursive calculation of the imaginary-time evolution amplitude and through several applications of variational perturbation theory we now want to discuss a few properties of both of them.
First of all we critically rate our recursion relation from Chapter 3 in Section 7.1, comparing it to other methods like for instance evaluating Feynman diagrams. In Section 7.2 we will discuss its limitations. Then we review the convergence behaviour of variational perturbation theory in Section 7.3. In Section 7.4 we will overview possible further applications of the recursion relation and of variational perturbation theory such as Bose-Einstein condensates, Type-II super conductors, Markov processes, and stochastic resonance. Thereafter we quickly look at the results obtained for the two boundary-layer problems in Section 7.5.

7.1 Bearing of the Combined Differential and Algebraic Recursion

The recursive technique that has been developed throughout Chapter 3 of this thesis definitely out classes all diagrammatical perturbative calculations. Using the conventional evaluation of Feynman diagrams, the partition function and the free energy have been evaluated up to third order [18]. Diagrammatical results for the density matrix came as far as up to second order [33]. In contrast to that we could drive our recursive calculations up to seventh order for the free energy and for the ground state wave function. Variationally we came us high as the fifth order in the case of the free energy and up to seventh order for the wave function. The free energy requires more computational resources due to the subtle expansion of the logarithm (4.3). State of the art computer algebra programmes such as `Maple` can evaluate the imaginary-time evolution amplitude up to the seventh order perturbatively within a couple of hours, whereas the integrals represented by eight loop Feynman diagrams are not solvable with such programmes, nor by hand. Variational perturbation theory costs even more time and five variational orders for the free energy is at the edge of what can be done at the moment.
Possible future applications of the combined differential and algebraic recursion are discussed

in Section 7.4.

7.2 Limitations

The combined differential and algebraic recursion definitely is a challenge for every computer algebra program. Going up order by order and thus making use of the cache memory of our PCs it still took `Maple` 15 hours to calculate the seventh order of the imaginary-time evolution amplitude.[1] Comparing the computation times for each order roughly yields an exponential growth. Also the further simplification procedures and especially the "series"-command (`Maple`) required a lot of computation time again. This was the price we had to pay for the idea, to get one universal recursion relation for all the quantum statistical anharmonic oscillator quantities at the same time.
Still it is easy to overcome diagrammatical calculations and further streamlining of the `Maple` script should probably push the limits further.

7.3 Exponential Convergence of Variational Perturbation Theory

For the free energy as well as for the ground state wave function the convergence of variational perturbation theory was found to be exponential. The fact that the principle of least sensitivity [48] as interpreted by Kleinert produces extrema for the odd variational orders and inflection points for even orders, both in the case of the free energy and in the case of the ground state wave function, is reflected in the respective convergence behaviours: Odd and even orders can best be fitted separately by exponentials. Thus we obtained intervals of convergence for certain values of the free energy or the ground state wave function which always turned out to contain the exact numerical result when taking into account the statistical errors associated with the boundaries of the intervals. For the free energy the numerical results were obtained using its spectral representation reverting on the first ten energy eigenvalues obtained with the "shooting method", sketched in Section 4.4. And for high temperatures the classical free energy was available for comparison. For the ground state wave function numerical results could be obtained directly from the "shooting method".

7.4 Next Steps

There are quite a few interesting problems which could now be tackled with either recursive techniques or with variational perturbation theory or both:

[1] We used a Pentium III, 450MHz and later an AMD with 1.5GHz which was much quicker. But at that stage this thesis was almost finished.

Quantum statistics

Recently a lot of research has been done on the stochastic and dynamic properties of flux lines in high-T_c super conductors with arbitrary pinning centres [70, 71]. Of all the possible pinning mechanisms, one seems to be most promising, namely the interaction of the flux lines with columnar defects [72, 73]. From a theoretical point of view, this mechanism has been examined by Nelson and Vinokur [74] on the foundation of the Bose analogy [75, 76]. Only recently Ettouhami succeeded in describing the physics of a single flux line without using columnar defects and their pinning effect [77], but instead he employed the Feynman-Kleinert variational perturbation theory [6], to generate the partition function and the effective pinning energy. It turned out that the mean square deviation of the flux lines from the pinning centre diverges for a certain critical temperature. This was taken as a hint for a localization-non localization phase transition. The final experimental and theoretical evidence of such a phase transition is still missing though [77].
Therefore it would be very interesting to investigate the question whether other pinning potentials than the Gaussian potential chosen by Ettouhami could create a phase transition. Also the competing influences of different pinning centres on the localization properties of the flux line can be studied. Finally one could check, whether the results of the Feynman-Kleinert variational perturbation theory is altered for higher orders. Especially for a Gaussian pinning potential corrections from higher variational perturbative orders could be evaluated by means of the smearing formula [12].

Bose-Einstein condensates, Type-II super conductors

After the pioneering work, that has been done to realize Bose-Einstein condensates of atomic gases in magnetic traps [78, 79, 80], these condensates are now routinely produced in labs around the world.[2] Therefore scientific interest has shifted from production and structure of these condensates to a deep understanding of their dynamics [83]. Especially for the interpretation of experimental data it is indispensable to examine the dynamics of collapsing and exploding Bose-Einstein condensates and the influence of interaction between the matter in the condensate and the radiation. For low temperatures the mean-field theory has proved to be successful. It assumes that all atoms are in the same one-particle state [84]. The Bose-Einstein condensate is then described by a macroscopic wave function $\Psi(\mathbf{r},t)$ which is the order parameter. Its modulus squared is interpreted as the residence probability of the atoms in the condensate. The unitary time evolution of the macroscopic wave function $\Psi(\mathbf{r},t)$ obeys the Gross-Pitaevskii equation [85], which reads

$$i\hbar\frac{\partial}{\partial t}\Psi(\mathbf{r},t) = \left[-\frac{\hbar^2\Delta}{2M} + V_{\text{ext}}(\mathbf{r}) + g\,|\Psi(\mathbf{r},t)|^2\right]\Psi(\mathbf{r},t)\,. \tag{7.1}$$

[2] In December 2001, for the second time in ten years, the Nobel Prize was awarded to three physicists who worked on Bose-Einstein condensates [81, 82].

We have to solve equation (7.1) with the wave function $\Psi(\mathbf{r},t)$ being normalized for all times:

$$\int d^3x|\Psi(\mathbf{r},t)|^2 = 1\,. \tag{7.2}$$

Contrarily in experiments atoms can be scattered out of the trap inelastically. We can account for that loss by adding imaginary loss terms to the Gross-Pitaevskii equation (7.1) which then destroy the normalization of $\Psi(\mathbf{r},t)$ [85].
Up to now the Gross-Pitaevskii equation has been solved either numerically [84] or in the Thomas-Fermi approximation [86, 87]. In the latter case one assumes that the evaluation of the wave function of the condensate can be simplified by neglecting the term for the kinetic energy in the limiting case of many atoms. It turns out that the Thomas-Fermi approximation is quite rough [86] and, moreover, it depends on the properties of the trap [87]. It is therefore necessary to improve the Thomas-Fermi approximation with the help of variational techniques [87]. It would be worth a try to solve the Gross-Pitaevskii equation by means of a Bender-Wu like double expansion ansatz. Afterwards one could resum the perturbative result with the help of variational perturbation theory. We expect that this procedure would improve the accuracy of the results for the Bose-Einstein condensate as well as in other applications of the Thomas-Fermi approximation like for instance the physics of atoms and molecules [2].
As the Gross-Pitaevskii equation is also used to describe super fluid Helium and super conductivity in the mean-field approach [88], a recursive ansatz would be very promising in these fields, too.

Dissipative quantum mechanics

The recursive methods which have been developed in chapter 3 of this thesis can also be extended to dissipative quantum systems. Such a system consists of a few macroscopic degrees of freedom which are coupled to a large number of microscopic degrees of freedom and is usually described by the path integral quantization [2, 42]. As the microscopic structure of the reservoir is of no importance, one usually integrates over these degrees of freedom. For simplicity the reservoir is modeled by independent oscillators. What is left over is the *reduced density matrix* which now depends on the coordinates of the macroscopic degrees of freedom only. The essential kernel of the path integral is the so called *influence functional* that effectively contains the complete influence of the reservoir [89]. Both the Caldeira-Leggett model [43, 44, 42, 90] and the model of optical and acoustic polarons [5, 42, 91] are of this general form. The actual evaluation of the reduced density matrix in the framework of these models unfortunately is very difficult, because the underlying action is bilocal.
One could try to find more efficient methods for this computation. A double expansion ansatz for the imaginary-time evolution amplitude would solve the Schrödinger equation. Again one would obtain a set of recursive ordinary differential equations. Taking the trace over the reservoir coordinates in the imaginary-time evolution would yield a perturbative result for the reduced density matrix, which could then undergo variational perturbation theory. The recursive technique would allow for higher orders, such that the first-order results [43] based on the variational methods by Giachetti and Tognetti [22] could be exceeded.

Especially a study of the g-dependence of the density of states of the damped harmonic oscillator [92] would be interesting.

Markov processes, Brownian motion

Bender-Wu like recursive solutions may also be useful for Markov processes [93, 94, 95, 96, 24]. Following Ref. [23] for a nonlinear drift coefficient [97]

$$K(x) = -\kappa x - g x^3 \,, \tag{7.3}$$

the probability density will factorize according to

$$P(x_b\, t_b | x_a\, t_a) = P_\kappa(x_b\, t_b | x_a\, t_a) F(x_b\, t_b | x_a\, t_a) \,, \tag{7.4}$$

where $P_\kappa(x_b\, t_b | x_a\, t_a)$ denotes the probability density of a Brownian particle. The resulting Fokker-Planck equation for the correction $F(x_b\, t_b | x_a\, t_a)$ then reads

$$\begin{aligned} \frac{\partial}{\partial t_b} F(x_b\, t_b | x_a\, t_a) \;=\; & \left\{ D \frac{\partial^2}{\partial x_b^2} + \left[\kappa x_b + g x_b^3 - 2\kappa \frac{x_b - x_a e^{-\kappa(t_b - t_a)}}{1 - e^{-2\kappa(t_b - t_a)}} \right] \frac{\partial}{\partial x_b} \right. \\ & \left. + \left[3 g x_b^2 - \frac{\kappa}{D} g x_b^3 \frac{x_b - x_a e^{-\kappa(t_b - t_a)}}{1 - e^{-2\kappa(t_b - t_a)}} \right] \right\} F(x_b\, t_b | x_a\, t_a) \,. \end{aligned} \tag{7.5}$$

Diagrammatical considerations suggest to solve this partial differential equation with the ansatz

$$F(x_b\, t_b | x_a\, t_a) = 1 + \sum_{n=1}^{\infty} \sum_{m=0}^{4n} g^n c_m^{(n)}(x_a, t_b, t_a) x_b^m \,. \tag{7.6}$$

Similar to the recursion which was developed in chapter 3 of this thesis, the expansion coefficients $c_m^{(n)}(x_a, t_b, t_a)$ should obey an ordinary partial differential equation. With the help of a computer algebra program it should be possible to drive this perturbative calculation to very high orders as seen in the case of the quantum statistical imaginary-time evolution amplitude. Initial results leading in this direction have now been shown in Ref. [24].

Stochastic resonance

Normally an increase of the noise background leads to a higher signal-to-noise ratio. Some 20 years ago it was discovered that under certain circumstances also the opposite counterintuitive effect can happen. This phenomenon is know as stochastic resonance [98]. Stochastic resonance is believed to explain many physical problems, as well as it has applications in chemistry and biology. Even the periodicity of the ice ages can be modeled by means of stochastic resonance.

Consider a particle in the double well potential together with a periodic external weak force. This weak force can induce periodic movements of the particle. This stochastic synchronization occurs when the mean time between two noise induced transitions is of the order of half the period of the external force. This model of stochastic resonance has been studied in the adiabatic limit, in the fully non-adiabatic regime and by means of linear-response approximation (compare the bibliography in [98]).
So similarly to the above described approach to Markov processes one could in this case solve the Fokker-Planck equation for the explicitly time-dependent drift coefficient

$$K(x,t) = -\kappa x - gx^3 + F(t) \tag{7.7}$$

for arbitrary forces $F(t)$ and especially for periodic forces $F(t) = A\cos(\omega t + \phi)$. But also other time dependencies as, for instance, the competition between two Fourier modes could be interesting.

Theory of reaction rates

One of the most important applications of Markov theory is the description of thermally activated transitions between meta stable states. This process is especially significant for the theory of reaction rates in chemistry and biology which was founded by Kramers [98]. A typical model is the over damped Brownian motion of a particle in a double well potential where the position of the particle is identified with the reaction rate coordinate. By solving the underlying Fokker-Planck equation, the mean transition rate between the two minima can be calculated. Using several different approximations one can show that the mean transition rate grows with a decreasing damping whereas the rate drops again for strong damping [99]. Variational perturbation theory would enable us to investigate this interesting transition further on the scaffolding of the results obtained for Markov theory mentioned earlier. For low temperatures also quantum mechanical tunneling becomes more important compared to thermally activated transitions. The competing influence of these two phenomena is described by the Caldeira-Leggett model. It predicts a critical temperature: Above this temperature thermally activated transitions are dominant, below this temperature only quantum mechanical tunneling processes are relevant. A variational perturbative study of these phenomena could refer to previous work [2, 28, 29, 30, 100] where purely quantum mechanical tunneling has been described. For instance one could compute the splitting in the double well potential by resumming the weak coupling perturbation series into a strong coupling series with the help of variational perturbation theory which then is analytically continued to negative coupling constants. The results are practical for low barriers and high tunneling rates. Combining variational perturbation theory with the semiclassical approximation, one could extend their practicability to high barriers and low tunneling rates.

Brownian motors

Is it possible to transform the arbitrary microscopic fluctuations of Brownian motion into mechanical work? This basic question can be studied by means of the stochastic ratchet

model [99] which is based on a gedanken experiment by Smoluchowski [101] and Feynman [102]. Consider the over damped Brownian motion of a particle in a spatially periodic potential $V(x) = V(x + L)$ with spatially broken symmetry. This could be realized for instance by superimposing two Fourier modes

$$V(x) = A \sin \frac{2\pi x}{L} + B \sin \frac{4\pi x}{L} \,. \tag{7.8}$$

Then one solves the underlying Fokker-Planck equation with the drift coefficient

$$K(x) = -V'(x) \,. \tag{7.9}$$

The ratchet effect occurs when appropriately chosen system parameters do not let the particle current vanish

$$\langle \dot{x}(t) \rangle = - \int_{-\infty}^{+\infty} dx \left[-V'(x) + D \frac{\partial}{\partial x} \right] P(x\, t | x_0\, t_0) \,. \tag{7.10}$$

Investigating such stochastical systems with ratchet effects, which are also referred to as Brownian motors, has become very important especially for the biology of cells. Recently it was discovered that the ratchet effect is responsible for the intra cellular transport of so-called molecular motors, which migrate along polymer filaments (compare the extensive bibliography in [99]).
This ratchet effect can be studied with the help of variational perturbation theory. To this end one of the few exactly solvable cases of the stochastic ratchet model [99] can be chosen as the reference system, around which one can then expand perturbatively. Its parameters become the variational parameters. The results could be compared with approximative results [99] for the particle current (7.10). Moreover it would be interesting to find out which system parameters can change the current (7.10) most efficiently.
Also one could extend the studies on quantum ratchets. Their microscopic fluctuations are both of thermal and quantum mechanical origin. Important experimental realizations are Josephson junctions and SQUIDS [103]. Quantum ratchets are described in the framework of the Caldeira-Leggett model of dissipative quantum mechanics, which has already been mentioned in connection with quantum dissipation.

7.5 Boundary-Layer Theory, Strong-Coupling Series, Large-Order Studies

Unfortunately we did not succeed in finding a systematic resummation algorithm for the instanton problem and for the Blasius equation, solved on the lattice in the limit as the lattice spacing goes to zero. This would have enabled us to quickly switch from difference equations to differential equations and vice versa. Also our analytic understanding of field theories would have benefited. However, we could study the respective large-order behaviours. May be these considerations will enable us, to at least push the convergence radii further out. Or

they might tell us which set of base functions can be used to re-expand the two weak-coupling series in such a way that they converge even for infinite coupling. What definitely can be said at this stage is, that the numerics have been pushed to the limits. Our `Maple` programs blocked various computer clusters on both sides of the Atlantic[3] for periods of time as long as two weeks.

7.6 Concluding Thoughts

We have seen that recursive techniques in quantum statistics together with powerful computer algebra systems enhance our possibilities to obtain high-order perturbative results for all the relevant quantities. Furthermore we could use these results to study variational perturbation theory for the anharmonic oscillator systematically. It is now about time to apply the two formalisms — the recursion techniques and variational perturbation theory — to the very interesting problems that have been mentioned in Section 7.4.
The boundary-layer problems from Chapter 6, solved on the lattice in the limit as the lattice spacing goes to zero, still wait for a suitable systematic resummation algorithm.

[3] At the Freie Universität in Berlin and at the Washington University in St. Louis, Missouri.

Acknowledgements

I am deeply grateful to Prof. Hagen Kleinert whom I first met in winter 1999, when I attended his lectures on "Advanced Quantum Mechanics". The main theoretical tool of this thesis, variational perturbation theory, was an integral part of this course as well as of his seminar on path integrals taught in the same semester. Prof. Kleinert later enthusiastically agreed to supervise this diploma thesis. He always kept up the spirits by coming up with new creative ideas which always turned out to work. And he always found time for very fruitful discussions.
In autumn 2001 I had the possibility to visit Prof. Carl Bender at Washington University in St. Louis, Missouri. After I had presented preliminary results from Chapters 3, 4, and 5 to him and his colleagues from the Physics Department at WashU, he offered several ideas how I could round off this work. Moreover, he taught me a lot of techniques which then layed the foundation for Chapter 6 of this thesis which is a result of our close collaboration. For this and for the warm reception at Washington University I want to thank him deeply.
Prof. Bodo Hamprecht provided me with his perturbative results for the free energy which he had obtained with `Mathematica`. Thus I had an excellent cross check for the expressions I generated with `Maple`. Prof. Hamprecht's generousity will not be forgotten.
Also Dr. Axel Pelster's advice was extremely helpful. Especially his well educated guesses concerning `Maple` helped to overcome many problems. And even the most technical mathematical question could not puzzle him. He also sacrificed a couple of public holidays to discuss this work with me.
Moreover I appreciate my parents' generous support. They made my life easier and more comfortable by ameliorating the income I get as a tutor at the Physics Department of Freie Universität Berlin. They also cheered me up during the dark phases, and their additional financial support finally enabled me to go to St. Louis. And even when I had a crash with my mother's staff car on the occasion of her 50th birthday in December 2001, neither my mother nor my father lost patience.
The money I got from my parents was also spent in the "Cafe Atlantic". My sessions there yielded quite a few ideas which are now part of this thesis. Moreover their kitchen was open till midnight — that helped me to survive this work physically. And Katharina was (and still is) a very warm-hearted waitress. However, I am disappointed that the "Atlantic" shamelessly raised all prices by 10 percent after conversion to Euros.
My grandparents always kept track of my academic efforts and they, too, helped me over financial obstacles. Therefore I want to thank them from the bottom of my heart and I promise to try to explain to them in plain German what this diploma thesis is all about.
My sister Julia kept distracting me from work with endless telephone calls. Still I am grateful

to her as she also joined me in the “Atlantic”. So did Christian Joas, Rolf Minkwitz, and Alekos Tsamaloukas. Alekos also gave me innumerable valuable hints concerning TEX. And Konstantin Glaum, Ceyda Öçalır, as well as Sebastian Schmidt were pleasant and easy-going office mates.

Berlin, in the Year of the Lord MMII
Florian Weißbach

List of Figures

List of Tables

Bibliography

[1] C. M. Bender and T. T. Wu: *Anharmonic oscillator*, Phys. Rev. **184**, 1231 (1969); *Anharmonic oscillator. II. A study of perturbation theory in large order*, Phys. Rev. D **7**, 1620 (1973)

[2] H. Kleinert: *Path integrals in mechanics, statistics, polymer physics, and stock markets*, 3rd edition, World Scientific, Singapore (2002)
`http://www.physik.fu-berlin.de/~kleinert/kleiner_reb3/3rded.html`

[3] R. P. Feynman: *Space-time approach to non-relativistic quantum mechanics*, Rev. Mod. Phys. **20**, 367 (1948)

[4] R. P. Feynman and A. R. Hibbs: *Quantum mechanics and path integrals*, McGraw-Hill, Inc., New York (1965)

[5] R. P. Feynman: *Statistical mechanics*, Reading, Massachusetts (1972)

[6] R. P. Feynman and H. Kleinert: *Effective classical partition functions*, Phys. Rev. A **34**, 5080 (1986)

[7] H. Kleinert: *Systematic corrections to variational calculation of effective classical potential*, Phys. Lett. A **173**, 332 (1993)

[8] H. Kleinert and V. Schulte-Frohlinde: *Critical properties of ϕ^4-theories*, World Scientific, Singapore (2001)

[9] J. Jaenicke and H. Kleinert: *Loop corrections to the effective classical potential*, Phys. Lett. A **176**, 409 (1993)

[10] H. Kleinert: *Effective potentials from effective classical potentials*, Phys. Lett. B **181**, 324 (1986)

[11] W. Janke and H. Kleinert: *Effective classical potential and particle distribution of a Coulomb system*, Phys. Lett. A **118**, 371 (1986)

[12] H. Kleinert, A. Pelster, and W. Kürzinger, *Smearing formula for higher-order effective classical potentials*, J. Phys. A **31**, 8307 (1998)

[13] M. Bachmann, H. Kleinert, and A. Pelster: *Quantum statistics of hydrogen in strong magnetic fields*, Phys. Lett. A **279**, 23 (2001)

[14] M. Bachmann, H. Kleinert, and A. Pelster: *Variational approach to hydrogen atom in uniform magnetic field of arbitrary strength*, Phys. Rev. A **62**, 52509 (2000)

[15] D. Klakow, C. Toepffer, and P.-G. Reinhard: *Semiclassical molecular dynamics for strongly coupled Coulomb-systems*, Journal of Chemical Physics **101**, 10766 (1994)

[16] D. Klakow, C. Toepffer, and P.-G. Reinhard: *Hydrogen under extreme conditions*, Phys. Lett. A **192**, 55 (1994)

[17] W. Ebeling and B. Militzer: *Quantum molecular dynamics of partially ionized plasmas*, Phys. Lett. A **226**, 298 (1996)

[18] H. Kleinert and H. Meyer: *Variational calculation of effective classical potential at* $T \neq 0$ *to higher orders*, Phys. Lett. A **184**, 319 (1994)

[19] W. Janke and H. Kleinert: *Convergent strong-coupling expansions from divergent weak-coupling perturbation theory*, Phys. Rev. Lett. **75**, 2787 (1995)

[20] H. Kleinert: *Variational interpolation algorithm between weak- and strong-coupling expansions*, Phys. Lett. A **207**, 133 (1995)

[21] H. Kleinert: *Variational resummation of divergent series with known large-order behaviour*, Phys. Lett. B **360**, 65 (1995)

[22] R. Giachetti and V. Tognetti: *Variational approach to quantum statistical mechanics of nonlinear systems with applications to Sine-Gordon chains*, Phys. Rev. Lett. **55**, 912 (1985)

[23] H. Kleinert, A. Pelster, and M. Putz: *Variational perturbation theory for Markov processes*, accepted for publication in Phys. Rev. **E**

[24] J. Dreger: *Untersuchung des Starkkopplungsverhaltens der Fokker-Planck-Gleichung mit anharmonischer Drift*, diploma thesis at Freie Universität Berlin (2002)

[25] A. Okopinska: *The Fokker-Planck equation for bistable potential in the optimized expansion*, e-print: cond-mat/0111389 (2001)

[26] H. Kleinert and W. Janke: *Convergence behavior of variational perturbation expansion – A method for locating Bender-Wu singularities*, Phys. Lett. A **206**, 283 (1995)

[27] W. Janke and H. Kleinert: *Scaling property of variational perturbation expansion for general anharmonic oscillator with* x^P*-potential*, Phys. Lett. A **199**, 287 (1995)

[28] H. Kleinert: *Variational approach to tunneling. Beyond the semiclassical approximation of Langer and Lipatov – perturbation coefficients to all orders*, Phys. Lett. B **300**, 261 (1993)

[29] R. Karrlein and H. Kleinert: *Precise variational tunneling rates of anharmonic oscillator for* $g < 0$, Phys. Lett. A **187**, 133 (1994)

[30] H. Kleinert and I. Mustapic: *Decay rates of metastable states in cubic potential by variational perturbation theory*, Int. J. Mod. Phys. A **11**, 4383 (1996)

[31] H. Kleinert: *Higher-order variational approach to non-Borel systems. The energies of the double-well potential*, Phys. Lett. A **190**, 131 (1994)

[32] H. Kleinert: *Particle distribution from effective classical potential*, Phys. Lett. A **118**, 267 (1986)

[33] M. Bachmann, H. Kleinert, and A. Pelster: *Variational perturbation theory for density matrices*, Phys. Rev. A **60**, 3429 (1999)

[34] A. Okopinska: *Optimized perturbation method for the propagation in the anharmonic oscillator potential*, Phys. Lett. A **249**, 259 (1998)

[35] H. Kleinert: *Effective classical potential for fluctuating field systems of finite size*, Phys. Lett. A **118**, 195 (1986)

[36] M. Bachmann, H. Kleinert, and A. Pelster: *Strong-coupling calculation of the fluctuation pressure of a membrane between walls*, Phys. Lett. A **261**, 127 (1999)

[37] M. Bachmann, H. Kleinert, and A. Pelster: *Fluctuation pressure of a stack of membranes*, Phys. Rev. E **63**, 051709 (2001)

[38] H. Kleinert: *Strong-coupling behaviour of ϕ^4-theories and critical exponents*, Phys. Rev. D **57**, 2264 (1998), Add. Phys. Rev. D **58**, 107702 (1998)

[39] H. Kleinert: *Critical exponents without β-function*, Phys. Lett. B, **463**, 69 (1999)

[40] A. Pelster and F. Weißbach: *Variational perturbation theory for the ground state wave function*, in: W. Janke, A. Pelster, H.-J. Schmidt, M. Bachmann (Editors): *Fluctuating Paths and Fields – Festschrift dedicated to Hagen Kleinert on the occasion of his 60th birthday*, World Scientific, Singapore (2001), p. 315

[41] T. Hatsuda, T. Kunihiro, and T. Tanaka: *Optimized perturbation theory for wave functions of quantum systems*, Phys. Rev. Lett. **78**, 3229 (1997)

[42] U. Weiss: *Quantum dissipative systems*, 2nd edition, World Scientific, Singapore (2000)

[43] A. Cuccoli, A. Rossi, V. Tognetti, and R. Vaia: *Thermodynamics of dissipative quantum systems by effective potential*, Phys. Rev. E **55**, 4849 (1997)

[44] A. O. Caldeira and A. J. Leggett: *Influence of dissipation on quantum tunneling in macroscopic systems*, Phys. Rev. Lett. **46**, 211 (1982)

[45] A. O. Caldeira and A. J. Leggett: *Path integral approach to quantum Brownian motion*, Physica A **121**, 587 (1983)

[46] D. Cohen: *Quantum dissipation versus classical dissipation for generalized Brownian motion*, Phys. Rev. Lett **78**, 2878 (1997)

[47] Y. C. Chen, M. P. A. Fisher, and A. J. Leggett: *The return of a hysteretic Josephson junction to the zero-voltage state: I-V characteristic and quantum retrapping*, Journal of Applied Physics **64**, 3119 (1988)

[48] P. M. Stevenson: *Optimized perturbation theory*, Phys. Rev. D **23**, 2916 (1981)

[49] C. Öçalır: *Correlation functions in quantum statistics*, diploma thesis at Freie Universität Berlin (2003)

[50] H. Kleinert, A. Pelster, and M. Bachmann: *Generating functional for harmonic expectation values of paths with fixed end points: Feynman diagrams for nonpolynomial interactions*, Phys. Rev. E **60**, 2510 (1999)

[51] The expansion coefficients $c^{(n)}_{2k|l}(\tau)$ up to seventh order can be found at `http://www.physik.fu-berlin.de/~weissbach/coeff.html`

[52] I. S. Gradshteyn and I. M. Ryzhik, *Table of integrals, series, and products,* corrected and enlarged edition, Academic Press, New York (1980)

[53] C. M. Bender, and S. Orszag: *Advanced mathematical methods for scientists and engineers*, McGraw-Hill, Inc., New York (1978)

[54] C. M. Bender, F. Cooper, G. S. Guralnik, and D. H. Sharp: *Strong-coupling expansion in quantum field theory*, Phys. Rev. D **19**, 1865 (1979)

[55] C. M. Bender, F. Cooper, G. S. Guralnik, R. Roskies, and D. H. Sharp: *Improvement of an extrapolation scheme for strong-coupling expansions in quantum field theory*, Phys. Rev. Lett. **43**, 537 (1979)

[56] C. M. Bender, F. Cooper, G. S. Guralnik, H. Rose, and D. H. Sharp: *Strong coupling expansion for classical statistical dynamics*, Jour. Stat. Phys. **22**, 647 (1980)

[57] C. M. Bender, F. Cooper, G. S. Guralnik, R. Roskies, and D. H. Sharp: *"Renormalizing the strong-coupling expansion for quantum field theory: Present status*, in *Recent Developments in High-Energy Physics*, Ed. by B. Kursunoglu, A. Perlmutter, and L. F. Scott (Plenum, New York, 1980), p. 211.

[58] C. M. Bender, F. Cooper, R. Kenway, and L. M. Simmons, Jr.: *Continuum regulation of the strong coupling expansion for quantum field theory*, Phys. Rev. D **24**, 2693 (1981)

[59] C. M. Bender and R. Z. Roskies: *Effect of renormalization of the large-order behavior of weak- and strong-coupling perturbation theory*, Phys. Rev. D **25**, 427 (1982)

[60] C. M. Bender, F. Cooper, R. Kenway, and L. M. Simons, Jr.: *Problems with continuum regulation of strong-coupling expansions*, Phys. Lett B **109**, 63 (1982)

[61] C. M. Bender, L. R. Mead, and L. M. Simmons, Jr.: *Large-order behavior of lattice strong-coupling expansions*, Phys. Rev. D **28**, 936 (1983)

[62] C. M. Bender, F. Cooper, and A. Das: *Continuum limit of supersymmetric field theories on a lattice*, Phys. Rev. Lett. **50**, 397 (1983)

[63] C. M. Bender, F. Cooper, G. S. Guralnik, E. Mjolsness, H. A. Rose, and D. H. Sharp: *A novel approach to the solution of boundary-layer problems*, Adv. Appl. Mathematics **1**, 22 (1980)

[64] C. M. Bender: *A novel approach to boundary-layer problems*, Los Alamos Science **2**, 76 (1981)

[65] C. M. Bender and A. Tovbis: *Continuum limit of lattice approximation schemes*, J. Math. Phys. **38**, 3700 (1997)

[66] The first 200 weak-coupling coefficients for the instanton equation can be found at `http://www.physik.fu-berlin.de/~weissbach/inst.html` .

[67] H. Blasius: *Grenzschichten in Flüssigkeiten mit kleiner Reibung*, Z. Math. Phys. **56**, 1 (1908)

[68] Z. Belhachmi, B. Brighi, and K. Taous: *On the concave solutions of the Blasius equation*, Acta Math. Univ. Comenianae, Vol. **LXIX**, 199 (2000)

[69] The first 300 weak-coupling coefficients for the Blasius equation can be found at `http://www.physik.fu-berlin.de/~weissbach/blas.html` .

[70] G. Blatter, M. V. Feigel'man, V. B. Geshkenbein, A. I. Larkin, and V. M. Vinokur: *Vortices in high-temperature superconductors*, Rev. Mod. Phys. **66**, 1125 (1994)

[71] T. Nattermann and S. Scheidl: *Vortex-glass phases in type II-superconductors*, Advances in Physics **49**, 607 (2000)

[72] L. Civale et al.: *Vortex confinement by columnar defects in $YBa_2Cu_3O_7$ crystals: Enhanced pinning at high fields and temperatures*, Phys. Rev. Lett. **67**, 648 (1991)

[73] M. Konczykowski et al.: *Effect of 5.3GeV Pb-ion irradiation on irreversible magnetization in Y-Ba-Cu-O crystals*, Phys. Rev. B **44**, 7167 (1991)

[74] D. R. Nelson and V. M. Vinokur: *Boson localization and correlated pinning of superconducting vertex arrays*, Phys. Rev. B **48**, 13060 (1993)

[75] D. R. Nelson: *Vortex entanglement in high-T_c superconductors*, Phys. Rey. Lett. **60**, 1973 (1988)

[76] D. R. Nelson and H. S. Seung: *Theory of melted flux liquids*, Phys. Rev. B **39**, 9153 (1989)

[77] A. M. Ettonhami: *Possible depinning transition of a single flux line near a columnar defect in type II-superconductors*, cond-mat/0106322 (2001)

[78] M. H. Anderson et al.: *Observation of Bose-Einstein condensate in a dilute atomic gas*, Science **269**, 198 (1995)

[79] K. B. Davis et al.: *Bose-Einstein condensation in a gas of sodium atoms*, Phys. Rev. Lett. **75**, 3969 (1995)

[80] C. C. Bradley et al.: *Evidence of Bose-Einstein condensation in an atomic gas with attractive interactions*, Phys. Rev. Lett. **75**, 1687 (1995)

[81] E. Cornell, and C. E. Wiemann: *Physicists create new state of matter at record low temperature*, joint press release by The National Institute of Standards and Technology and The Univereity of Colorado (1995)

[82] W. Ketterle: *MIT physicists demonstrate first atom laser*, MIT News Office (1997)

[83] L. Ginzburg, and L. P. Pitaevskii: *On the theory of superfluidity*, Sov. Phys. JETP **7**, 858 (1958); F. Dalfovo, S. Giorgini, L. P. Pitaevskii, and S. Stringari: *Theory of Bose-Einstein condensation in trapped gases*, Rev. Mod. Phys. **71**, 463 (1999)

[84] H. Saito and M. Ueda: *Mean-field analysis of collapsing and exploding Bose-Einstein condensates*, cond-mat/0107248

[85] E. P. Gross: *Structure of a generalized vortex in boson systems*, Nuovo Cimento **20**, 454 (1961); J. Math. Phys. **4**, 195 (1963); L. P. Pitaevskii: *Vortex lines in an imperfect Bose gas*, Sov. Phys. JETP **13**, 451 (1961); A. J. Leggett: *Bose-Einstein condensation in the alkali gases: Some fundamental concepts*, Rev. Mod. Phys. **73**, 307 (2001)

[86] I. Haering and J. M. Rost: *Atomic scattering from Bose-Einstein condensates*, quant-ph/0108027 (2001)

[87] A. L. Zubarev and Y. E. Kim: *Beyond the Thomas-Fermi approximation for nonlinear dynamics of trapped Bose-condensed gases*, cond-mat/0107512

[88] H. Kleinert: *Gauge fields in condensed matter, vol. 1: Superflow and vortex lines - disorder fields, phase transitions*, World Scientific, Singapore (1989)

[89] R. P. Feynman and F. L. Vernon: *The theory of a general quantum system interacting with a linear dissipative system*, Ann. of Phys. **24**, 118 (1963)

[90] A. O. Caldeira and A. J. Leggett: *Quantum tunneling in a dissipative system*, Ann. of Phys. **149**, 374 (1983)

[91] R. P. Feynman: *Slow electrons in a polar crystal*, Phys. Rev. **97**, 660 (1955)

[92] A. Hanke and W. Zwerger: *Density states of a damped quantum oscillator*, Phys. Rev. E **52**, 6875 (1994)

[93] R. L. Stratonovich, *Topics in the theory of random noise, vol. 1 — General theory of random processes, nonlinear transformations of signals and noise,* Second Printing, Gordon and Breach (1967)

[94] N. G. van Kampen, *Stochastic processes in physics and chemistry,* North-Holland Publishing Company (1981)

[95] H. Haken, *Synergetics — An introduction, nonequilibrium phase transitions and self-organization in physics, chemistry and biology,* third revised and enlarged edition, Springer, Berlin (1983)

[96] H. Risken, *The Fokker-Planck equation – Methods of solution and applications,* second edition, Springer, Berlin (1988)

[97] H. Haken, *Laser theory*, Encyclopedia of Physics, Vol. XXV/2c, Springer, Berlin (1970)

[98] L. Gammaitoni, P. Hänggi, P. Jung, and F. Marchesoni: *Stochastic resonance*, Rev. Mod. Phys. **70**, 223 (1998)

[99] P. Reimann: *Brownian motors: noisy transport far from equilibrium*, cond-mat/0010237

[100] P. Hänggi, P. Talkner, and M. Borkovec: *Reaction-rate theory: Fifty years after Kramers*, Rev. Mod. Phys. **62**, 251 (1990)

[101] M. v. Smoluchowski: *Experimentell nachweisbare, der üblichen Thermodynamik widersprechende Molekularphänomene*, Physik. Zeitschr. **13**, 1069 (1912)

[102] R. P. Feynman, R. B. Leighton, and M. Sands: *The Feynman lectures on physics*, vol. 1, chapter 46, Addison Wesley, Reading MA (1963)

[103] S. Weiss et al.: *Ratchet effects in dc SQUIDs*, Europhys. Lett. **51**, 499 (2000)